Lattice-Renormalization of the Polyakov loop

Dissertation

zur Erlangung des Doktorgrades
der Fakultät für Physik
der Universität Bielefeld

vorgelegt von
Felix Zantow

Dezember 2003

Acknowledgments

I would like to thank all the people who have helped and supported me during the make up of this thesis.

It is with the greatest pleasure that I thank my supervisor, Prof. Dr. Frithjof Karsch, for his guidance and collaboration. He was always open for questions and many fruitful discussions. He also provided me with the possibility of participating in conferences and workshops around the world. I also would like to thank Prof. Dr. Helmut Satz and Prof. Dr. Jürgen Engels for their cooperativeness and for supervising this thesis. I am particularly indebted to Dr. Olaf Kaczmarek, who introduced me into the computational aspects of my research work, providing me most of the tools I needed to get numerical results safely and efficiently. Many illuminating discussions with him about our research field have brought this thesis to a successful conclusion. In addition I would like to thank Dr. Peter Petreczky for his help and support during the whole time of my research work on this thesis, especially for kindly hosting me during my visit at BNL. In fact, this thesis is a result of the fruitful common work of all the people mentioned above. It is a great pleasure for me to have the possibility to keep working with them also in future.

I gratefully acknowledge Michael Seniuch and Sanatan Digal for reading carefully the manuscript. I also would like to express all my gratefulness to the staff of the Particle Physics group at Bielefeld, especially Gudrun Eickmeyer and Susi von Reeder, for all the help and support I received from them in all circumstances. I have benefited immensely from the friendly and quite pleasant atmosphere at the Particle Physics group in Bielefeld.

Ganz besonders möchte ich mich bedanken bei meiner Gaby sowie meinen Eltern für ihre Unterstützung und ihr Verständnis im gesamten Zeitraum meines Studiums.

Felix Zantow, Bielefeld, December 2003

Contents

Introduction

The theoretical background for this work is provided by Quantum Chromodynamics (QCD), the theory of strong interactions (see for instance [1]). QCD is part of the $SU(3) \times SU(2) \times U(1)$-Standard model for the elementary particle interactions. Describing all features of hadronic matter QCD is expected to explain such different properties as confinement and asymptotic freedom [2, 3, 4]. These widely different properties of strong interactions led to the speculation that strongly interacting hadronic matter has a qualitatively new behavior at asymptotic large temperatures and/or hadron densities. In fact, it is expected [5] that the structure of hadronic matter becomes rather simple in the high energy regime (for reviews see [6, 7, 8]). For instance, in the limit of large temperatures hadronic matter is expected to dissolve into their elementary constituents, the quarks and the gluons, forming a new state of matter, the so-called quark-gluon plasma. To some extent this new plasma state is comparable to an ideal gas of quarks and gluons. As the qualitative behavior of matter in this high temperature phase is quite different from ordinary hadronic matter, which confines quarks and gluons, this presumably implies the existence of a phase transition between these two phases. Many qualitative aspects of the confinement deconfinement phase transition in QCD can already be discussed in the quenched approximation, *i.e.* $SU(3)$ gauge theory. Here the Polyakov loop can be used as an order parameter to distinguish both phases [9, 10]. Its properties and in particular its proper definition which allows to give it a physically meaningful interpretation are the central topics of this thesis.

Due to asymptotic freedom one may expect that QCD can be analyzed with perturbative methods (for an introduction into these methods see [1, 11, 12]). Unfortunately, however, the well-established perturbative treatment of field theories in general is insufficient in its application to QCD. For instance, the ordinary perturbative treatment of QCD does not signal confinement and, due to asymptotic freedom, perturbative methods are limited in QCD to the high energy sector. This situation becomes even more complicated at finite temperature as with the weakening of the coupling at high temperatures different well separated length scales dominate the quark gluon plasma, *i.e.*

$$1/T \ll 1/(gT) \ll 1/(g^2T) \tag{1}$$

The different scales call for different perturbative re-summation techniques [13, 14]. At the ultra-soft scale, *i.e.* at distances of about $1/(g^2T)$, perturbation theory will break down even at extremely large temperatures [15, 16, 17]. Thus, although the break-down

of perturbation theory is not that obvious to take place even in the high energy, weakly coupled plasma phase, the long wave-length plasma contributions in general cannot be handled as small perturbations. This indeed prevents a perturbative analysis of long distance phenomena on quite general grounds [15]. Moreover, it cannot be expected that a perturbative approach is well suited for the study of inherently non-perturbative aspects of the confinement deconfinement phase transition. Thus, in order to study QCD in the full energy regime, even down to the low energy sector, one is indeed forced to use non-perturbative methods. For this reason the QCD thermodynamics is mainly a domain of the non-perturbative lattice approach (for an introduction to this field see [18]). MC simulation methods can provide a powerful tool to give unique quantitative results for the phase transition temperature, the order of the phase transition, the equation of state and different other quantities which are of interest for theory and experiment (for reviews see [19, 20]). The latter are, for instance, the zero temperature heavy quark potential as well as the heavy quark free energies at finite temperatures [21, 9].

Subject of this thesis is a detailed analysis of the thermal properties of the Polyakov loop and its correlation functions on the lattice in pure gauge theory ($SU(N = 3)$). The expectation value of the Polyakov loop and its (spatial) correlation functions are related to the change in free energy due to the presence of static quarks placed into the thermal gluonic heat bath. They are of considerable interest in particle physics as they reflect the screening properties of the medium in the high temperature phase as well as the confining properties in the low temperature, chiral symmetry broken phase. They are thus sensitive to the confinement deconfinement phase transition in QCD and allow to study the confining forces at finite temperatures. In fact, the QCD phase diagram has been analyzed in great detail in terms of the heavy quark free energies. Moreover, thermal modifications on the Polyakov loop correlation functions have been subject of quite a few studies in the past. Such studies refer to the pure gauge theory at finite temperature as well to full QCD and to QCD at finite baryon number densities (reviews and further references can be found in Refs. [22, 20]). However, although the Polyakov loop correlation functions have been analyzed in detail in the past, there are long standing problems which have not been solved so far. For instance, these are

- the *non-perturbative calculation of the color singlet and color octet quark antiquark free energies*. In fact, while the color averaged free energies are well-known from earlier studies, the color singlet and octet free energies are much less studied so far. This is to some extent due to the fact that up to quite recently [23] a satisfactory non-perturbative gauge invariant formulation has not be given. Indeed, the knowledge of the color singlet and color octet free energies is mainly based on perturbative arguments [24, 9]. It is therefore quite important to study the color singlet and color octet free energies in gauge invariant non-perturbative formulations in a confined and deconfined medium.

- the *renormalization of the Polyakov loop (TrL) and its correlation functions on the lattice*. This is a long standing problem which is not only of purely academic

interest [22]. For instance, $\langle \mathrm{Tr}L \rangle$ acts as an order parameter for the confinement-deconfinement phase transition which should have a physical meaning. The natural physical meaning of the order parameter is the heavy quark free energy ΔF_q which is related to the Polyakov loop expectation value via

$$\langle \mathrm{Tr}L \rangle \quad \simeq \quad \exp\left(-\Delta F_q(T)/T\right). \tag{2}$$

There also exist recent studies which claim that a renormalized Polyakov loop expectation value can be used to construct effective actions for the hadron dynamics near the phase transition [25, 26]. In this context the equation of state has been related to the temperature variation of the Polyakov loop [27, 28].

- the *calculation of the excess potential energies and entropies from free energies.* In general the Polyakov loop correlation functions refer to free energies of a system of n quarks and $\tilde{n}$ antiquarks,

$$\Delta F_{nq\tilde{n}\bar{q}} = \Delta E_{nq\tilde{n}\bar{q}} - T\Delta S_{nq\tilde{n}\bar{q}}, \tag{3}$$

which contain the internal energies $\Delta E_{nq\tilde{n}\bar{q}}$ and entropies $\Delta S_{nq\tilde{n}\bar{q}}$ which are of interest in heavy quark physics. For example, investigations of meson and hadron properties [29, 30] using thermal properties of the Polyakov loop and the Polyakov loop correlation functions in potential models [31, 32] show the need for an analysis of potential energies rather than the free energies. In fact, only phenomenological arguments could be used to motivate the potential energies in the past. Indeed, a non-perturbative evaluation of the potential energies and entropies is still outstanding at finite temperatures.

It should be obvious that these problems call for further investigations of the Polyakov loop and its correlation functions on the lattice. In the first chapter we discuss the thermal properties of the color singlet, octet and averaged free energies from large to quite small distances at temperatures ranging from $T = 0.9T_c$ to temperatures of about $12T_c$. The data for the color singlet and octet free energies we present here are calculated in a gauge independent way (following [23]). We also present here a new 1-loop perturbative calculation for the color averaged free energies.

In the second chapter we discuss the renormalization of the Polyakov loop and its correlation functions on the lattice. As the lattice renormalization of the Polyakov loop is a long standing problem we first introduce into the problem and discuss earlier and current concepts. We then outline our new renormalization scheme for the 2-point correlation functions of the Polyakov loops which leads to a proper and well-defined continuum limit for the Polyakov loop expectation value on the lattice. Clearly, to our scheme corresponds a renormalization constant. This effective renormalization constant will be calculated by us at several lattice couplings.

In the last chapter of this thesis we discuss a first application of the renormalized free energies. In particular, we calculate separately the potentials and entropies from the renormalized free energies using thermal relations. We discuss the thermal properties of

the finite temperature potentials and entropies.

In this thesis we restrict ourselves to the pure gauge theory, $SU(3)$, as we are in main parts interested in the inherent effects concerning the confinement deconfinement phases and the phase transition. We stress here, however, that the conceptual approach we develop here for $SU(3)$ can easily be generalized to the case of full QCD.

Chapter 1

Heavy quark free energy and the running coupling at finite temperature

In this first chapter we begin with our analysis of the thermal properties of the quark antiquark free energies[1] in both phases of $SU(3)$, in the confinement and deconfinement phases. We are interested in the thermal modifications at large ($rT \gg 1$), intermediate ($rT \simeq 1$) and small ($rT \ll 1$) quark antiquark separations, where r denotes the separation between the $q\bar{q}$-pair and T is the temperature of the thermal medium. We discuss in detail non-perturbative effects in the free energies, *i.e.* the thermal properties of color screening above T_c and the r-running of the coupling defined in terms of heavy quark free energies at finite temperatures. We close this chapter with general notes on the free energies at temperatures below the deconfinement point.

Nonetheless, we should first clarify our conventions and notations and also should summarize what is known about heavy quark free energies. Actually, the heavy quark free energies have been subject of many studies in the past. However, while the so-called *color averaged free energies* ($\Delta F_{q\bar{q}}$), which are defined in the case of $SU(3)$ on (and similarly for $SU(N)$) [9]

$$\Delta F_{q\bar{q}}(r,T) \;=\; -T \ln \left(\frac{1}{9} e^{-\Delta F_1(r,T)/T} + \frac{8}{9} e^{-\Delta F_8(r,T)/T} \right) , \tag{1.1}$$

have been studied to high accuracy at intermediate and large distances at finite temperatures, the color singlet (ΔF_1) and color octet (ΔF_8) quark antiquark free energies are

[1] The introduction of the Polyakov loop and its relation to the free energies we discuss here is subject of Sec. 1.2. At this level of the discussions of the thermal properties of the heavy quark antiquark free energies it is indeed sufficient to realize that the heavy quark free energies are *free energies*: As free energies (F) they contain the potential energies (E) as well as the entropies (S), *i.e.* $F = E - TS$. They are thus often called *potential energies* of the quark antiquark pair in the gluonic heat bath. In terms of potentials confinement is said to lead to increasing functional dependence with increasing distances while the plasma phase (deconfinement) is related to a flattening of the potentials at large distances.

much less known, so far. It follows from (1.1) that the thermal influence of the medium on the free energies becomes more transparent in terms of the color singlet and octet free energies.

Unfortunately, however, the formulation of free energies can be given a gauge independent, physically reasonable meaning only in the case of the color averaged free energies although the physical interest rather points at the color singlet and color octet free energies. Indeed, up to quite recently [23] the singlet and octet free energies could not be formulated (accurately) in a gauge independent manner [24]. In a recent study it is shown [23] that a formulation of the color singlet and color octet free energies can be given in terms of manifestly gauge invariant, non-local operators and this formulation is equivalent to a formulation of the free energies in Coulomb gauge. We mainly discuss in this chapter the thermal effects on the color singlet and color octet quark antiquark free energies calculated in the latter, thus gauge independent way (following [23]). In this chapter we summarize various *new* aspects of the different thermal properties of Polyakov loop correlation functions.

We begin with some general notes on the thermal properties of the (color averaged) heavy quark free energies. We follow here closely the discussion outlined in [33] as it summarizes the present knowledge on this field.

1.1 Heavy quark free energies

In order to show the basic features of the free energies in a confining medium we show in Fig. 1.1 lattice results for the color averaged heavy quark antiquark free energies ($\Delta F_{q\bar{q}}(r,T)$) in quenched QCD (pure $SU(3)$ gauge theory) at temperatures below T_c. As can be seen from this figure the free energies show the so-called *quark confinement* as the quark antiquark free energies increase with increasing distances. It follows that it is impossible to separate completely the two static color charges in this medium as it would cost an infinite amount of (free) energy. Consequently, the interaction between the static quarks in this phase is quite strong and gets stronger with increasing distance. It can also be seen from Fig. 1.1 that the slope of the free energies as function of the distance is decreasing when going to higher temperatures. This property may suggest that above some temperature (T_c) the strong interaction gets weak which may result in a (new) phase of almost interaction free particles.

It is well-known that a linearly increasing free energy of a $q\bar{q}$ pair at large distances arises from the *string picture* in the confined ($T < T_c$) phase. In this model[2] for the quark interactions an (infinite) thin color flux-tube, the one-dimensional so-called *string*, forces the quarks to be confined. One is now interested in the time evolution of this system: Hence, one is interested in the surfaces, so-called *world-sheets*, which are defined through

[2]We discuss here the string picture which arises for the pure gauge theory. In the absence of dynamic quarks the well-known *string breaking*, which is observed on the lattice [34, 35, 36] and is subject of several models [37], does not take place. An excellent review and further going studies of the string models we refer to can be found in Ref. [38].

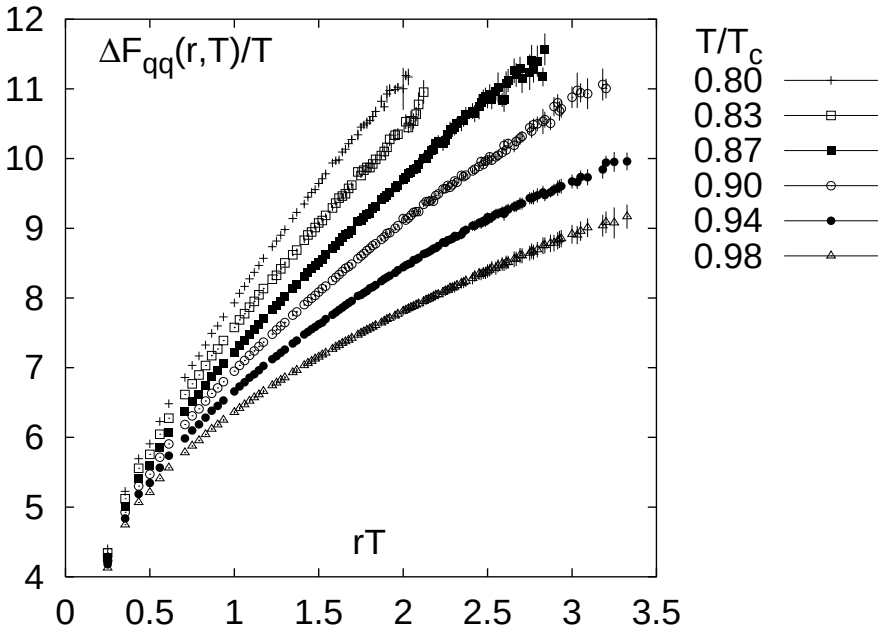

Figure 1.1: The color averaged heavy quark antiquark free energies at temperatures below the deconfinement point as a function of the distance rT. This figure shows lattice data from simulations on lattices with size $32^3 \times 4$.

the time evolution of the string [39]. In terms of heavy quark free energies, these are given by

$$e^{-\Delta F_{q\bar{q}}(r,T)/T} \simeq \langle \mathrm{Tr} L(\mathbf{x}) \mathrm{Tr} L^\dagger(\bar{\mathbf{x}}) \rangle \simeq \sum_{\text{surfaces}} e^{-S_{\text{eff}}(\text{surfaces})} \tag{1.2}$$

where S_{eff} parameterizes the surfaces which appear due to the time evolution of the fluctuating string where the Polyakov loops ($L(\mathbf{x})$, $L^\dagger(\bar{\mathbf{x}})$) describe the propagations of the static quark and antiquark. One often uses the *Nambu-Goto* action (S_{NG}) [39] in the *Gaussian approximation* (S_{NG}^{Gauss}), defined as

$$S_{\text{eff}} \to S_{NG}^{Gauss} = \sigma \int d^2\xi \; \partial_a x_t \partial_a x_t, \tag{1.3}$$

where x_t describes the transversal displacement of the string from the flat surface and σ is the string tension. It is interesting to realize that the Gaussian approximation (1.3) does assume that x_t is the *only relevant dynamic variable* and therefore this approximation of string fluctuation does describe a whole class of different string models [40, 41]. In fact, as one neglects any internal degrees of freedom of the string, *i.e.* the color structure or the space-like extent of the color flux tube, this estimate is restricted to (asymptotic) large distances where the color flux tube is allowed to be approximately described through an one-dimensional string. These models are therefore called the *asymptotic string models* [42]. Following these models, the surface fluctuations are bound to vanish at the static boundaries given by the Polyakov loops, and the boundary conditions in time and spatial

directions are respecting the bosonic properties of the gauge fields. As the Polyakov loops in (1.2) are spatially separated by a distance, $r = |\mathbf{x} - \bar{\mathbf{x}}|$, the string is called *open*. The mathematical tool needed to analyze the properties of fluctuating surfaces was established in [43, 44].

At finite temperatures, the inverse temperature, T^{-1}, is related to the time-like extent of the world sheet and thus the lowest order approximation of the world sheet by a flat surface leads to $S_{NG}^{Gauss} \simeq \sigma r T^{-1}$. This is similar to the so-called *area law* which is related to the confinement signal in the free energies [18]. The transverse displacements of the string fluctuations from the flat surface have been approximated in different limits, one is the ordinary $T \to 0$ limit [40] and another one gives the leading temperature corrections [45]. A third approximation is to increase the dimension of space-time (D) in which the string is embedded and then to calculate the string fluctuations by means of a $1/D$-expansion [46]. The first method leads to the zero temperature approximation ($T \to 0$),

$$V_{q\bar{q}}(r) = \sigma r - \frac{\pi}{12r} + \mathcal{O}(1/r^3), \tag{1.4}$$

where we have assumed that the string is placed in a $D = 4$ dimensional space-time. This is the well-known zero temperature heavy quark potential in the free (bosonic) string picture [40, 47]. As the underlying effective string action unifies a whole class of string pictures, the Coulomb factor will arise in all these asymptotic string models. However, it is a long range Coulomb-like correction to the linear term and should not be confused with the short range Coulombic perturbative term. Higher orders are indeed known to result in a series in odd powers of $1/r$ which can be resummed leading again to a close expression for $V_{q\bar{q}}(r)$ [38]. In the second case one deals with the leading T-dependent corrections in the confinement phase. The asymptotic behavior of (1.2) is then given by [45]

$$\Delta F_{q\bar{q}}(r,T) = \left(\sigma - \frac{\pi}{3}T^2\right) r + T\ln(2rT) + \mathcal{O}(rT^3) + \mathcal{O}(T^2). \tag{1.5}$$

In contrast to the Coulomb-like term $-\pi/12r$ in (1.4) a universal term appears which leads to a temperature correction of the string tension, $\sigma \to \sigma(T)$. From this expression the string tension is supposed to decrease with increasing temperatures. This property can indeed be seen from the free energies shown in Fig. 1.1. The third approximation mentioned above leads to a different temperature dependence of the string tension at temperatures close to T_c [46]. One finds $\Delta F_{q\bar{q}}(r,T) = \sigma(T) r$ with

$$\sigma(T) = \sigma\sqrt{1 - \frac{T^2}{T_c^2}} \tag{1.6}$$

and T_c is obtained as

$$T_c^2 = \frac{3}{\pi(D-2)}\sigma. \tag{1.7}$$

From the string picture it is thus expected that the string tension in the free energies will continuously vanish at some (critical) temperature T_c. This is the critical temperature where the confinement deconfinement phase transition is supposed to appear. We note,

however, that the phase transition of $SU(3)$ in $D = 4$ dimensions is of first order [48], while the transition in the string picture for $D \to \infty$ is a second order one. One thus expects deviations from (1.6) in color $SU(3)$.

Finally we note that also a general expression for the heavy quark antiquark free energies has been calculated at finite temperatures from the string picture [49]:

$$\begin{aligned} \Delta F_{q\bar{q}}(r,T) &= \left(\sigma - \frac{\pi}{3}T^2 + \frac{2}{3}T^2 \mathrm{arctan}(1/(2rT))\right) r \\ &\quad - \left(\frac{\pi}{12} - \frac{1}{6}\mathrm{arctan}(2rT)\right)\frac{1}{r} + \frac{1}{2}T\ln\left(1+(2rT)^2\right) \end{aligned} \tag{1.8}$$

It can easily be checked that this expression reproduces the limits given in (1.4) and (1.5), while it continuously changes between these two limits within increasing or decreasing r.

The predictions of the string picture have extensively been studied with MC lattice data in the past. A comparison of (1.4) with early $SU(3)$ lattice data shows a Coulomb term $\gamma = 0.25 \pm 0.02$ [50] in the Cornell potential, $V_{\mathrm{Cornell}}(r) = -\gamma/r + sr$, which is indeed quite close to $\pi/12$, while the findings of current studies enlarge this value, $\gamma \simeq 0.295$ [51]. Also the spatial extent of the strings have been investigated within different methods [52, 53]. In general one can say that these studies confirm that the field strength between the static charges in QCD is indeed quite large and the spatial extent of this kind of flux tube becomes thin when the charges get separated to large distances. In fact, recent studies of the string picture claim that at zero temperature the string behavior of heavy quark potential takes place at surprisingly small distances, $r \gtrsim 0.5$ fm [54]. At shorter distances, however, the string picture fails as the thin string approximation breaks down and, moreover, at very short distances QCD depends on a running, asymptoticly free coupling. In conclusion, at intermediate distances improved string pictures should be applied, which, for instance respect more degrees of freedoms than the asymptotic string picture does. At very short distances, however, the zero temperature quark potential is calculable perturbatively and shows the logarithmic weakening of the coupling [55].

A comparison of the string picture at finite temperature and MC studies of gauge theories has been performed in many studies. For instance, the second term in (1.5), which originates from the transverse fluctuations of the string at finite temperature, is established in the context of numerical calculations (see for instance [33]). The temperature dependence of the string tension at temperatures close to T_c has also been analyzed in detail. It is established that in color $SU(2)$, which also exhibits a second order phase transition, the string tension vanishes $\sim (1/T - 1/T_c)^\nu$ with a critical exponent ν taking its 3-D Ising value as suggested by universality [56]. In contrast to a critical behavior in $SU(2)$, in color $SU(3)$ one expects a discontinuous behavior and a non-vanishing string tension at the critical temperature as the confinement deconfinement phase transition in this case is (weakly) first order [48]. In fact, deviations from (1.6) were found at high temperatures while the presence of a logarithmic term with the predicted strength in (1.5) is well-established [33].

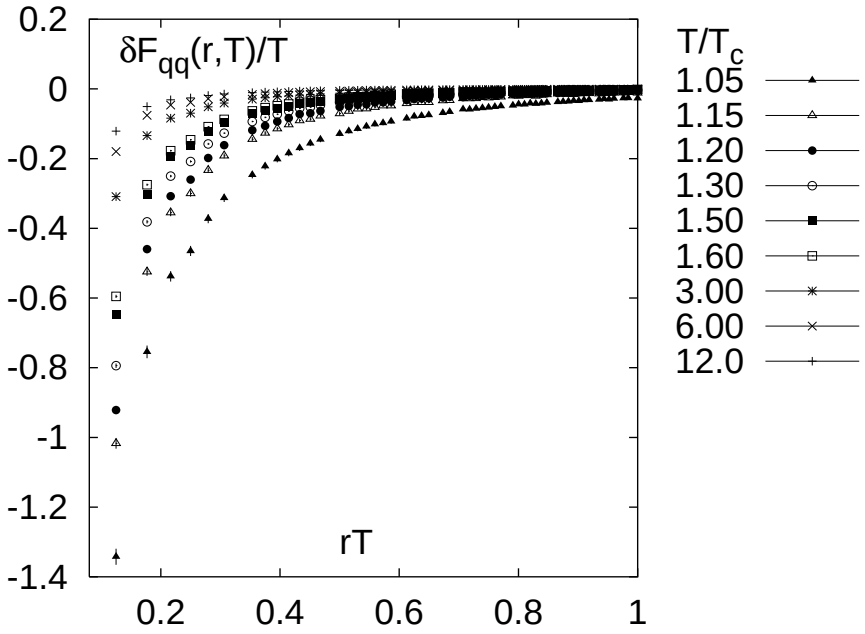

Figure 1.2: The color averaged heavy quark antiquark free energies at temperatures above the deconfinement point as functions of the distance rT. This figure shows lattice data from simulations on lattices of size $32^3 \times 8$.

Let us turn now to the thermal properties of the (color averaged) quark antiquark free energies in the deconfined medium. To get an idea of the general behavior of the free energies in this phase we show in Fig. 1.2 lattice data for the color averaged free energies at several temperatures above T_c. In general, the free energies at large distances flatten and approach some finite values. In this figure we have normalized the free energies such that they approach zero at large distances, $\delta F_{q\bar{q}}(r,T) = \Delta F_{q\bar{q}}(r,T) - \Delta F_{q\bar{q}}(r \to \infty, T)$. The flattening of the free energies is consistent with deconfinement. This suggests that the heavy quark pair can be separated from each other at large distances as the interaction of the color charges is weakening at large distances. In general the statement is that the static color charges get screened in the thermal medium which causes the flattening of the free energies. It can also be seen from that figure that the flattening of the free energies sets in at smaller distances as the temperature increases.

In fact, the deconfined medium is supposed to consist of weakly interacting quarks and gluons, $g^2(T) \to 0$. This property might result in an ordinary perturbative treatment of the free energies (in power-expansions of g^2). However, it is well-known (see for instance [18]) that perturbation theory has only a limited predictive power for the behavior of the free energies in the deconfined phase. In particular, it cannot be expected that the perturbative approach is well suited for the study of inherently non-perturbative aspects of the free energies at temperatures close to the phase transition separating the low from the high temperature plasma phase. Its range of validity is thus quite uncertain and infra-red problems appear which lead to the dynamical generation of chromo-electric and

chromo-magnetic mass scales which are of $\mathcal{O}(gT)$ and $\mathcal{O}(g^2T)$ and thus in general cannot be collected in a power series of g^2. This indeed prevents a perturbative treatment of the long distance properties of the free energies. At high temperatures, however, improvements of perturbation theory have been established (*i.e.* HTL-resummation techniques [13] or screened perturbation theory [14]) which allow to give at least reasonable estimates at length scales below $\mathcal{O}(1/gT)$. In the discussions of free energies in a deconfined medium one thus often resorts to these kind of high temperature perturbative methods.

In high temperature perturbation theory the color singlet and color octet free energies are given to leading order by one gluon exchange [57, 9]. Consequently, to this order δF_1 and δF_8 only differ by the Casimir[3]

$$\delta F_1(r,T) \;=\; -(N^2-1)\,\delta F_8(r,T) \;+\; \mathcal{O}(g^4). \tag{1.9}$$

As discussed above, at finite temperature the crucial point to respect is that the IR limit of the gluon polarization tensor ($\Pi_{00}(q)$) in general is non-zero as it is related to the Debye mass, $\Pi_{00}(q\to 0) = m_D$. In fact, from HTL-resummed lowest order perturbation theory one expects a *Debye screened Coulomb* behavior for δF_1 and δF_8 in position space. In this case, the Fourier transformation of the gluon propagator ($\sim 1/(q^2+m_D^2)$) leads to

$$\delta F_i(r,T) \;=\; C_i\frac{\alpha(T)}{r}e^{-m_D(T)r}, \tag{1.10}$$

where $C_1 = -4/3$ and $C_8 = +1/6$ for $N=3$ [57, 9]. In this relation we have introduced the coupling $\alpha(T) = g^2(T)/4\pi$ as a temperature dependent quantity. Although not in leading order, higher order contributions indeed will lead to a *running coupling* (after renormalization). In addition we have assumed that we work at such high temperatures that beside the temperature there is no other scale which could control the coupling. Therefore we use $g = g(T)$ which provides asymptotic freedom, $g^2(T)\to 0$, in the high temperature limit. Apart of the Debye mass, Eq. (1.10) does not respect any further momentum dependencies of the polarization tensor (in momentum space). It thus has been noted that this estimate of the color singlet free energy estimates only the IR limit [59]. In position space, this is the large distance regime. Consequently, at short distances and low temperatures we expect deviations from (1.10).

As noted above, because of the interaction with the heat bath the gluon acquires a chromo-electric mass, $m_e(T)$, which results from the non-zero IR limit of the polarization tensor. To lowest order in perturbation theory, this is obtained as (in $SU(N)$)

$$m_e^{(0)} \;=\; \sqrt{\frac{N}{3}}g(T)T. \tag{1.11}$$

In general, one identifies the leading order Debye mass with this chromo-electric mass, $m_D(T) = m_e^{(0)}(T)$. Note that the power in the coupling of the lowest order is reduced, $m_e^{(0)} \simeq gT$, which is the typical scale for electric screening. The electric screening mass is

[3] This relation is quite similar to the leading order relation of the color singlet (V_1) and color octet (V_8) potentials at zero temperature, $V_1 = -(N^2-1)V_8 + \mathcal{O}(g^4)$ [58]. At zero temperature, the leading order potentials in position space are given by the Fourier transformation of the gluon propagator ($\sim 1/q^2$) which leads to a Coulombic potential at this order [58].

also known in next-to-leading order in which it depends on an anticipated chromo-magnetic gluon mass although the magnetic gluon mass itself cannot be calculated perturbatively [60]. It is said to scale typically like $m_g \simeq g^2 T$, which is the non-perturbative scale recovered above.

In contrast to $\delta F_1(r,T)$ and $\delta F_8(r,T)$ the color averaged free energy to leading order perturbation theory is given by *two gluon exchange* diagrams [57, 9]. Correspondingly, at high temperatures one expects

$$\frac{\delta F_{q\bar{q}}(r,T)}{T} \;=\; -\frac{1}{16}\left(\frac{\delta F_1(r,T)}{T}\right)^2 \;\simeq\; -\frac{\alpha^2(T) e^{-2m_D(T)r}}{9(rT)^2}. \tag{1.12}$$

One can easily check that this relation follows also from the high temperature expansion of the exponentials in (1.1) by using the relation given in (1.9). In fact, the leading order term, which could behave like $1/r$, drops out in the color averaged free energies [57]. The validity of (1.12) is limited in the same way as (1.10). However, to justify the high temperature expansion of the exponential functions in (1.1), relation (1.12) is limited to small values of $\delta F_1/T$ and $\delta F_8/T$, which means large distances r and high temperatures. Nonetheless, also at quite large distances perturbation theory is known to break down as the spatial 3 dimensional confinement is entering at length scales $1/g^2T$. In fact, due to the spatial confinement the long distance behavior of any spatial correlation function is expected to be dominated by the exchange of some bound state of the effective three dimensional theory [61, 62]. Thus one would expect that the large distance behavior of the color averaged free energies is also described by a simple color screened Coulomb form. In practice, however, the relative strength of the perturbative $\sim 1/r^2$ and the non-perturbative $\sim 1/r$ contribution is not known and it is thus not clear at which distance the non-perturbative $1/r$-term will dominate the free energies.

Several MC studies have shown that non-perturbative phenomena prevail up to temperatures at least several times the critical temperature [63, 64, 65, 66]. In terms of the color averaged free energies non-perturbative effects have been studied in detail with MC methods at finite temperatures in the case of $SU(3)$ [33, 67] and in the case of $SU(2)$ [68, 23, 69, 70]. In particular, deviations from the perturbative $1/r^2$ behavior of the color averaged free energies have been found in color $SU(2)$ and color $SU(3)$ at intermediate distances, *i.e.* $1/4 \lesssim rT \lesssim 4$ [67, 33, 70]. They show that the r-dependence of these free energies can be well parameterized with the ansatz

$$\frac{\delta F_{q\bar{q}}(r,T)}{T} \;=\; -\frac{a}{r^d} e^{-mr} \tag{1.13}$$

with an arbitrary power-behavior d. The general statement is that at these distances and sufficiently large temperatures ($T \gtrsim 2T_c$) $d \to 2$ is approximately fulfilled while at temperatures close to T_c deviations are significant so that in general $d \lesssim 2$. In particular, it can be excluded that the 2-gluon exchange with an effective chromo-electric mass is the dominant screening mechanism [33]. This might not be too surprising as various non-perturbative modes may play a role in the long distance sector of the quark gluon plasma [71, 72]. It is thus important to quantify the color screening effects by a genuinely non-perturbative approach. By means of the exponential decrease of the color averaged

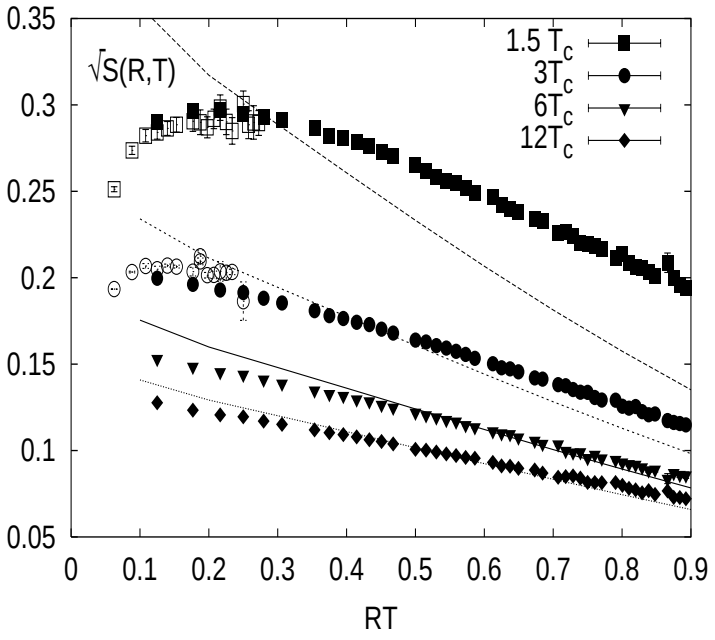

Figure 1.3: The screening functions in color $SU(3)$ in terms of $\sqrt{S_{q\bar{q}}(r,T)}$ from lattices of size $32^3 \times 8$ (filled symbols) and $32^3 \times 16$ (open symbols) at several temperatures above T_c. We also compare in this figure the HTL-like resummed perturbative calculation of the color averaged free energies to the lattice data (lines).

free energies the screening mass for color $SU(3)$ has been discussed in [33]. They note that the screening mass scales with the temperature like $m_D \simeq 2.5T$, thus a perturbative decrease due to the temperature dependent renormalized coupling $g(T)$ is not seen at least up to temperatures a few times the critical one, $T \lesssim 2T_c$. They conclude that it is very likely that non-perturbative phenomena and higher order perturbative contributions are needed to explain the screening behavior. Results on the color singlet and color octet (triplet) free energies defined in Landau gauge are reported for $SU(3)$ in [67] and in a gauge independent manner for $SU(2)$ in [23]. A recent related discussion of the free energies in the case of $SU(2)$ can be found in [69]. They also investigate the non-perturbative color screening masses from the color singlet free energies at temperatures close to T_c, *i.e.* $T \lesssim 3T_c$. They agree with the general findings discussed above.

The color averaged free energies have also been discussed in full 1-loop HTL-like resummed perturbation theory (see for instance our analysis in Ref. [73]). In Fig. 1.3 we compare our perturbative calculations to $SU(3)$ lattice data for the color averaged free energies at several temperatures in the deconfined phase. Details on our computations are summarized in Appendix B. In order to provide a detailed analysis of the quark antiquark free energy we refer in that figure to the dimension-less quantity defined as

$$S_{q\bar{q}}(r,T) \quad = \quad -9 \left[\frac{1}{rT}\right]^{-2} \times \frac{\delta F_{q\bar{q}}(r,T)}{T}. \tag{1.14}$$

This so-called *screening function* $S_{q\bar{q}}(r,T)$ [74] is defined in the spirit of high temperature leading order perturbation theory and hence should show the exponential fall-off due to color screening (hence its name) at large distances. It can be seen that our perturbative calculation does not fit the lattice data at $T \lesssim 3T_c$. This break-down of perturbation theory is not too surprising as the coupling at such small temperatures is presumably still large and inherent non-perturbative effects at temperatures close to T_c are well-known to enter the free energies [33]. At higher temperatures, however, the validity of perturbation theory is much improved at these distances.

At small distances the lattice data for $\sqrt{S_{q\bar{q}}(r,T)}$ in Fig. 1.3 show a weakening which is not expected from high temperature perturbation theory. We will see in the analysis performed in this chapter (and see also chapter 2) that this weakening of the screening function at short distances is caused by two effects. First of all it results from a weakening of the power-like behavior of the free energies at short distances, *i.e.* $\delta F_{q\bar{q}} \simeq -1/r^2 \to -1/r$. This reduction in the power behavior presumably suggests that at short distances the color averaged free energies are dominated by some effective one gluon exchange. Another reason for a decrease of the screening function is that Coulomb part of the the finite temperature free energies is dominated by vacuum physics at small distances, *i.e.* the running of the coupling, $g^2(r)$. The latter effect also means a *conceptual barrier* for a description of free energies in high temperature ($g^2(T) \to 0$) perturbation theory at such small distances. This is indeed expected from the separation of length scales at finite temperature discussed with (1).

In the following section we introduce the heavy quark free energies and their relation to the Polyakov loop and its correlation functions with more rigor. We follow here closely the analysis of Refs. [9, 23] as we pay attention to the formulations of the color singlet and color octet free energies in a genuinely gauge independent manner.

1.2 The Polyakov loop and its correlation functions

As we will be interested in the lattice formulation of the pure gauge theory at finite temperature in thermal equilibrium, we consider the *Euclidean* path integral throughout this thesis. In this case, the grand canonical partition function $Z(T,V)$ is basically given as an integral over the gluon fields A_μ,

$$Z(T,V) \;=\; \int \mathcal{D}A_\mu e^{-S_E[A_\mu]}, \tag{1.15}$$

where T denotes the temperature and V the finite volume. Both, the temperature and the volume, can be defined in the equilibrium as integration boundaries of the Euclidean Lagrangian $\mathcal{L}_E$ which gives the gauge action S_E,

$$S_E[A_\mu] \;=\; \int_0^{1/T} dx_0 \int_V d^3\mathbf{x}\; \mathcal{L}_E[A_\mu] = \frac{1}{2}\int_0^{1/T} dx_0 \int_V d^3\mathbf{x}\; \mathrm{Tr} F_{\mu\nu}(x)F_{\mu\nu}(x), \tag{1.16}$$

where $F_{\mu\nu}(x)$ is the usual field strength tensor of the $SU(N)$ gauge theory,

$$F_{\mu\nu} \;=\; \partial_\mu A_\nu - \partial_\nu A_\mu - ig[A_\mu, A_\nu]\;, \tag{1.17}$$

and $x = (x_0, \mathbf{x})$. The theory defined through (1.16) is quantized in terms of the path integral defining the partition function (1.15). For instance, any observable will be expressed through the expectation value of the corresponding *operator*, $\langle\hat{\mathcal{O}}\rangle$, which in the path integral formalism is calculated from its *classical* counter part, $\mathcal{O}$,

$$\langle\hat{\mathcal{O}}\rangle \;=\; \frac{1}{Z(T,V)}\int \mathcal{D}A_\mu\;\mathcal{O}\;e^{-S_E[A_\mu]}. \tag{1.18}$$

As in general the quantity $\langle\hat{\mathcal{O}}\rangle$ contains infinities, this quantity is related to the physical observable only up to renormalization. All thermodynamic information about the system can be deduced from the partition function (1.15), once it is known properly. A review on this topic in thermal QCD can be found in [19]. A general overview on finite temperature field theory is provided in textbooks (see for instance [11, 12]).

1.2.1 Polyakov loop and heavy quark free energy

We are now interested in the free energy of *one*[4] static quark placed into the gluonic heat bath. Following Ref. [9], this can be formulated in terms of the *thermal Wilson line* $L(\mathbf{x})$, the so-called Polyakov loop defined in [76],

$$\mathrm{Tr}L(\mathbf{x}) \;=\; \mathrm{Tr}\mathcal{T}\exp\left(i\int_0^\beta dx_0\lambda\cdot\mathbf{A}_0(x_0,\mathbf{x})\right), \tag{1.19}$$

which describes the propagation of the static quark along the time direction. In this relation the trace is normalized such that $\mathrm{Tr}\mathbb{1} = 1$. The expectation value of the thermal Wilson line is related to the *difference in free energy*, ΔF_q, due to the presence of a static quark in the gluonic heat bath, via

$$e^{-\beta\Delta F_q(\mathbf{x})} \;\simeq\; \langle\mathrm{Tr}L(\mathbf{x})\rangle. \tag{1.20}$$

Note that this relation is correct only up to renormalization. Some notes are in order: First we note that we define the *Polyakov loop* as the trace of the thermal Wilson line [77]. Thus, the Polyakov loop $\mathrm{Tr}L(\mathbf{x})$, is a gauge invariant quantity. Secondly, offhand, the Polyakov loop is an element of $SU(N)$ and is therefore *complex*. Moreover, the pure gauge theory has a global $Z(N)$ symmetry, where $Z(N)$ is the center of the group of $SU(N)$. The elements of the center of $SU(N)$ are given by the matrices

$$\exp(i\phi)\,\mathbb{1} \quad \text{where} \quad \phi = \frac{2\pi k}{N} \quad \text{and} \;\; k = 0, 1, ..., (N-1), \tag{1.21}$$

[4] As we are interested in this section in the Polyakov loop expectation value and not in its correlation functions, we examine here the case of one single test quark. The existence of a single test color charge in the gluonic heat bath is complicated as the Polyakov loop expectation value will vanish. We will not elaborate here any further on as we will define the Polyakov loop expectation value from the large distance properties of the 2-point correlation functions. In fact, the rather formal problems with single color charges drop out in this way. The general case with n quarks and $\bar{n}$ antiquarks is given in Ref. [9]. It should be noted, however, that this discussion is complicated through the problem of *triality* [9, 75].

which are complex for $N > 2$. Under such a transformation the Polyakov loop transforms like $\mathrm{Tr}L \to e^{i\phi}\mathrm{Tr}L$. It follows that the Polyakov loop expectation value is N-fold degenerate,

$$\langle \mathrm{Tr}L \rangle \;=\; \exp\left(i\frac{2\pi k}{N}\right)\; |\langle \mathrm{Tr}L \rangle|, \tag{1.22}$$

where in pure gauge theory each of these degenerate vacua is equivalent. In conclusion, the value of the Polyakov loop, $\mathrm{Tr}L$, is a complex number for $N > 2$ and its expectation value given in Eq. (1.20) vanishes. This situation changes much, however, in full QCD, for instance in the presence of massive quarks. In this case, the only stable vacuum is that for which $\langle \mathrm{Tr}L \rangle$ is *real* ($k = 0$). Another property of the Polyakov loop expectation value is the following one: Confinement implies a vanishing Polyakov loop expectation value, $|\langle \mathrm{Tr}L \rangle| = 0$ [76]. On the other hand, in the deconfinement phase one expects $|\langle \mathrm{Tr}L \rangle| \neq 0$ and moreover, a weak coupling will lead to $|\langle \mathrm{Tr}L \rangle| = 1$, which is supposed to be its high temperature limit. Therefore, $\langle \mathrm{Tr}L \rangle$ is said to be an order parameter for the confinement deconfinement phase transition, quite similar to the magnetization in a Z_N spin system. Thus, if $|\langle \mathrm{Tr}L \rangle|$ turns on continuously at T_c the transition is of second order. If it will behave discontinuously at T_c it indicates a first order phase transition. It is supposed, that the phase transition in $SU(3)$ is of first (or weakly first) order [48], while the transition in $SU(2)$ is a second order one [56].

1.2.2 Polyakov loop correlation functions

We are interested in the state of n static quarks at spatial positions $\mathbf{x}_1, \mathbf{x}_2, ..., \mathbf{x}_n$ and a number $\bar{n}$ of their charge conjugate partners, static antiquarks at positions $\bar{\mathbf{x}}_1, \bar{\mathbf{x}}_2, ..., \bar{\mathbf{x}}_{\bar{n}}$. In general, the heavy quark free energy $F_{nq,\bar{n}\bar{q}}$ is defined as the logarithm of the partition function $Z_{nq,\bar{n}\bar{q}}$ of the thermal (gluonic) system containing n static color sources and $\bar{n}$ static anti-color sources,

$$\begin{aligned} Z_{nq,\bar{n}\bar{q}}(V,T,\mathbf{x}_1,...,\mathbf{x}_n,\bar{\mathbf{x}}_1,...,\bar{\mathbf{x}}_{\bar{n}}) &\equiv \exp\left(-\frac{F_{nq,\bar{n}\bar{q}}(V,T,\mathbf{x}_1,...,\mathbf{x}_n,\bar{\mathbf{x}}_1,...,\bar{\mathbf{x}}_{\bar{n}})}{T}\right) \\ &= \int \mathcal{D}A_\mu e^{-S_E[A_\mu]} \prod_{i=1}^{n} \mathrm{Tr}L(\mathbf{x}_i) \prod_{i=1}^{\bar{n}} \mathrm{Tr}L^\dagger(\bar{\mathbf{x}}_i), \end{aligned} \tag{1.23}$$

where the trace is normalized such that $\mathrm{Tr}\mathbb{1} = 1$. The corresponding expectation value of the product of Polyakov loops is related to the difference in free energy due to the presence of static $q(\bar{q})$-sources in the gluonic thermal heat bath [9]:

$$\begin{aligned} \left\langle \prod_{i=1}^{n} \mathrm{Tr}L(\mathbf{x}_i) \prod_{i=1}^{\bar{n}} \mathrm{Tr}L^\dagger(\bar{\mathbf{x}}_i) \right\rangle &= \frac{Z_{nq,\bar{n}\bar{q}}(V,T,\mathbf{x}_1,...,\mathbf{x}_n,\bar{\mathbf{x}}_1,...,\bar{\mathbf{x}}_{\bar{n}})}{Z(V,T)} \\ &= \exp\left(\frac{-\Delta F_{nq,\bar{n}\bar{q}}(V,T,\mathbf{x}_1,...,\mathbf{x}_n,\bar{\mathbf{x}}_1,...,\bar{\mathbf{x}}_{\bar{n}})}{T}\right), \end{aligned}$$

where

$$\Delta F_{nq,\bar{n}\bar{q}}(V,T,\mathbf{x}_1,...,\mathbf{x}_n,\bar{\mathbf{x}}_1,...,\bar{\mathbf{x}}_{\bar{n}}) \equiv F_{nq,\bar{n}\bar{q}}(V,T,\mathbf{x}_1,...,\mathbf{x}_n,\bar{\mathbf{x}}_1,...,\bar{\mathbf{x}}_{\bar{n}}) - F(V,T). \tag{1.24}$$

In this relation $Z(V,T) = \exp(-F(V,T)/T)$ is the partition function of the pure $SU(N)$ gauge theory introduced in (1.15). The free energies described above consist of a contribution from the (internal) energy $\Delta E_{nq,\bar{n}\bar{q}}$ and of a contribution from the entropy $\Delta S_{nq,\bar{n}\bar{q}}$. In general the statement is $\Delta F_{nq,\bar{n}\bar{q}} = \Delta E_{nq,\bar{n}\bar{q}} - T\Delta S_{nq,\bar{n}\bar{q}}$, where

$$\begin{aligned}\Delta E_{nq,\bar{n}\bar{q}}(V,T,\mathbf{x}_1,...,\mathbf{x}_n,\bar{\mathbf{x}}_1,...,\bar{\mathbf{x}}_{\bar{n}}) &\equiv E_{nq,\bar{n}\bar{q}}(V,T,\mathbf{x}_1,...,\mathbf{x}_n,\bar{\mathbf{x}}_1,...,\bar{\mathbf{x}}_{\bar{n}}) - E(V,T),\\ \Delta S_{nq,\bar{n}\bar{q}}(V,T,\mathbf{x}_1,...,\mathbf{x}_n,\bar{\mathbf{x}}_1,...,\bar{\mathbf{x}}_{\bar{n}}) &\equiv S_{nq,\bar{n}\bar{q}}(V,T,\mathbf{x}_1,...,\mathbf{x}_n,\bar{\mathbf{x}}_1,...,\bar{\mathbf{x}}_{\bar{n}}) - S(V,T). \quad (1.25)\end{aligned}$$

In this relations we consider the quantities $E(V,T)$ and $S(V,T)$ with respect to the free energy $F(V,T)$,

$$F(V,T) \;=\; E(V,T) - TS(V,T). \quad (1.26)$$

In particular, we will consider in our discussion the 2-point Polyakov loop correlation functions ($n = \bar{n} = 1$) and the Polyakov loop expectation value $\langle \mathrm{Tr}L\rangle$. A convenient starting-point for a discussion of these quantities is to consider the correlation function of the Polyakov loop, $G(r,T)$, and the correlation function of the (untraced) Polyakov loop, $H(r,T)$, where the latter one is a gauge dependent quantity:

$$\begin{aligned}G(r,T) &= \left\langle \mathrm{Tr}L(\mathbf{x}_1)\mathrm{Tr}L^\dagger(\bar{\mathbf{x}}_1)\right\rangle \quad (1.27)\\ H(r,T) &= \left\langle L(\mathbf{x}_1)L^\dagger(\bar{\mathbf{x}}_1)\right\rangle, \qquad r \equiv |\mathbf{x}_1 - \bar{\mathbf{x}}_1|. \quad (1.28)\end{aligned}$$

The Polyakov loop expectation value $\langle \mathrm{Tr}L\rangle$ is defined through the disconnected part of the correlation function $G(r,T)$. Since the r-dependence of a correlation function of operators is controlled through the connected parts, which vanish if the distance between the operators becomes large, it is possible to define the Polyakov loop expectation value through the large distance behavior of n-point Polyakov loop correlation functions. We define $\langle \mathrm{Tr}L\rangle$ through the large distance behavior of $G(r,T)$,

$$|\langle \mathrm{Tr}L\rangle| = \lim_{r\to\infty} \left(G(r,T)\right)^{1/2}. \quad (1.29)$$

In this way $|\langle \mathrm{Tr}L\rangle| \in \mathbb{R}$ can be related to the free energy $\Delta F_q \in \mathbb{R}$ of a single test quark. The decomposition of the 2-point Polyakov loop correlation function of the traced Polyakov loops in Eq. (1.27) in the (color) singlet and the adjoint ($\sim$ color octet for $N \equiv 3$) representation is expressed in terms of projection operators P_1 and P_{N^2-1} defined as

$$\begin{aligned}P_1 &= \frac{1}{N^2}\mathbb{1}\otimes\mathbb{1} - \frac{2}{N}\bar{T}^a \otimes T^a,\\ P_{N^2-1} &= \frac{N^2-1}{N^2}\mathbb{1}\otimes\mathbb{1} + \frac{2}{N}\bar{T}^a \otimes T^a, \quad (1.30)\end{aligned}$$

where T^a ($a = 1,...,(N^2-1)$) denote the generators of the gauge group $SU(N)$ [58, 57]. The color singlet ($\Delta F_1(r,T)$) and the color adjoint ($\Delta F_{N^2-1}(r,T)$) quark antiquark free energies are defined in terms of the projection operators applied to the correlation function of the untraced Polyakov loop $H(r,T)$, which leads to (see [23])

$$\exp\left(-\frac{\Delta F_1(r,T)}{T}\right) = \frac{\mathrm{Tr}(P_1 H(r,T))}{\mathrm{Tr}P_1} = \left\langle \mathrm{Tr}L^\dagger(\bar{\mathbf{x}}_1)L(\mathbf{x}_1)\right\rangle \quad (1.31)$$

and

$$\exp\left(-\frac{\Delta F_{N^2-1}(r,T)}{T}\right) = \frac{\mathrm{Tr}(P_{N^2-1}H(r,T))}{\mathrm{Tr}P_{N^2-1}}$$
$$= \frac{N^2}{N^2-1}\left\langle \mathrm{Tr}L^\dagger(\bar{\mathbf{x}}_1)\mathrm{Tr}L(\mathbf{x}_1)\right\rangle - \frac{1}{(N^2-1)}\left\langle \mathrm{Tr}L^\dagger(\bar{\mathbf{x}}_1)L(\mathbf{x}_1)\right\rangle . \qquad (1.32)$$

As it stands, the color singlet and color adjoint free energies defined in (1.31) and (1.32) are gauge dependent quantities. In order to determine ΔF_1 and ΔF_{N^2-1} properly one has to fix the gauge. However, it has recently been shown [23], that a gauge independent definition of the color singlet and color adjoint free energies can be achieved in terms of dressed Polyakov lines, $\tilde{L}(\mathbf{x}) = \Omega^\dagger(x_0,\mathbf{x})L(\mathbf{x})\Omega(x_0,\mathbf{x})$ with $\Omega \in SU(N)$, and that such a definition coincides with (1.31) and (1.32) in Coulomb gauge. In general the statement is that one has to fix a gauge which is local in time and leads to a positive transfer matrix[5].

According to the decompositions given above, the 2-point correlation function of the traced Polyakov loop, $G(r,T)$ in (1.27), is related to the color singlet and color adjoint free energy through [9]

$$\begin{aligned} G(r,T) &= \frac{1}{N^2}\left(e^{-\Delta F_1(r,T)/T} + (N^2-1)e^{-\Delta F_{N^2-1}(r,T)/T}\right) \\ &= \exp\left(-\frac{\Delta F_{q\bar{q}}(r,T)}{T}\right) \end{aligned} \qquad (1.33)$$

which defines $\Delta F_{q\bar{q}}(r,T)$. According to the statistically weighted decomposition of $G(r,T)$ into the color singlet and color octet free energy, $\Delta F_{q\bar{q}}(r,T)$ is referred to as the color averaged free energy.

1.2.3 Lattice formulation of the $q\bar{q}$-free energy and lattice artifacts

The path integral appearing in Eq. (1.15) is regularized by introducing a four dimensional space-time lattice of size $N_\sigma^3 \times N_\tau$ with a lattice spacing a. The volume and the temperature introduced in (1.16) are then related to the number of lattice points in the space (N_σ) and in the time (N_τ) directions, respectively,

$$V = (N_\sigma a)^3 \quad , \quad T = (N_\tau a)^{-1} . \qquad (1.34)$$

Enforced by the requirement of gauge invariance one introduces *link variables* $U_\mu(x)$ which are associated with the link between two neighboring sites of the lattice and describe the parallel transport of the field A_μ from the site x to the neighboring site in the $\hat{\mu}$ direction, $x + \hat{\mu}a$,

$$U_\mu(x) = \mathcal{T}\ \exp\left(ig\int_x^{x+\hat{\mu}a} dx_\mu A_\mu(x)\right). \qquad (1.35)$$

[5]It has recently been shown with numerical lattice data that modifications appear in the color octet and singlet free energies when using different gauges which are local in time [78]. They conclude that this may indicate that the statement made in Ref. [23], *i.e.* that one can fix to *any* local-in-time gauge, is too strong. As it is, however, explicitly shown that the results in Coulomb gauge fixed by us coincide with the gauge independent definition of the singlet and octet free energies, this statement does not affect our analysis.

The link variables $U_\mu(x)$ are thus elements of the $SU(N)$ color group. We will not elaborate here any further on details of the lattice formulation as it is described in textbooks and review articles [18, 19].

The straightforward formulation of the Polyakov loop in (1.19) on a lattice with periodic boundary conditions in time direction is

$$\mathrm{Tr}L(\mathbf{x}) \;=\; \mathrm{Tr}\prod_{x_0=0}^{N_\tau-1} U_0(x_0,\mathbf{x}), \tag{1.36}$$

where $U_0(x_0,\mathbf{x}) \in SU(N)$ denotes the gauge link variable on the lattice in time direction with respect to (1.35). Inserting (1.36) in Eqs. (1.33), (1.31) and (1.32) we calculate the color averaged, the color singlet and color octet ($N \equiv 3$ in our calculations) heavy quark antiquark free energy on the lattice. As discussed above, we need to fix the Coulomb gauge. On the lattice, this can be done by maximizing

$$\mathrm{ReTr}\sum_{\mu=1,2,3}\Big(U_\mu(x_0,\mathbf{x}) + U_\mu^\dagger(x_0,\mathbf{x}+\hat{\mu})\Big), \tag{1.37}$$

which is local in time. In fact, the equivalence of maximizing this quantity and fixing the Coulomb gauge ($\partial_i A_i = 0$) is explicitly shown [23]. Finally we note that

$$\Delta F_i(r,T) = F_i(r,T) - F(T) \tag{1.38}$$

for $i = 1, 8, q\bar{q}$, where $F(T)$ is defined through (1.26) and we have assumed the infinite volume limit.

For our study of the short distance properties of the 2-point Polyakov loop correlation functions we also use lattice calculations at off-axis separations on the lattice. At short distances these calculations suffer from violations of rotational symmetry although a tree level improved lattice gauge action will be used by us. At short distances deviations from the continuum remain also in the on-axis data. In order to correct for these violations we used the lattice Coulomb potential to redefine the distances ($r \to r_I$) as suggested in [55]: We replace $F_i(r,T)$ with $F_i(r_I,T)$ for $i = 1, 8, q\bar{q}$ where

$$1/r_I = 4\pi\int_{-\pi}^{+\pi}\frac{d^3k}{(2\pi)^3}\exp(i\mathbf{kr})D_{00}^{(0)}(k) \tag{1.39}$$

denotes the lattice Coulomb term. For our improved action, $D_{00}^{(0)}(k)$ denotes the tree level gluon propagator on the lattice [79, 80]:

$$D_{00}^{(0)}(k) \;=\; \left(\sum_{i=1,2,3}\sin^2(k_i/2) + \frac{1}{3}\sin^4(k_i/2)\right)^{-1}. \tag{1.40}$$

As an example we show in Fig. 1.4 the short distance lattice data of the color singlet quark antiquark free energy $\delta F_1(r,T) \equiv \Delta F_1(r,T) - \Delta F_1(r\to\infty,T)$ at $T/T_c = 1.5$ calculated with the tree level improved Symanzik gauge action using the lattice distances $a\sqrt{n}$ ($n = 1, 2, 3, ...$) (in units of the string tension) and with the improvement through

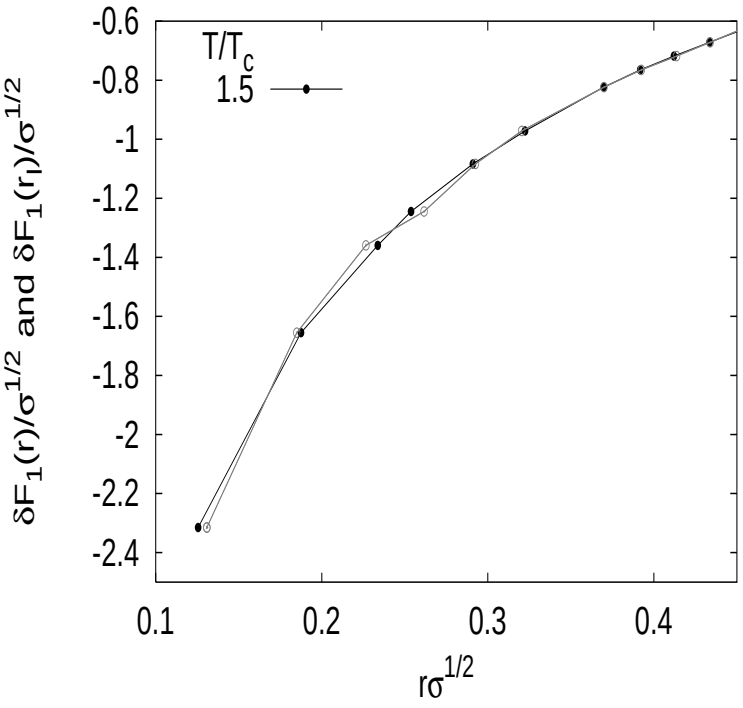

Figure 1.4: The color singlet free energy $\delta F_1(r,T) \equiv \Delta F_1(r,T) - \Delta F_1(r \to \infty, T)$ compared to $\delta F_1(r_I, T)$ at fixed temperature $T/T_c = 1.5$. The black filled data points refer to the improved distance r_I while the grey open symbols show the bare lattice distance in units of the string tension $\sqrt{\sigma}$. This figure shows the results of our calculation for small quark antiquark separations, which in units of the lattice spacing a are defined at $a\sqrt{n}$ with $n = 1, 2, ...$

the lattice Coulomb potential, respectively. The open circles show the free energy as a function of r and the closed symbols show results corrected with r_I. Following Ref. [55], the data of $\delta F_1(r_I, T)$ are supposed to show less lattice artifacts than $\delta F_1(r, T)$ at short distances. In fact, although we have used a tree level improved action, at short distances $\delta F_1(r, T)$ shows deviations from a smooth curve, while $\delta F_1(r_I, T)$ seems to correct for these deviations, as the closed symbols rather look like 'interpolating' between $\delta F_1(r, T)$, while at distances $a\sqrt{n}$ and $n \gtrsim 6$ the corrections become less important as the improved lattice gauge action shows a better behavior with respect to rotations. Similar results have been obtained by us at all temperatures.

In our discussions of the free energies we are also interested in the derivatives of the free energy with respect to distance, r, which at short distances is sensible to lattice artifacts. In order to avoid any fit to the quite complex structure of the free energies at short distances we want to perform the differentiation using directly the lattice data. For instance, we calculate

$$D_{on}(\tilde{r}, T) = \frac{\Delta F_1(r_I[(n+1)a], T) - \Delta F_1(r_I[na], T)}{r_I[(n+1)a] - r_I[na]}\ , n = 1, 2, 3, ..., \tag{1.41}$$

where $\tilde{r} = r_I[na + a/2]$. When replacing r with r_I the quantity $\tilde{r}^2 D_{on}(\tilde{r}, T)$ is known to

reproduce the continuum limit up to $\mathcal{O}(a^4)$ corrections [79]. This method has successfully been applied at distances $r \gtrsim 2a$ [55]. However, as we are interested in the properties of the free energy at quite short distances it is convenient to include also off-axis data since at short distances the free energies change a lot as function of the separation of the color sources. In fact, this allows us to analyze the lattice data at shorter distances than $r_I[a(2+1/2)]$. For instance, the shortest distance resolved by us in terms of derivatives is $\tilde{r} = r_I[a(1+1/\sqrt{2})]$.

In this thesis we are interested in an analysis of the different thermal properties of the Polyakov loop and its correlation functions in color $SU(3)$. In our numerical calculations we use a tree level Symanzik-improved gauge action on the lattice consisting of 1×1 and 2×1 loops. This construction of the gauge action on the lattice is known to correct for the leading ultra-violet cut-off effects and improves the approach to the continuum limit [79, 81]. In the Polyakov loop correlation functions this influences in particular the regime of short quark antiquark separations, as the rotational symmetry gets improved at distances which become comparable to the lattice spacing a, $r \sim \mathcal{O}(a)$. We have calculated the color singlet, color octet and color averaged free energies with the methods described above using lattices of size $32^3 \times N_\tau$ with $N_\tau = 4, 8$ and 16. In parts of our analysis we also used lattices of size $48^3 \times 4$ and $64^3 \times 4$. This allows us to discuss the free energies from large ($rT \gg 1$) to quite small ($rT \ll 1$) distances. In fact, the smallest distance which can be resolved on the lattice is given by $rT = 1/N_\tau$ while the largest distance is limited through $rT = N_\sigma/(2N_\tau)$. We have calculated the free energies for temperatures close to the deconfinement point in both phases up to temperatures about $12T_c$. We thus mainly discuss here the thermal modifications of the free energies in the deconfined medium.

The rest of this chapter is organized as follows: We begin with our analysis of the free energies at temperatures above T_c. We study the thermal properties of the color singlet and color octet free energies in detail at small, intermediate and large distances. For instance we extract the chromo-electric screening masses from the color singlet free energies up to temperatures of about $12T_c$ and compare our results to leading order perturbation theory. We also investigate the r-running of the finite temperature coupling extracted from the free energies. Finally we discuss our lattice results for the free energies at temperatures below T_c.

We should note here that earlier studies of the color singlet and octet free energies performed by us were based on the *cyclic Wilson loop* [73, 82]. The cyclic Wilson loop is a gauge independent operator and is suggested [57] to give the color singlet free energies at small distances. Throughout this thesis we will, however, present and discuss only lattice data for the free energies calculated from (1.31) and (1.32) in Coulomb gauge as these data yield the color singlet and octet free energies in a gauge independent manner at all distances.

1.3 Further analysis of the quark antiquark free energies at high temperature

For the study of the color singlet and octet free energies in the deconfinement phase we follow here the conceptual approach we have used for the color averaged free energies. We normalize the free energies such that they vanish at large distances by means of subtracting the disconnected part from the correlation functions, for instance

$$\frac{\delta F_1(r,T)}{T} \equiv -\ln \frac{\langle \mathrm{Tr} L(\mathbf{x}) L^\dagger(\bar{\mathbf{x}})\rangle}{|\langle L\rangle|^2}\,, \qquad |\mathbf{x}-\bar{\mathbf{x}}| = r\,, \tag{1.42}$$

and similarly we define $\delta F_8(r,T)$. This normalization, however, leads to a strong temperature dependence in the free energies at short distances. Although this normalization is physically unmotivated as one would expect zero temperature vacuum physics at small distances, this normalization allows to study relations from high temperature perturbation theory and also screening effects become transparent when using this normalization.

1.3.1 Short versus long distances

We will first discuss the cross-over from the short distance Coulomb-like behavior of the color singlet free energies to the color screened long distance behavior. It is indeed convenient to do this in terms of color singlet free energies as they have the advantage that perturbative calculations at small distances, $rT \ll 1$, which are supposed to be valid for $g^2(r) \ll 1$, as well as at large distances, $rT \gg 1$, which are supposed to be valid at high temperatures where $g^2(T) \ll 1$, are both dominated by one gluon exchange diagrams [58, 24]:

$$\delta F_1(r,T) \simeq -\frac{g^2(r)}{3\pi r} \qquad \text{for } rT \ll 1 \tag{1.43}$$

while

$$\delta F_1(r,T) \simeq -\frac{g^2(T)}{3\pi r} e^{-\mu(T) r} \qquad \text{for } rT \gg 1. \tag{1.44}$$

Motivated by these asymptotic forms we introduce the screening functions, $S_1(r,T)$, for the color singlet free energies as

$$S_1(r,T) = -\frac{3}{4}\left[\frac{1}{rT}\right]^{-1} \times \frac{\delta F_1(r,T)}{T}. \tag{1.45}$$

In the spirit of perturbation theory this quantity is supposed to be related to the coupling $g^2(r,T)$ while at large distances it carries information about color screening (hence its name) and is thus supposed to drop exponentially. At very short distances, however, one would expect that the screening functions recover the properties of vacuum physics in terms of a logarithmic weakening of the coupling $g^2(r)$. Consequently we expect that $S_1(r,T)$ will exhibit a maximum at some intermediate distance which we can identify as the point separating the short distance regime from the long distance regime.

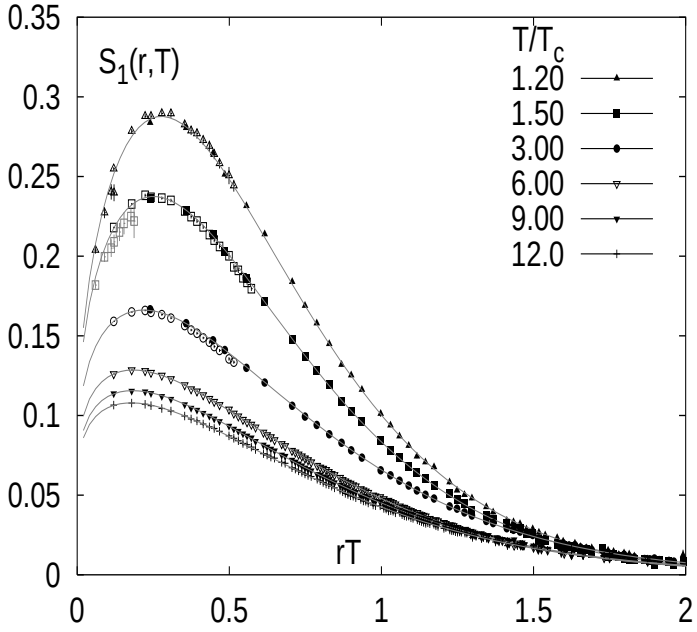

Figure 1.5: Lattice results for the color singlet free energies at temperatures above T_c. In this figure we have normalized the free energies such that they approach zero at large distances. The screening function we show here in terms of the color singlet free energies is defined in (1.45). We summarize in this figure lattice data from simulations on lattices of size $32^3 \times 4, 8$ and 16. The grey lines which match the lattice data correspond to fits with respect to an r- and T-dependent coupling. These fits are discussed in Sec. 1.3.3.

In Fig. 1.5 we show lattice results for the color singlet free energies at several temperatures in the deconfined phase in terms of the screening functions, $S_1(r,T)$. The expected features discussed above are clearly seen in this figure. At temperatures below $3.0T_c$ a clear maximum is visible in the screening functions. At higher temperatures the tendency to develop a maximum is also apparent. However, in those cases our simulations could not be performed at sufficiently small distances to demonstrate this property clearly. We find that the maximum occurs at $rT \simeq 0.3$ at a temperature about $1.2T_c$, corresponding to $r \simeq 0.2$ fm, and slowly shifts to smaller values at higher temperatures. Beyond this scale $S_1(r,T)$ drops rapidly and thus exhibits screening. We note, however, that the screening function takes on a proper exponential form only for distances $rT \gtrsim 1$. This property can clearly be seen when plotting the screening functions on a logarithmic scale.

In Fig. 1.6 we show our lattice results for the color octet free energies at several temperatures above the deconfinement point. Similarly to the data for the color singlet free energies we have subtracted from these free energies the disconnected part of the correlation functions. It can be seen from that figure that the color octet free energies behave indeed repulsive at small distances. In general, to leading order high temperature perturbation theory the color octet free energies are given similarly to the singlet free energies by

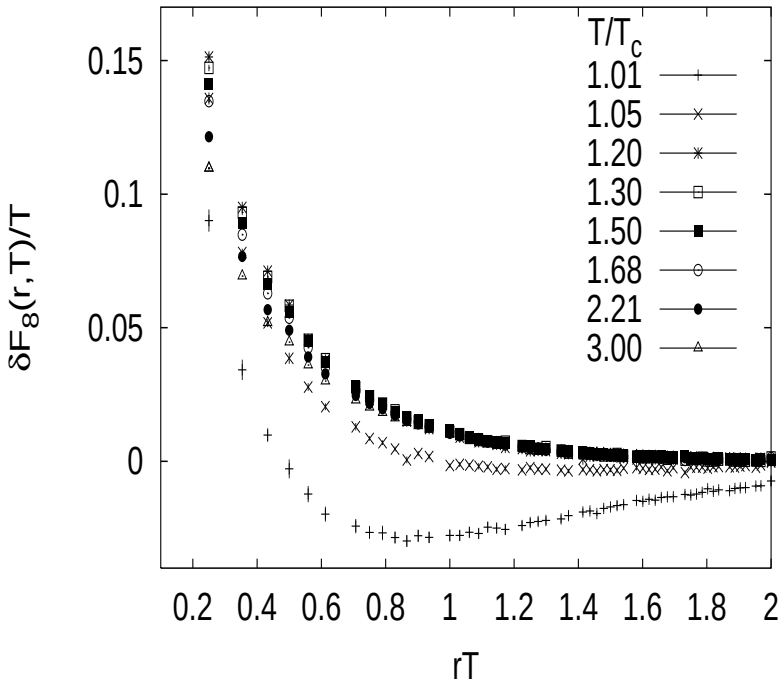

Figure 1.6: The color octet free energies from lattice simulations with lattices of size $32^3 \times 8$ at several temperatures above T_c. The free energies in this figure are normalized such that they approach zero at large distances.

one gluon exchange. Thus, a proper Coulombic behavior is expected to dominate the color octet free energies. While this behavior can indeed be identified at high temperatures, the behavior of the free energies at temperatures smaller than $1.05T_c$ clearly deviates from this simple behavior. For instance, the octet free energy at $1.01T_c$ exhibits a minimum as function of the distance. At small distances the color octet free energy at that small temperature behaves repulsive while it behaves attractive at distances larger than $rT \gtrsim 0.8$. This property is not expected from perturbation theory and shows that at small temperatures still strong non-perturbative effects dominate the color octet free energies.

In conclusion, from the large distance behavior of the color singlet free energies we can extract screening masses while in the short distance range the r-running of the coupling can be studied from the finite temperature free energies. We note that $S_1(r,T)$ shows strong temperature effects even at quite small distances. As discussed above this is to a large extent due to the normalization of the screening functions, *i.e.* we have subtracted a temperature dependent constant, $\Delta F_1(\infty,T)$, which forces $S_1(r,T)$ to approach zero at large distances and at the same time introduces an artificial temperature dependence at small distances.

1.3.2 Non-perturbative color screening

We discuss the large distance behavior of the free energies at high temperatures and determine the screening masses from the color singlet free energies. Unfortunately, the data for the color octet free energies turn out to be still too noisy to investigate their large distance exponential decay. As we aim to analyze correlated data a fit method is required which respects the correlation between the data. We thus use *correlated fits* as they include also off-diagonal elements of the correlation matrix in this analysis (for details on this method see for instance [84]). However, with this method it is not possible to fit the free energies directly. To determine the screening masses from the free energies within this approach we thus perform a correlated fit of the connected Polyakov loop correlation function in the color singlet channel

$$K_1(r,T) \quad = \quad \langle \mathrm{Tr} L(\mathbf{x}) L^\dagger(\bar{\mathbf{x}}) \rangle - |\langle \mathrm{Tr} L \rangle|^2. \tag{1.46}$$

Due to the exponential screening this correlation function has the same large distance behavior as the corresponding free energy. Hence it is mandatory that the correlation function above is fitted carefully at large distances. In our fits we use the general exponential ansatz,

$$K_1(r,T) \quad = \quad \frac{a(T)}{r^d} \exp(-m(T)r) + c, \tag{1.47}$$

which includes an additive constant c. For the color singlet free energies one expects $d = 1$ from perturbation theory as they are dominated by one gluon exchange and this is also expected from the $3D$-effective theory. We thus have fixed $d = 1$ in this case[6]. We then analyzed the correlation function by varying the upper and lower distance limit of the fit range. On finite lattices the upper limit is given by $rT = N_\sigma/(2N_\tau)$. We thus have fixed the upper limit to a distance close to this limitation where we still find reasonable small χ^2/d.o.f.. We used lattices with spatial extent $N_\sigma = 32$ and $N_\tau = 4, 8$. The lower fit range is chosen such that we find a region where the fit results behave stable against the variation of the lower fit range and in addition we find reasonable small values of χ^2/d.o.f.. In general, this leads to a lower fit range of about $rT \gtrsim 1$. The errors on these values are obtained from a Jack-knife analysis. We note that the additive constant c in our fits are compatible to zero within the statistical errors although they were essential to find small values for χ^2. Our results from this study of the screening masses of the color singlet free energies are shown in Fig. 1.7 as function of the temperature. In that figure we also show results for the screening masses of the color averaged free energies ($d = 1$) at temperatures $T \lesssim 1.03$ calculated from correlated fits and we also summarize the data from [33]. As the latter data respect an arbitrary d, however, we show these results normalized with $\mu_{av} = \mu/d$. Our numerical results from the correlated fit analysis are summarized in

[6]The fit analysis can equally well be done with the color averaged correlation functions. In this case we fixed both cases, $d = 1$ and $d = 2$. At temperatures close to T_c we noticed that only the case with $d = 1$ led to reasonable small values for χ^2/d.o.f.. For large temperatures both, $d = 1$ and $d = 2$, gave acceptable χ^2 values. This may imply that at high temperatures the true large distance behavior of the color averaged free energies sets in at distances which are considerable larger than those available by the present study. In our analysis we thus stick to the temperature range where $d = 1$ is well-established, $T \lesssim 1.03 T_c$ [85].

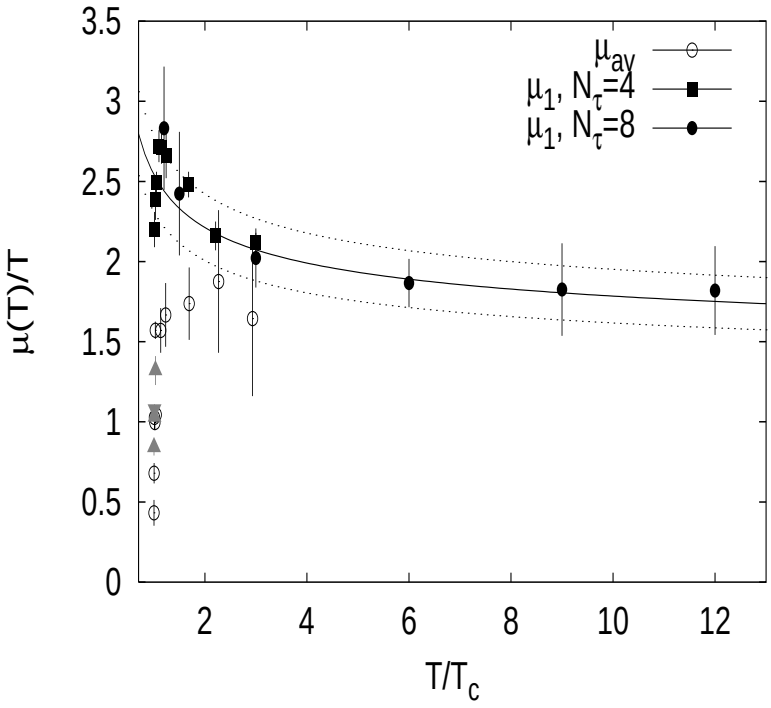

Figure 1.7: The color singlet screening masses (μ_1) from correlated fits of the correlation functions at large distances and the masses (μ) from [33] as function of the temperature. We have normalized the color averaged masses with the arbitrary power (d), *i.e.* $\mu_{av} \equiv \mu/d$. They grey triangles at temperatures close to T_c denote the results for μ_{av} calculated with the correlated fit method with $d = 1$ from lattices of size $32^3 \times 4$ (triangles up) and $48^3 \times 4$ (triangles down) [83].

Tab. 1.1.

It can be seen from that figure that the color singlet screening masses at temperatures close to the deconfinement point still approach large values while the results for the color averaged screening masses drop drastically at temperatures close to T_c. For instance, $\mu_1/T \gtrsim 2.2$ is obtained at the lowest temperature analyzed by us while the masses of the color averaged free energies from [33] approach values which are quite small, *i.e.* $\mu_{av}/T \lesssim 0.5$. As the screening masses determined from the color averaged free energies become that small it is an interesting question whether they will vanish at the deconfinement point or will stay finite [12]. To analyze this question in more detail and to take care of effects from the finite spatial lattice volume at small temperatures we also calculated the color averaged screening masses using the correlated fit method with $d = 1$ on lattices of size $32^3 \times 4$ and of size $48^4 \times 4$. In fact, $d = 1$ is suggested up to $T \lesssim 1.03 T_c$ [85]. The data from this study are shown in Fig. 1.7 with the grey triangles ($32^3 \times 4$: triangles up, $48^3 \times 4$: triangles down, see also Tab. 1.1). The screening masses determined by us with this method are larger at temperatures close to T_c than the normalized values, $\mu_{\rm av} = \mu/d$, of Ref. [33]. This is mainly due to the fact that we use an uncorrelated fit analysis. From

Non-perturbative screening masses							
singlet				averaged			
$32^3 \times 4$		$32^3 \times 8$		$32^3 \times 4$		$48^3 \times 4$	
T/T_c	$\mu_1(T)/T$	T/T_c	$\mu_1(T)/T$	T/T_c	$\mu_{q\bar{q}}(T)/T$	T/T_c	$\mu_{q\bar{q}}(T)/T$
1.0128	2.20 (11)	1.2	2.83 (39)	1.0128	1.03 (3)	1.0034	0.84 (5)
1.031	2.39 (13)	1.5	2.42 (39)	1.031	1.32 (9)	1.0128	1.08 (3)
1.05	2.49 (07)	3.0	2.02 (19)				
1.10	2.72 (10)	6.0	1.87 (16)				
1.15	2.71 (10)	9.0	1.83 (29)				
1.24	2.66 (14)	12.0	1.82 (28)				
1.68	2.48 (08)						
2.21	2.16 (09)						
3.00	2.12 (06)						

Table 1.1: The non-perturbative screening masses determined from the large distance exponential screening of the correlation functions. We used here the correlated fit method. The error estimate respects the Jack-knife analysis for the statistical uncertainty and the systematic uncertainty from the variation of the fit range.

a comparison of the correlated fit data of both lattices it follows that the finite size effects are negligible. Form our analysis it follows that the discontinuity in the screening mass for the color averaged free energy is about $\mu_{av}(T_c) \simeq 0.7T_c$. It is thus most likely that the screening masses for the color averaged free energies will stay finite at the deconfinement point. This behavior thus signals a first order phase transition. Further discussions of the screening masses will be presented elsewhere (see Ref. [83]).

We have also analyzed the color singlet screening masses at high temperatures. At high temperatures the color singlet masses (in units of the temperature) deduced by us, $\mu_1(T)/T$, decrease continuously with increasing temperature. In general this behavior is suggested by leading order perturbation theory (1.11) due to the weakening of the coupling, $g(T)$. To make contact with high temperature perturbation theory we adjusted the leading order color electric screening mass to our data at the highest three temperatures analyzed by us (*i.e.* $T \gtrsim 6T_c$) using the ansatz $m_e/T = Ag(T)$. For the temperature dependent (renormalized) coupling $g^2(T)$ we used the two-loop formula

$$g^{-2}(T) \;=\; 2b_0 \ln\left(\frac{2\pi T}{\Lambda_{\overline{MS}}}\right) + \frac{b_1}{b_0}\ln\left(2\ln\left(\frac{2\pi T}{\Lambda_{\overline{MS}}}\right)\right) \tag{1.48}$$

where $b_0 = 11/(16\pi^2)$ and $b_1 = 102/(16\pi^2)^2$. The scale is set by $T_c/\Lambda_{\overline{MS}} = 1.14(4)$ [86, 87] and the lowest Matsubara frequency $2\pi T$. Perturbation theory suggests $A = 1$ for the color singlet screening mass. The fit, however, leads to $A = 1.52(15)$ which is incompatible with this value, although the temperature dependence of the lattice data can be well-described with this perturbative inspired ansatz down to surprisingly small temperatures about $T \gtrsim 2T_c$.

Finally we note that the values for the screening masses deduced by us for the color

averaged free energies are close to recent results for the screening masses from plane-plane correlations of Polyakov loops using a simple exponential fit [88], *i.e.* without power-like pre-factors. We also note that the screening masses extracted from recent analysis of the Landau gauge gluon propagator yield similar results to ours [89].

1.3.3 Notes on the running coupling at finite temperature

We now turn to a discussion of the color singlet free energies at small distances. In order to eliminate any dependence of the free energies on (arbitrary) temperature dependent normalization which for instance get introduced due to the normalization of the screening functions we follow here the approach which is frequently used at zero temperature in order to eliminate the dependence on zero temperature renormalization constants. We calculate the derivative of the finite temperature free energies with respect to distance as discussed in Sec. 1.2.3 at each fixed temperature, $d\Delta F_1(r,T)/dr$. This eliminates undetermined constant contributions to $\Delta F_1(r,T)$. The quantity

$$\alpha_{\mathrm{eff}(1)}(r,T) \;=\; \frac{3r^2}{4} \times \frac{d\Delta F_1(r,T)}{dr} \tag{1.49}$$

then is supposed to provide an estimate of the running coupling constant at finite temperatures. We thus call $\alpha_{\mathrm{eff}(1)}(r,T)$ the *effective running coupling*. At zero temperature a corresponding detailed analysis has recently been performed by analyzing the short distance properties of the heavy quark potential [55]. At high temperatures and large distances, however, $\alpha_{\mathrm{eff}(1)}(r,T)$ will be dominated by the temperature scale and color screening effects will set in. We thus expect that the effective coupling will smoothly change from the temperature dominated region at large distances ($rT \gg 1$) to the r-dominated region at short distances ($rT \ll 1$) where vacuum physics is expected.

We compare our finite temperature results to the high statistics calculation of Ref. [55] in Fig. 1.8. In this figure the results of the numerical calculation of the zero temperature heavy quark potential at distances $r \gtrsim 0.1$ fm are summarized by the fat black line. Also shown in this figure is the Cornell potential from the string picture with the thin grey line. This line agrees with the lattice data at zero temperature for $r \gtrsim 0.1$ fm but strong deviations from the finite temperature data are expected at small distances.

Our numerical results on $\alpha_{\mathrm{eff}(1)}(r,T)$ in the QCD plasma phase clearly show a running with the dominant length scale r at small distances. For temperatures below $3T_c$ we find that $\alpha_{\mathrm{eff}(1)}(r,T)$ agrees with the zero temperature lattice data in its entire regime of validity. Only at larger distances thermal effects become visible and lead, as expected, to a decrease of the coupling relative to the coupling at zero temperature. For temperatures higher than $3T_c$ this effect is also visible at smaller distances. At small distances the effective couplings coincide at different temperatures while the thermal effects become visible at large distances. In fact, at large distances the effective coupling will be effected much by screening. The high temperature data for $\alpha_{\mathrm{eff}(1)}(r,T)$ indeed show this behavior as they vanish at large distances.

The study of the effective coupling at finite temperature could equally well be done in

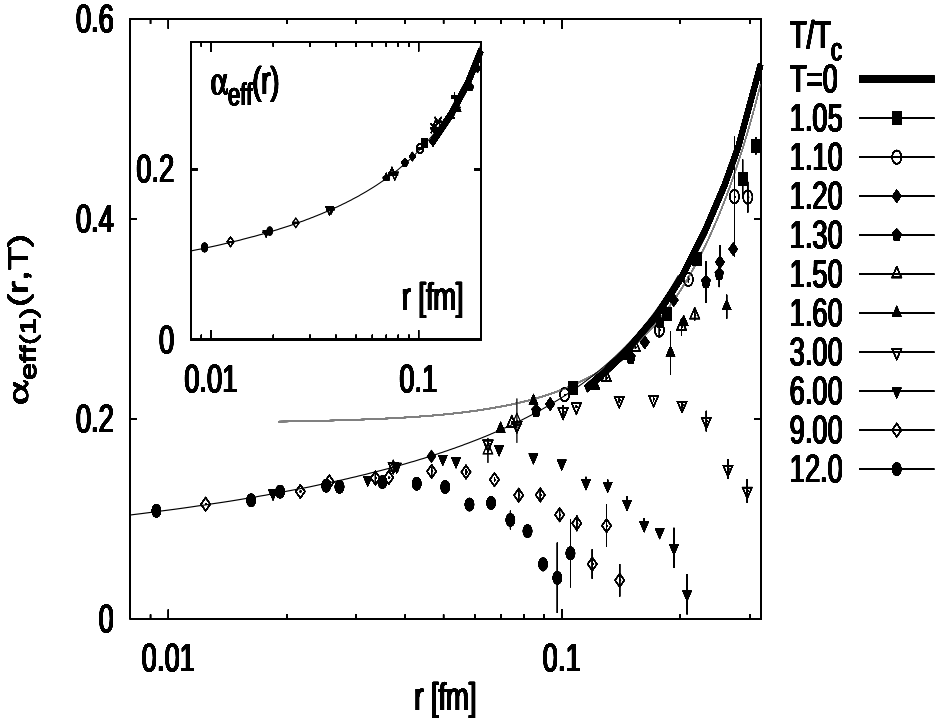

Figure 1.8: The derivative of the color singlet free energies with respect to r at different temperatures in terms of (1.49) and the zero temperature running coupling from [55] (thick black line). Also shown is in this figure the potential from the zero temperature string picture (thin grey line) and the 3-loop calculation from [55] (thin black line). The inserted figure contains only the values of the derivatives of the free energies at the shortest distances available by us. These values are also compared to the perturbative 3-loop coupling [55] in the so-called qq-scheme. In this small figure we also summarize values at temperatures below T_c (stars and crosses). For more details see the text.

terms of the data for the free energies in the color octet channel. In this case, leading order perturbation theory suggests that the effective coupling defined as

$$\alpha_{\mathrm{eff}(8)}(r,T) \quad = \quad -\frac{r^2}{6} \times \frac{d\Delta F_8(r,T)}{dr} \tag{1.50}$$

yields similar results than $\alpha_{\mathrm{eff}(1)}(r,T)$ at small distances. We have indeed analyzed this relation and find that both estimates for the effective running coupling yield consistent results at small distances. At large distances differences become visible. They are, however, quite small at temperatures larger than $6T_c$.

The conclusions drawn from our analysis of the color singlet free energies at small distances are twofold: First of all it follows that the color singlet and color octet free energies cannot be described by a simple color screened Coulombic term, *i.e.* $\simeq -a(T)e^{-m(T)r}/r$ at small distances ($rT \ll 1$), as the logarithmic r-running of the coupling becomes quite important. In contrast to this, at large distances ($rT \gg 1$) the scale in the coupling is clearly set by the

temperature as the color singlet free energies can be well-fitted with this simple screened Coulombic ansatz. The analysis of the r- and T-dependence is more transparent in terms of color singlet free energies[7].

Moreover, it follows that the finite temperature effective coupling $\alpha_{\text{eff}(1)}(r,T)$ can be described at small distances by zero temperature perturbation theory. This property can clearly be seen from the small inserted figure in Fig. 1.8. In that figure we compare $\alpha_{\text{eff}(1)}$ at the two smallest distances for each temperature. They indeed give the coupling at zero temperature from distances of about $r \simeq 0.1$ fm down to $r \simeq 0.01$ fm and agree well with the lattice data from [55] at larger distances. In that figure we have also summarized lattice data for the color singlet free energies at temperatures below T_c. They are denoted by crosses ($T = 0.75T_c$), by switched crosses ($T = 0.90T_c$) and by stars ($T = 0.94T_c$). In conclusion, it is possible to extract the zero temperature part from the finite temperature free energies below and above T_c.

We should stress here that the observation of vacuum physics in our finite temperature free energies at small distances will be conceptually essential for our approach used in the renormalization of the Polyakov loop on the lattice. This long standing problem is subject of the next chapter. Before we turn to details on this we briefly discuss the thermal properties of free energies in a confined medium.

1.4 Notes on the quark antiquark free energies below T_c

In the string picture (in the Gaussian approximation) discussed in Sec. 1.1 the string does not contain any internal degrees of freedom nor does it have reference to internal color

[7] It is also of considerable importance (see for instance our discussions in chapter 3) to find an accurate *parameterization* for the free energies which allows to fit the data from short to large distances. Naively, one would expect that the scale ($\mu(r,T)$) in the coupling $\alpha_{\text{eff}(1)}(\mu)$ could be set by $\mu \simeq 1/r + T$ as this leads to a dominant temperature scale at large distances while the scale is set by the distance at small r. By setting the scale in this way the singularity in the perturbative coupling at zero temperature, $\alpha(r) \simeq 1/\ln(1/r\Lambda)$, at distances which become comparable to the (inverse) QCD-Λ-scale is removed at finite temperature. Thus, this scale-ansatz could indeed be used to parameterize $\alpha_{\text{eff}(1)}(r,T)$ and the screening functions $S_1(r,T)$. We used the leading order perturbation theory to motivate a parameterization $g^2(r,T) \simeq 1/\ln(\mu/\Lambda)$ with $\mu \simeq 1/r + T$ for the coupling in the cross-over regime. In terms of the screening functions we thus use

$$S_1(r,T) \quad \simeq \quad g^2(r,T)\exp\left(\rho(T)g(r,T)\times r\right) \tag{1.51}$$

as this ansatz in addition to the scale dependence in the coupling $g^2(r,T)$ could also respect the onset of screening as function of distance, $\rho(T)g(r,T)$. Our results of fits of this function to lattice data for $S_1(r,T)$ are shown as grey lines in Fig. 1.5. It can be seen from that figure that such a kind of parameterization can fit the lattice data for the screening functions from short to large distances. Once the free parameters in (1.51) are fixed this parameterization allows to study separately the coupling $g^2(r,T)$ and the exponential screening as function of T and r. We note here that we find a reasonable functional dependence of the coupling and the values for $\rho(T)g(r,T)$ at distances about $rT \gtrsim 1$ are close to the values summarized in Tab. 1.1. The values $m(T) = \lim_{r\to\infty}\rho(T)g(r,T)$, which could be used to define screening masses, are about 15% larger than the values in Tab. 1.1.

However, also other (energy-) scales, *i.e.* rT^2, $1/Tr^2$, ..., may become important in the cross-over region. A different discussion from ours can be found in [90].

structures. It thus equally well should describe the color singlet and color octet quark antiquark free energies. Indeed, no additional[8] boundary conditions are introduced on the surfaces which cover the operator correlation given by $\langle \mathrm{Tr} L(\mathbf{x}) L^\dagger(\bar{\mathbf{x}}) \rangle$ in (1.31) and (1.32). In conclusion, the string picture in the Gaussian approximation suggests a confining color singlet and color octet free energy, and, more importantly, the string tension of the quark antiquark free energies in all three color channels is supposed to show a unique temperature dependence, *i.e.* $\sigma_{1,8,q\bar{q}}(T) = \sigma(T)$.

We present our lattice results for the Polyakov loop correlation functions at temperatures below T_c. Our results for the color singlet and color octet free energies at various temperatures are shown in Fig. 1.9. The left figure (A) shows the color singlet free energies while the right figure (B) shows our results for the color octet free energies. In both figures the free energies are given in units of the temperature ($\Delta F_{1,8}(r,T)/T$) as functions of the distance rT. The lattice data we summarize in these figures are related to the free energies only up to renormalization. It can be seen from these figures that the color singlet and color octet free energies indeed signal confinement at large distances as they increase with increasing distances. Thus, the color octet contributions to the color averaged free energies turn out to be quite important in a confined medium [82]. Similar findings are reported for color $SU(2)$ [23, 69].

Deviations from a common behavior of the color singlet and octet free energies can be seen at intermediate and small distances. While the color singlet free energies behave attractive in the entire distance range covered by the lattice data, the color octet free energies signal the beginning of a repulsive behavior at small distances. A repulsive color octet free energy is indeed expected from perturbation theory through (1.9). We thus expect to find agreement with perturbation theory at smaller distances.

It follows from our discussion given above that deviations of the free energies at some fixed temperature from a common behavior in all three color channels indicate an incompatibility with the Gaussian string picture. From a closer inspection of the free energies in Fig. 1.9 it follows that the color singlet, octet and averaged free energies start to coincide at distances $rT \gtrsim 2.5$ which thus gives a lower limit for the validity of the Gaussian string picture. At those large distances also the predicted term $\ln(rT)$ from Eq. (1.5) can be well identified with the predicted strengths in the color singlet and octet free energies. For instance, when subtracting this term from the color singlet, octet and averaged free energies (not explicitly shown here) one can clearly observe that the free energies describe a simple linear behavior at such large distances. At smaller distances the color averaged

[8] This property may change when analyzing the *cyclic Wilson loop* in the string picture instead of $\langle \mathrm{Tr} L L^\dagger \rangle$. In fact, in the case of the cyclic Wilson loop, one would in addition to the usual boundary conditions demand that the fluctuations of the string vanish on the (straight) gauge link connection between the two loops. This condition will indeed not affect the leading order term, which is still given by $\sigma r T^{-1}$, but may change the sub-leading corrections to $\Delta F_1/T$. In spirit of (1.32), also the sub-leading terms to ΔF_8 may change. It is an interesting question whether the different properties of the color singlet and octet free energies can be reproduced at intermediate distances. Obviously, however, such a kind of investigation will run into problems at small and large distances as the cyclic Wilson loop is bound to short distances while the string picture is to large ones.

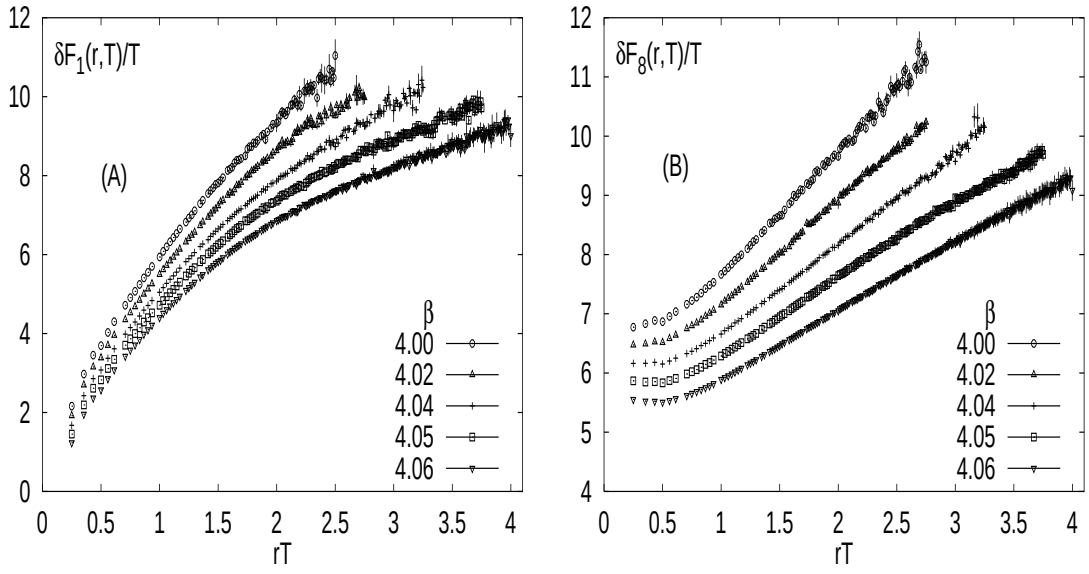

Figure 1.9: The color singlet (A) and the color octet (B) free energies (up to renormalization) as functions of rT at several temperatures below T_c. The couplings β and the corresponding temperatures are given in Tab. A.1. These data summarize our calculations on lattices of size $32^3 \times 4$.

free energies still follow this behavior while the color singlet and octet free energies significantly deviate from the linear behavior. In fact, the color averaged free energies can be well fitted to the string picture [33, 54] at much smaller distances than $rT \simeq 2.5$. In view of our discussions above, however, this agreement at small distances is quite surprising as the Gaussian string formation will clearly take place only at larger distances.

Chapter 2

Lattice-Renormalization of the Polyakov loop

Universal properties of the confinement deconfinement phase transition in QCD are often discussed in its quenched approximation ($\sim SU(3)$) where the Polyakov loop is treated as an order parameter although it is affected by UV divergences and thus requires renormalization. Moreover, $\langle \mathrm{Tr} L \rangle$ is said to be related to the change in free energy ΔF_q due to the presence of a single test color charge put into a gluonic heat bath [9],

$$\langle \mathrm{Tr} L \rangle \simeq \exp(-\Delta F_q / T). \tag{2.1}$$

Implicitly, this assumes that it is possible to go from the bare Polyakov loop expectation value to its renormalized counterpart. However, although the Polyakov loop is known to be a renormalizable quantity for a long time [43, 91], how to do this explicitly on the lattice is still an outstanding problem. Actually, using the lattice formulation, $\langle \mathrm{Tr} L \rangle$ vanishes due to the presence of these divergences in the continuum limit at fixed temperature and consequently the heavy quark free energy in (2.1) gets physically ill-defined. Recently we suggested [92, 93] a new concept of a non-perturbative renormalization prescription for the Polyakov loop *and* its n-point correlation functions, which, for instance, works on a lattice.

In this chapter we discuss this non-perturbative renormalization scheme for the 2-point Polyakov loop correlation functions which will lead us to a proper evaluation of the Polyakov loop expectation value. As the Polyakov loop is a (non-local) composite operator, one expects[1] its renormalization through

$$L^R(\mathbf{x}) \;=\; Z_L \prod_{x_0=1}^{N_\tau} Z_U U(x_0, \mathbf{x}) = Z_L Z_U^{N_\tau} \prod_{x_0=1}^{N_\tau} U(x_0, \mathbf{x}), \tag{2.2}$$

where the renormalization constant Z_U is introduced in order to renormalize the field and the gauge coupling while Z_L respects the composition of the lattice link variables. While

[1] Or one would think of an even more complicated renormalization structure as composite operators in general mix with other operators under renormalization. However, this is not the case with the Polyakov loop [43].

the renormalization of the correlation functions is performed in our scheme in the short distance regime, the renormalized Polyakov loop expectation value follows from the infinite distance limit of the renormalized 2-point correlation functions. In fact, as in this approach we rather estimate the renormalized counterpart of $|\langle \mathrm{Tr} L \rangle|$ rather than of $\langle \mathrm{Tr} L \rangle$, the relation (2.1) can be formulated properly. Moreover, since ΔF_q signals confinement at temperatures below T_c while, consistent with deconfinement, it approaches finite values at $T > T_c$, it follows that the renormalized Polyakov loop expectation value works as an order parameter for the confinement deconfinement phase transition which is indeed physically meaningful through (2.1).

This second chapter is organized as follows: In the first section we discuss the problems with the renormalization of the Polyakov loop and review what is known so far. We then outline the theoretical background for our new renormalization concept for the 2-point Polyakov loop correlation functions and the Polyakov loop. Following this discussion we present a detailed analysis of the thermal properties of the Polyakov loop correlation functions in the three color channels. For instance, we relate the color singlet, octet and averaged $q\bar{q}$ free energies to each other and show that the temperature effects on the color singlet and octet free energies become negligible at short distances. The properties of the correlation functions at short distances lead us to a proper renormalization prescription for the 2-point Polyakov loop correlation functions and we analyze their properties in the continuum limit. We then re-analyze the thermal features in terms of the renormalized finite temperature heavy quark free energies in all color channels. In the last sections of this chapter we present the non-perturbatively renormalized Polyakov loop expectation value and deduce from it the corresponding *effective renormalization constant* for the Polyakov loop. Finally, we comment on the structure of divergences present in n-point Polyakov loop correlation functions. Indeed, we conclude that the renormalization prescription formulated by us can be generalized to any n-point Polyakov loop correlation function once the renormalization constants in spirit of (2.2) are fixed. We close this chapter after a final discussion of the things done so far and comment on related problems with the Polyakov loop which are discussed in the current literature.

We note that we analyze the color singlet, octet and averaged quark antiquark free energies down to distances $r \gtrsim 0.01$ fm and in a temperature range from $T \simeq 0.9 T_c$ to about $12 T_c$. Actually, the shortest distance which can be resolved on a lattice with finite temporal extent N_τ is $rT = 1/N_\tau$. Thus, in order to analyze such small distances on the lattice it is mandatory to use lattices with large temporal extent. For instance we use lattices of size $32^3 \times N_\tau$ with $N_\tau = 4, 8$ and 16. This is the first time that we have utilized lattices of that large temporal extent for an analysis of the free energy at finite temperature. In fact, the shortest distances resolved by us are of about 5 to 10 times smaller than the distances studied in current lattice studies of other observables at finite temperature [33, 69].

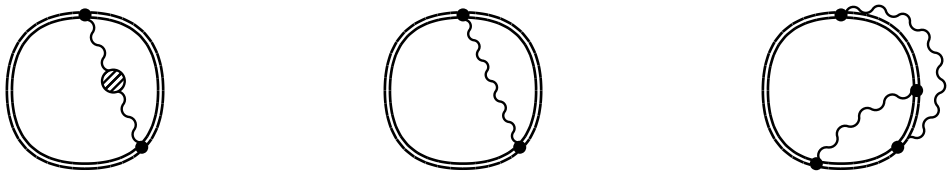

Figure 2.1: The perturbative contributions in (2.6) to the Polyakov loop expectation value in the diagram language. The double line represents the time-like closed propagation of the static quark including the one (A') and two (B) gluon exchange (wavy lines). The blob in the left diagram (A) indicates the $\mathcal{O}(g^2)$ radiative part of the gluon self energy.

2.1 On the problem addressed and on current concepts

We are interested in the evaluation of the expectation value of a special thermal Wilson line, the Polyakov loop expectation value $\langle \mathrm{Tr}L \rangle$, defined through

$$\langle \mathrm{Tr}L \rangle \equiv \langle \mathrm{Tr}\mathcal{T} \exp\left(ig \int_0^\beta dx_0 A_0(x_0, \mathbf{x}) \right) \rangle, \tag{2.3}$$

where we assume that the dynamics of the gauge fields A_μ is given by the pure gauge theory with $SU(N)$ gauge group. In (2.3) we consider the trace to be normalized to unity, $\mathrm{Tr}\mathbb{1} = 1$, and β denotes the inverse temperature, $\beta = 1/T$. Due to the finite integration in the time direction the gauge fields obey the usual periodic boundary conditions, i.e. $A_\mu(0, \mathbf{x}) = A_\mu(\beta, \mathbf{x})$, and $\mathcal{T}$ in (2.3) is the usual time ordering operator. In this section we consider the problem with divergences which are present in (2.3) and discuss the problem of their cancellation through regularization and renormalization, which is indeed far from trivial since L is a non-local composite operator (see for instance [94, 95]). We note, however, that we are in a somewhat 'lucky' position as earlier studies have succeeded to solve this problem (starting with [43]) at least partly.

The best way to get a first insight into this problem is to analyze (2.3) in the framework of perturbation theory ($g \to 0$) in the continuum and we should therefore first clarify what we mean with $\langle ... \rangle$, namely

$$\begin{aligned} \langle ... \rangle &\equiv \frac{1}{Z_0} \int \mathcal{D}A_\mu \mathcal{D}\bar{C}\mathcal{D}C \, (...) \, e^{-\int_0^\beta dx_0 \int d\mathbf{x} \mathcal{L}(x)} \\ \text{with } \mathcal{L}(x) &= \frac{1}{4} F^a_{\mu\nu} F^a_{\mu\nu} + \frac{1}{2\xi} \left(\partial_\mu A^a_\mu \right)^2 + \partial_\mu \bar{C}^a \left(\partial_\mu C^a - g t^{abc} A^b_\mu C^c \right). \end{aligned} \tag{2.4}$$

In this Lagrangian we denote with C, $\bar{C}$ the ghost fields and for convenience we assume that the partition function is normalized such that $\langle 1 \rangle = 1$. In order to stay close to the current literature (for instance [96]), we work in the $\partial_\mu A_\mu = 0$ gauge. The Polyakov loop, $\mathrm{Tr}L$, in Eq. (2.4) is, however, a gauge invariant quantity.

In order to calculate the first two non-vanishing orders in the (bare) coupling constant g, one expands the exponential function in (2.3) to $\mathcal{O}(g^4)$ and averages over the gauge and

ghost fields with respect to (2.4),

$$\langle \mathrm{Tr}L\rangle \simeq \langle 1\rangle - g^2\mathrm{Tr}\left(\lambda^a\lambda^b\right)\langle\int_0^\beta d\tau_1\int_0^\beta d\tau_2 A_0^a(\tau_1,\mathbf{x})A_0^b(\tau_2,\mathbf{x})\rangle \tag{2.5}$$

$$-ig^3\mathrm{Tr}\left(\lambda^a\lambda^b\lambda^c\right)\langle\int_0^\beta d\tau_1\int_0^\beta d\tau_2\int_0^\beta d\tau_3 A_0^a(\tau_1,\mathbf{x})A_0^b(\tau_2,\mathbf{x})A_0^c(\tau_3,\mathbf{x})\rangle$$

$$+g^4\mathrm{Tr}\left(\lambda^a\lambda^b\lambda^c\lambda^d\right)\langle\int_0^\beta d\tau_1\int_0^\beta d\tau_2\int_0^\beta d\tau_3\int_0^\beta d\tau_4 A_0^a(\tau_1,\mathbf{x})A_0^b(\tau_2,\mathbf{x})A_0^c(\tau_3,\mathbf{x})A_0^d(\tau_4,\mathbf{x})\rangle,$$

where we have separated the color structure from the gauge field according to the representation $A_\mu(x) = \lambda^a A_\mu^a(x)$. Since the $\mathcal{O}(g^3)$-term vanishes after the averaging for symmetry reasons of the 3-gluon vertex, one finds a series expansion of the form [43, 96]

$$\langle \mathrm{Tr}L\rangle \;=\; 1 - g^2\mathcal{L}_2 + \frac{1}{2}\left(g^2\mathcal{L}_2^0\right)^2 + g^4\mathcal{L}_4 + \ldots\,. \tag{2.6}$$

Let us first consider the lowest order term denoted with $\mathcal{L}_2$: It is given by the diagram A in Fig. 2.1, where the blob represents the gauge field self energy including the $\mathcal{O}(g^2)$ radiative corrections, $\Pi(\mathbf{q}^2)$. (In order to be precise, $\Pi(\mathbf{q}^2)$ is given through the 1-loop diagrams of the gluon propagator. These are the gluon loop, the ghost loop as well as the tadpole diagram shown in Fig. 3e-3g of Ref. [91].) In momentum space, after performing the frequency sum at finite T, $\mathcal{L}_2$ reads

$$g^2\mathcal{L}_2 \;\simeq\; g^2\frac{1}{T}\mathrm{Tr}\left(\lambda^a\lambda^b\right)\int\frac{d^3q}{(2\pi)^3}\frac{1}{\mathbf{q}^2+\Pi(\mathbf{q}^2)}. \tag{2.7}$$

It follows that this term is (UV) divergent and thus needs a regularization: In fact, the insertion of $\Pi(\mathbf{q}^2)$ produces *logarithmic divergences*. The second term in (2.6), $\mathcal{L}_2^0$, is given by single one gluon exchange which is shown in Fig. 2.1 through the diagram A'. As the wavy line represents the usual gluon propagator ($\sim 1/\mathbf{q}^2$), its evaluation leads to

$$(g^2\mathcal{L}_2^0)^2 \;\simeq\; \left(g^2\frac{1}{T}\int\frac{d^3q}{(2\pi)^3}\frac{1}{\mathbf{q}^2}\right)^2. \tag{2.8}$$

From power counting it follows that this integral is *linear divergent* and therefore also needs a regularization. Moreover, $\mathcal{L}_4$ produces in parts linear divergences which have to be regulated, too. An example for this kind of diagram is shown in Fig. 2.1 as diagram B. The questions which arise now are how to handle the divergences and, more importantly, how to remove them. At this point of the discussion two[2] basic properties of the divergent structures are important: First of all this discussion includes the *degree of the divergences*

[2]The discussion in the present literature concerns rather five than two topics. In addition to the two topics which we examine it is also discussed:
3) Renormalization in general includes the reference to the space-time dimension (D) in which the theory is incorporated into. In our discussion we ignore this reference as we are rather interested in the physical case, $D = 4$, from which we know that the theory is (strictly) renormalizable. This property has been

as this property is closely related to the question which kind of regularization prescription is the most comfortable one. And secondly, the discussion of the renormalization gets complicated as TrL is a *composite operator*. The last property usually leads to a complicated renormalization procedure as composite operators in general need their own renormalization constants and additional renormalization conditions. Moreover, the renormalization procedure becomes even more difficult as a proper renormalization of composite operators in general requires a calculation of a matrix of renormalization constants since such operators can mix under renormalization with any other operator that has the same quantum numbers and a (canonical) dimension equal or smaller than the initial composite operator. This shows that the discussion of the renormalization of the Polyakov loop is indeed complex.

It was Polyakov who first *conjectured* a surprisingly 'simple' fragmentation of the different divergent structures (logarithmic/linear) of $\langle \mathrm{Tr}L \rangle$ [43]: The linear divergent parts appear in any order perturbation theory and could be collected together forming a factor $\exp(-Kf(l/a))$, where $f(l/a)$ is a linear function in l/a (here l denotes the length of the loop and a the (lattice) cut-off parameter),

$$\langle \mathrm{Tr}L \rangle \quad \simeq \quad e^{-Kf(l/a)} \times G_{\mathrm{ren}}, \tag{2.10}$$

while G_{ren} consists only of the logarithmic divergences and of the finite contributions. The most striking statement of *Polyakov's suggestion*, however, is that it claims that *all* logarithmic divergences can be removed in perturbation theory, order by order, within the standard field and coupling renormalization. Indeed, Polyakov's suggestion has been

discussed extensively in the current literature; see [43, 97, 98].

4) The geometric structure of the loop contour plays a role: In our considerations we refer only to *smooth contours* without self interactions. Otherwise, assuming that the contour has a corner with an angle γ (see Fig. 2 of Ref. [43]), divergences will appear which depend on this angle. For instance, in leading order one finds [43]

$$f^{(1)}(l/a) \quad = \quad \pi \frac{l}{a} + (\gamma \cot \gamma - 1) \log \frac{l}{a}, \tag{2.9}$$

where l denotes the length of the loop and a is the lattice spacing. The first term originates from the smooth part of the contour and the second part is produced at the corner. Its qualitative nature can be related to the bremsstrahlung which gets emitted from the color charge through the rapid change of motion at the corner [43, 91]. It is worth noting that such γ-divergences will not cancel out within the standard renormalization procedure. As they are rather 'anomalous' we restrict our discussion to the case of smooth loops.

5) Furthermore, the problem of divergences which appear in higher powers of L is discussed. For instance, 1-loop calculations of k-powers in the Polyakov loop, $\langle \mathrm{Tr}L^k \rangle$, $k = 1, 2, ..., N-1$, in a background gauge field are presented in [99]. The result is that they are finite by renormalization, but *real*, $\langle \mathrm{Tr}L^k \rangle \in \mathbb{R}$. More important in that discussion, however, is the statement that the untraced counterparts are *infinite*, and the corresponding matrices become diagonal which are neither *unitary* nor *special*. From some point of view one may argue that the (untraced) Polyakov loop is not a gauge invariant quantity and therefore its renormalization would be without any relevance. It is argued in that reference, however, that a gauge transformation cannot remove the infinity. In this sense, there are even unsolved problems in the continuum renormalization of the Polyakov loop. We note, however, that we will not go into a discussion of such kind of divergences. Note that L is a *non-local* operator while k-powers in L with $k > 1$ build up *local* composite operators.

proven to fourth order in perturbation theory [98] and to any order in perturbation theory, too [91]: In the case of a smooth contour, the (renormalized) quantum average of the quantity

$$\mathrm{Tr}\mathcal{T}\exp\left(iZ_gZ_A^{-1}g\int_0^\beta dx_0A_0(x_0,\mathbf{x})\right) \tag{2.11}$$

is free from logarithmic divergences in any order perturbation theory, where Z_g and Z_A^{-1} denote the renormalization constants associated with the coupling (Z_g) and with the field (Z_A^{-1}) renormalization. Disregarding the linear divergences, this expression shows that the Polyakov loop, although it is a composite operator, does not mix with any other operator under renormalization. In conclusion, it is proven that the Polyakov loop expectation value is a (standard) renormalizable object and we should calculate it.

In practice now, the question arises which is the most suitable regularization scheme. Indeed, the divergence structure of (2.10) invites to use the *dimensional regularization*, as the linear divergence simply cancels out ($e^{Kf(l/a)}=1$). Using this regularization method, there only remain the parts denoted by G_{ren} in (2.10), but which are known to be renormalizable. Then, at finite temperature, the essential thing is to include the effects from Debye screening. In fact, the HTL re-summation suggests $\Pi(\mathbf{q}^2=0)=m_D^2$, where $m_D\sim gT$ is the typical scale of the Debye mass. An evaluation of $\langle\mathrm{Tr}L\rangle$ to fourth order in g using this method can be found in [96]. They calculate the coefficients in (2.6) being:

$$\langle\mathrm{Tr}L\rangle=1+2\pi^2Q_0\Big\{\left(\frac{2}{3}N\right)^{\frac{1}{2}}\left(\frac{g^2}{8\pi^2}\right)^{\frac{3}{2}}+N\left(\frac{g^2}{8\pi^2}\right)^2\left(\ln\left(\frac{g^2}{8\pi^2}\right)+\ln(\frac{2\pi^2N}{3})+\frac{3}{2}\right)\Big\}, \tag{2.12}$$

where $Q_0=\mathrm{Tr}\sum_a\lambda^a\lambda^a$, which is $(N^2-1)/(2N)$ in the fundamental representation and N in the adjoint case. Some comments are in order: Firstly, the power-enhancement in g of the first term compared to the initial expansion (2.6) - and its change in sign - follow from the insertion of $\Pi(\mathbf{q}^2=0)=m_D^2$: (2.7) leads to a power behavior in g like $-g^2\times(-m_D)\simeq+g^3$. Secondly, $\langle\mathrm{Tr}L\rangle\simeq1+f(g)$ with f being a (positive) decreasing function with decreasing coupling. Following the discussion above, the *renormalized* Polyakov loop expectation value ($\langle\mathrm{Tr}L^R\rangle$) is given by replacing the bare coupling g with the renormalized coupling, g_R. Strictly speaking, at this order, the renormalized coupling is given by a constant and consequently $\langle\mathrm{Tr}L^R\rangle\simeq1+c$, where c is some positive number. However, disregarding the possible effects from the Linde problem [15, 11], higher order corrections to (2.12) are known to be renormalizable by renormalization of the coupling and will lead to a running (renormalized) coupling, $g_R(T)\simeq1/\ln(T^2/\Lambda^2_{\mathrm{QCD}})$. Therefore (2.12) can be estimated as giving the leading order behavior of the renormalized Polyakov loop expectation value when replacing g with its renormalized quantity, $g_R(T)$ [96]. For this reason, $\langle\mathrm{Tr}L^R\rangle$ is supposed to approach its high temperature limit *from above*, $\lim_{T\to\infty}\langle\mathrm{Tr}L^R\rangle=1$. Being a perturbative expansion, (2.12) is supposed to estimate $\langle\mathrm{Tr}L^R\rangle$ in the high temperature limit, $\beta\to0$, while at temperatures close to T_c, or even below T_c, the validity of (2.12) will

break down as one runs into a non-perturbative temperature regime. Moreover, the usual uncertainties are present in the perturbative estimate (2.12). In conclusion, in this temperature range one requires *non-perturbative methods* in order to evaluate $\langle \mathrm{Tr} L^R \rangle$ properly.

One possibility to get non-perturbative insights into the Polyakov loop is to apply MC simulation techniques on the lattice (for a related discussion see [100, 101]). Within the *lattice regularization* method, however, one has to face the problem which results from the linear divergence in (2.10): As it stands, for any finite lattice spacing a one will find finite results while $\langle \mathrm{Tr} L \rangle$ will vanish in the continuum limit where $a \to 0$. We note that our MC lattice data indeed show this effect. We have calculated the Polyakov loop expectation value in terms of $|\langle \mathrm{Tr} L \rangle|$ at fixed physical temperature T using lattices with different N_τ (see Fig. 2.2). The data indeed show that $|\langle \mathrm{Tr} L \rangle|$ calculated on lattices with larger N_τ ($\sim$ smaller a) approach smaller values than the results calculated on lattices with smaller N_τ at a fixed T (see also Fig. 2.2). This suppression of $\langle \mathrm{Tr} L \rangle$ with vanishing lattice spacing a is indeed due to the presence of the linear divergence.

It is worth noting that this property is visible in lattice perturbation theory, too. $SU(N)$ 1-loop ($\mathcal{O}(g^4)$) calculations on the lattice are presented in [102, 103]. They compute the 1-loop correction terms to the Polyakov loop using finite lattices in pure gauge theory defined with the standard Wilson gauge action. On a lattice one expects a rather straightforward power series in the bare coupling, $\langle \mathrm{Tr} L \rangle \simeq 1 + \sum_i c_i g^{2i}$. To $\mathcal{O}(g^4)$ the perturbative coefficients are

$$\langle \mathrm{Tr} L \rangle = 1 - g^2 \frac{N^2-1}{N} Q^{(2)} - g^4 (N^2-1) Q^{(4a)} - g^4 \frac{(2N^2-3)(N^2-1)}{N^2} Q^{(4b)} + \mathcal{O}(g^6), \tag{2.13}$$

where the N-independent coefficients $Q^{(i)}$ are listed in Tab. 5 of Ref. [102]. In fact, these coefficients reflect the linear divergence; For instance, the first coefficient in (2.13) is constant in units of N_τ, $Q^{(2)}/N_\tau \simeq 0.057....$ In conclusion, the perturbative expansion of $\langle \mathrm{Tr} L \rangle$ on a lattice given in (2.13) is not only a function of the temperature but in addition depends on the lattice extent $N_\tau \equiv 1/Ta$, *i.e.* on the cut-off.

In order to remove the lattice dependence of $\langle \mathrm{Tr} L \rangle$ one is forced to eliminate the linear divergence. For instance, we checked whether the subtraction of the perturbative expansion from the MC data compensates the lattice effect. We note, however, that subtracting the leading order part from our MC measurements does not bring the data with $N_\tau = 4$ and $N_\tau = 8$ on a common curve. We have also subtracted the (in spirit of (2.10)) re-exponentiated leading order term from our MC data. Also in this case the dependence of the data on the temporal extent of the lattice is not removed. This indeed indicates that the leading order term in (2.13) does not resolve the linear divergence completely on the lattice in the coupling regime which is analyzed by us.

Let us finally remark that the interest in a proper renormalization of the Polyakov loop is not only pure academic but also physically motivated, for instance through (2.1) (more background notes and links to related problems which motivate the non-perturbative renormalization of $\mathrm{Tr} L$ were given in the introduction of this thesis). Thus, not only

a *non-perturbative renormalization* concept for $\langle \mathrm{Tr}L \rangle$ is required, but also the question *how to relate* $\langle \mathrm{Tr}L \rangle$ *to the free energy* is important to answer. In our approach[3] we are rather interested in a renormalization of $|\langle \mathrm{Tr}L \rangle|$ than of $\langle \mathrm{Tr}L \rangle$ as the relation (2.1) can be formulated properly with $|\langle \mathrm{Tr}L \rangle|$ once the renormalization works.

2.2 Outline of the non-perturbative renormalization concept

Recently we suggested that the renormalization of the Polyakov loop on a lattice can be obtained by *first renormalizing the quark antiquark free energies* calculated at small quark antiquark separations [92]. At short distances the finite temperature free energy is given by the zero temperature heavy-quark potential. From this property we concluded that the divergent self energy contribution in the finite temperature free energy can be removed through a matching of its short distance behavior to that of the heavy-quark potential at zero temperature, which is known from lattice studies [87, 104, 55] and in perturbation theory [105, 106, 107]. As it is usually the case in the renormalization process of quantities at finite temperature, their renormalization takes place at energy scales μ (renormalization scale) where the temperature does not influence the theory, so that $\mu \gg T$ [11, 12]. According to our suggestion, the 2-point Polyakov loop correlation functions can be renormalized at short distances, where for example $1/r \gg T$ ($r \ll 1/T$). In conclusion, we suppose that

$$T\frac{d\Delta F_i(r,T)}{dT} = 0 \qquad (i = 1, 8) \tag{2.14}$$

is fulfilled at sufficiently small distances r. This equation can be considered as the renormalization group equation for the renormalized free energies. We note here, that in general the temperature variation of the free energy yields the entropy. Relation (2.14) is thus closely related to the term $T\Delta S_i$ in the free energies and tells us that the finite temperature free energy at short distances is indeed given by the potential energy. Therefore we pay attention to the short distance behavior of the correlation functions as we expect that at small distances its renormalization can be obtained.

Once having performed the renormalization of the Polyakov loop correlation function at short distances, also the large distance behavior of the finite temperature part of the free energy is fixed through

$$|\langle \mathrm{Tr}L \rangle| = \lim_{|\mathbf{x}-\bar{\mathbf{x}}|\to\infty} \Big(\langle \mathrm{Tr}L(\mathbf{x}) \mathrm{Tr}L^\dagger(\bar{\mathbf{x}}) \rangle \Big)^{1/2}. \tag{2.15}$$

[3] A different way how to relate the Polyakov loop to the free energy is suggested in Ref. [22]. In this approach, the Polyakov loop L is estimated as the propagator of an infinitely heavy test charge in a background gauge field. Although the particle is infinitely heavy, which means static, it will carry the Aharonov-Bohm phase factor. This is the Polyakov loop. Thus, the expectation value of the traced Polyakov loop, $\langle \mathrm{Tr}L \rangle$, is the expectation value of the trace of the propagator. For instance, confinement then means that the trace of this propagator vanishes.
In chapter 4 of this reference one also finds a comfortable review of what is known on the renormalization of $\mathrm{Tr}L$.

In general no additional divergences get introduced in (2.15) at finite temperature once the correlation function on the right hand side of (2.15) is properly fixed at small distances. We suggest that this property can be utilized to extract the renormalized Polyakov loop from the large distance behavior of the renormalized 2-point Polyakov loop correlation function.

Clearly, this renormalization prescription corresponds to some *effective renormalization constant* $Z^R(g^2)$ for the Polyakov loop (which in general will depend on the color and flavor group of the theory) and it is worth noting that the Polyakov loop and its n-point correlation functions are composite operators and as such need their own renormalization constants and conditions on the lattice. It turns out, however, that once having fixed this effective renormalization constant for the Polyakov loop operator on the lattice, the renormalization scheme applies to any n-point Polyakov loop correlation function calculated at finite temperature on the lattice. This important feature follows from the hierarchic divergence structure of the n-point Polyakov loop correlation functions, which allows to remove the divergences through one single renormalization constant. Therefore it is indeed sufficient to calculate only 2-point Polyakov loop correlation functions at finite temperature in order to extract both, the renormalized Polyakov loop and the renormalization constant. In order to avoid here any misunderstandings, however, we note that the renormalization constant $Z^R(g^2)$, that will be determined by us[4], renormalizes the operator while the action in our MC calculation is still the bare lattice gauge action. We therefore have called $Z^R(g^2)$ the effective renormalization constant for the Polyakov loop.

In the renormalization scheme described above, however, the renormalized quantities are defined only up to an arbitrary overall constant (c) which fixes the heavy quark potential at zero temperature. In the case of 2-point correlation functions we will fix this constant through a definite (but arbitrary) choice of the zero temperature heavy quark potential relatively to the potential of the string picture at large quark antiquark separations. The exact definition, however, of the zero temperature heavy quark potential used in our discussions will be presented in the analysis of Sec. 2.3.2. We simply clarify here, that any renormalization group equation contains operations in terms of derivatives with respect to some scales $(T, r, ...)$, see for instance (2.14), and thus a constant shift will not affect the dynamics of such kind of equations. In this sense, $c = 0$ (Cornell potential) appears as a 'natural' choice.

In order to be definite now, we introduce the renormalized Polyakov loop L^R and its effective renormalization constant $Z^R(g^2)$ on the lattice in spirit of (2.2) through

$$L^R(\mathbf{x}) \;\equiv\; Z_L \prod_{x_0=1}^{N_\tau} Z_U U(x_0, \mathbf{x}) \;=\; \left(Z^R(g^2)\right)^{N_\tau} L(\mathbf{x}), \tag{2.16}$$

where $(Z^R(g^2))^{N_\tau} = Z_L (Z_U)^{N_\tau}$. In this notation g is the bare coupling which is related to

[4] A different renormalization concept from ours has recently been suggested in Ref. [101]. They calculate the renormalized Polyakov loop from the divergence structure given through Eq. (2.10) using different temporal lattice spacings. They find, in contrast to us, explicit temperature dependent renormalization constants.

the lattice coupling β via $\beta = 2N/g^2$. We note that the multiplication of the renormalization constant in the lattice operator respects the center symmetry of $SU(N)$. Moreover, (2.16) implies ($\mathbf{x} \neq \bar{\mathbf{x}}$)

$$\begin{aligned} \left\langle \mathrm{Tr}L^R(\mathbf{x})\mathrm{Tr}L^{R\dagger}(\bar{\mathbf{x}}) \right\rangle &= \left(Z^R(g^2)\right)^{2N_\tau} \left\langle \mathrm{Tr}L(\mathbf{x})\mathrm{Tr}L^\dagger(\bar{\mathbf{x}}) \right\rangle \\ &= \exp\left(-\frac{\Delta F_{q\bar{q}}(r,T)}{T}\right). \end{aligned} \tag{2.17}$$

The behavior of (2.17) at infinite separations of the quark and antiquark sources leads to the renormalized Polyakov loop expectation value as the large distance behavior is controlled by (2.15). In the language of the renormalized quantities this relation can be rewritten as

$$\frac{\Delta F^\infty_{q\bar{q}}(T)}{T} \equiv \lim_{r\to\infty} \frac{\Delta F_{q\bar{q}}(r,T)}{T} = -\ln|\langle \mathrm{Tr}\left(Z^R(g^2)\right)^{N_\tau} L\rangle|^2 = -\ln|\langle \mathrm{Tr}L^R\rangle|^2. \tag{2.18}$$

At this point of our discussion some comments are in order: First of all we note that (2.18) respects the usual color structure of a quark antiquark pair. In fact, it can form a color singlet or a color octet state ($N \equiv 3$). However, if the separation between the quark sources becomes large, the relative orientation of the charges in color space will not influence the screening of the individual charges. Consequently, the expectation value of the renormalized Polyakov loop, which, with respect to (2.18), can be estimated from

$$|\langle \mathrm{Tr}L^R\rangle| = \exp(-\Delta F^\infty_{q\bar{q}}(T)/2T) = \exp(-\Delta F_q(T)/T), \tag{2.19}$$

does not reflect a particular color structure. Moreover, its magnitude is properly related to the difference in free energy $\Delta F_q(T)/T$ due to the presence of one single heavy-quark placed into the gluonic heat bath. In this spirit the renormalized Polyakov loop is related to the confining/deconfining properties of the free energies rather than to the formal Z_N symmetry properties[5] of $\mathrm{Tr}L$. The expectation value of the renormalized Polyakov loop defined in (2.19) will vanish below T_c as $\Delta F_{q\bar{q}}(r\to\infty,T)$ will signal confinement in the pure gauge theory while in the case of full QCD $|\langle \mathrm{Tr}L^R\rangle|$ will lead to finite values even in the confinement phase. In this case, $\Delta F_{q\bar{q}}(r,T)$ will reflect the string breaking property. However, as $\Delta F_q/T$ will diverge in the limit $T \to 0$ in any case, a vanishing expectation value of the renormalized Polyakov loop will follow at $T = 0$ also in full QCD.

Secondly we note, that due to (2.18) also the renormalization constant can be deduced. If one is interested in a renormalization prescription of the Polyakov loop in the high temperature phase only, one may estimate $Z^R(g^2)$ in terms of $(|\langle \mathrm{Tr}L^R\rangle|/|\langle \mathrm{Tr}L\rangle|)^{1/N_\tau}$ [93]. It is more convenient, however, to estimate the renormalization constant for the Polyakov loop correlation functions from

$$Z^R(g^2) = \exp\left(-\frac{\Delta F_{q\bar{q}}(r,T) - T\ln\langle \mathrm{Tr}L(\mathbf{x})\mathrm{Tr}L^\dagger(\bar{\mathbf{x}})\rangle}{2TN_\tau}\right), \tag{2.20}$$

as this relation is properly defined also below T_c. In fact, (2.20) is related to the shift $C_{q\bar{q}}$ of the bare quark antiquark free energy that leads to the renormalized free energy,

[5] A recent discussion of the Z_3 symmetry and its relation with the confinement deconfinement phase transition is given in [108].

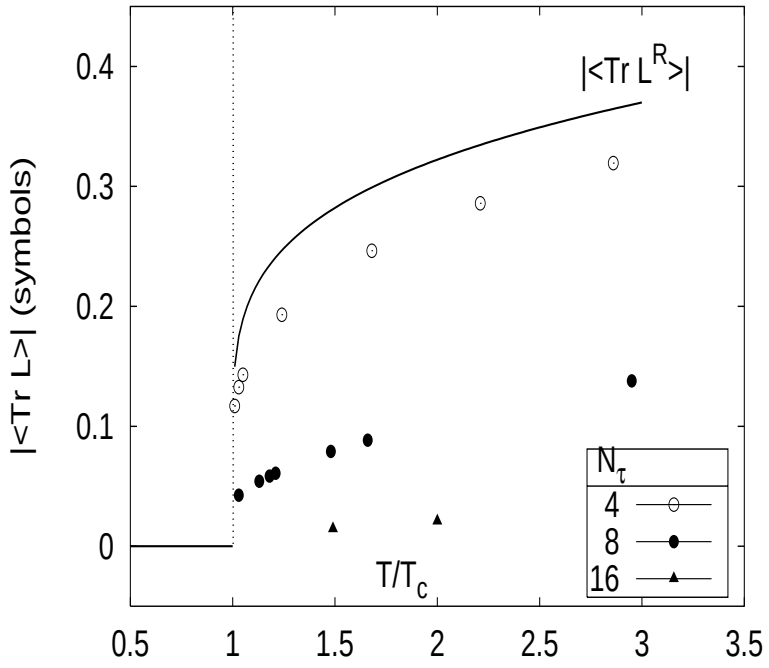

Figure 2.2: The bare Polyakov loop expectation value as a function of the physical temperature. The data points show the bare lattice results deduced in MC studies of $SU(3)$ gauge theory on lattices of size $32^3 \times N_\tau$ with $N_\tau = 4, 8, 16$. The black line illustrates the universal curve of the renormalized Polyakov loop that we expect from a multiplicative renormalization, $|\langle \mathrm{Tr} L^R \rangle| = |\langle Z^{N_\tau} \mathrm{Tr} L \rangle|$.

$C_{q\bar{q}} \equiv \Delta F_{q\bar{q}} - \Delta F^{bare}_{q\bar{q}}$. It can therefore also be used to give a renormalization prescription for the Polyakov loop correlation function below T_c, as for instance

$$C_{q\bar{q}} = -2TN_\tau \ln Z^R(g^2) \qquad (\forall T). \tag{2.21}$$

In conclusion, the renormalization prescription suggested by us can be used to renormalize the 2-point Polyakov loop correlation function below and above T_c once the renormalization constant $Z^R(g^2)$ is known. And thirdly we note that the projection operators introduced in (1.30) do not act on the renormalization constant. This leads to the fact, that the renormalization constant cancels out not only the divergence in the 2-point Polyakov loop correlation functions of the traced Polyakov loop, but in the same way also renormalizes 2-point Polyakov loop correlation functions of the untraced Polyakov loop. It follows from (1.27) and (1.28) that the color singlet, the color octet and the color averaged quark antiquark free energies will stay finite and well-behaved in the continuum limit through the introduction of the effective renormalization constant in the untraced Polyakov loop, $Z^R(g^2)L$. In conclusion, the 2-point Polyakov loop correlation functions for the color singlet, color octet and color averaged free energy produce equal divergent structures.

Let us finally discuss Fig. 2.2 as it illustrates the renormalization scheme we have suggested

above. The data points in that figure show the (bare) Polyakov loop expectation values, $|\langle \mathrm{Tr} L \rangle|$, calculated in MC studies on lattices of size $32^3 \times N_\tau$ with $N_\tau = 4, 8$ and 16. It can be seen from that figure, that the expectation values of the bare Polyakov loop calculated on the lattices with larger temporal extents ($N_\tau = 8, 16$) results in smaller values than the data from the lattice with a smaller temporal extent ($N_\tau = 4$). This suppression of the bare lattice values with increasing N_τ is due to the presence of linear UV divergences as described through (2.10). We suggest here that this effect can be absorbed through a multiplicative renormalization with a renormalization constant $Z^R(g^2)$ introduced in (2.16). Following the discussion above, a proper renormalization of the 2-point correlation function at short distances will result in a unique behavior of the renormalized Polyakov loop expectation value, $|\langle Z^R(g^2) \mathrm{Tr} L \rangle|$, on lattices with finite temporal extent N_τ as the N_τ dependence of $|\langle \mathrm{Tr} L \rangle|$ gets removed through renormalization. In Fig 2.2 we have illustrated this property through the black line: From the definition (2.19) it follows that the renormalized Polyakov loop expectation value is identical to zero at temperatures below T_c, as the free energy is controlled by confinement, while $|\langle \mathrm{Tr} L^R \rangle|$ will approach finite values due to the presence of color screening, which is consistent with deconfinement. Usually the (bare) Polyakov loop expectation value is used as an order parameter for the confinement deconfinement phase transition and as such its temperature dependence should not only indicate the phase transition but should also indicate the order of the phase transition. Since the renormalized Polyakov loop is related to the free energy ΔF_q through Eq. (2.18) we indeed expect that $\langle \mathrm{Tr} L^R \rangle$ is also sensible to the order of the phase transition. In the case of $SU(3)$, the first (or weakly first) order phase transition will result into a discontinuity of $|\langle \mathrm{Tr} L^R \rangle|$ at T_c. This feature is shown in Fig. 2.2 through the jump of the black line at T_c. Moreover, we expect that the renormalized Polyakov loop expectation value will lie above the bare lattice data, $|\langle \mathrm{Tr} L^R \rangle| \gtrsim |\langle \mathrm{Tr} L \rangle|$, as the suppression through the divergence in spirit of (2.10) is removed. Because of this reason we have drawn the line that illustrates the renormalized Polyakov loop expectation value *above* the bare data. In this spirit, the bare data in Fig. 2.2 tell us already that the discontinuity of $|\langle \mathrm{Tr} L^R \rangle|$ will be larger than 0.1 at T_c.
In the following we discuss this issue in more detail.

2.3 Renormalization prescription for 2-point Polyakov loop correlation functions

At distances much shorter than the inverse temperature, $rT \ll 1$, the dominant scale is set by the distance r and the running coupling will be controlled by this scale, $g(r, T) \simeq g(r, T = 0) \equiv g(r)$. As the quark antiquark separation becomes smaller than the inverse QCD-Λ-scale, $r \ll 1/\Lambda_{QCD}$, ordinary zero temperature perturbation theory should be valid. In this limit, the color singlet and color octet free energies are dominated by *one-gluon exchange* [9, 58]. In the following subsections we analyze different aspects of the short distance properties of the finite temperature heavy quark free energy which show us that the quark antiquark free energies are indeed dominated by the distance scale. In fact, we deduce some (new) features and relations which will lead us to the renormalization

prescription for the Polyakov loop correlation functions and the Polyakov loop.

2.3.1 Relations between ΔF_1, ΔF_8 and $\Delta F_{q\bar{q}}$

As we have seen in the first chapter of this thesis, the lattice data for the color singlet free energy are attractive while the data for the color octet free energy behave repulsive at small r. These properties are indeed expected in leading order (zero temperature) perturbation theory. Due to this feature, the color averaged free energy will be dominated by the contribution of the color singlet free energy as in this limit the repulsive contribution from the color octet free energy gets exponentially suppressed in the 2-point correlation function and thus also in the color averaged free energy determined from the logarithm of this correlation function. Since additional linear terms in the free energies, which signal confinement below T_c, become negligible at short distances, too, we conclude from Eq. (1.33)

$$\lim_{r\to 0} \left(\Delta F_{q\bar{q}}(r,T) - \Delta F_1(r,T)\right) \quad = \quad T \ln N^2 \tag{2.22}$$

at *all* temperatures [73]. This is a remarkable relation: First of all it is important to realize that this relation indeed holds for the *finite contributions* to the correlation functions $\langle \mathrm{Tr} L(\mathbf{x}) \mathrm{Tr} L^\dagger(\bar{\mathbf{x}})\rangle$ and $\langle \mathrm{Tr} L(\mathbf{x}) L^\dagger(\bar{\mathbf{x}})\rangle$ as the divergences are eliminated by identical renormalization constants in both operator correlations. Secondly we note, that from this relation it follows that the color averaged as well as the color singlet free energies will behave similar at small distances, $\delta F_1 \simeq \delta F_{q\bar{q}}$. This property implies that, *up to the temperature dependent constant shift* in (2.22) and exponentially suppressed terms, the color averaged free energy will agree with the zero temperature heavy quark potential, $V_{q\bar{q}}(r)$, too. For instance, from the leading order perturbative contribution to the color singlet free energy we expect a Coulomb-like behavior at short distances,

$$\delta F_{q\bar{q}} \quad \simeq \quad \delta F_1 \quad \simeq \quad -\frac{g^2}{3\pi r} + \mathcal{O}(g^4). \tag{2.23}$$

Note that this power-like behavior at short distances is quite different from the perturbative high temperature behavior of the color averaged free energy at large distances ($rT \gg 1$), where the dominant scale is set by the temperature. In this case, high temperature perturbation theory is used to show that the leading order contribution to the color averaged free energy is given by *two-gluon exchange* [57, 9]. In a somewhat loose sense it thus often is argued that $\Delta F_{q\bar{q}}/T \simeq (\Delta F_1/T)^2$ [57, 9] (instead of $\delta F_{q\bar{q}}/T \simeq (\delta F_1/T)^2$) at large quark antiquark separations. In spirit of our previous discussion, however, this statement has to be formulated a bit more carefully as $\Delta F(r \to \infty, T)$ in general will not be zero. When fixing the overall renormalization of the free energies at short distances one no longer has the freedom to assume that they approach zero at large distances. Actually, the color averaged as well as the color singlet and color octet free energies will approach a finite value as function of temperature at large quark antiquark separations. Moreover we note that due to (2.22) it is obvious that both, the color singlet and color averaged free energies, will coincide at *zero temperatures*. In this limit both finite temperature free

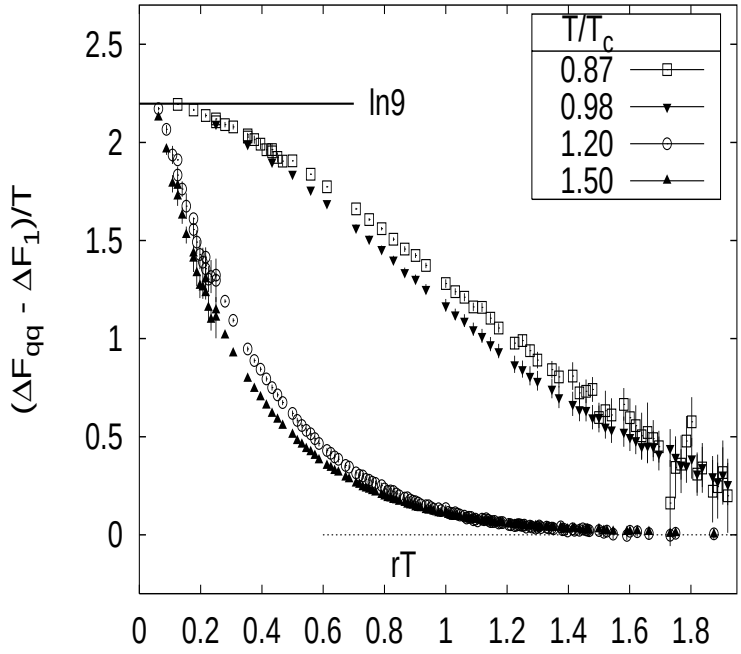

Figure 2.3: The difference of the color averaged and color singlet heavy quark free energies in units of the temperature calculated at temperatures below and above the critical temperature. This figure includes lattice data from simulations with lattices of size $32^3 \times N_\tau$ with $N_\tau = 4, 8$ and 16.

energies will coincide with the heavy quark potential as the entropy contribution to the free energy cancels out at $T = 0$ ($F = U - TS$).

Let us finally discuss the physical interpretation of the difference in free energies at short distances. We argue that the difference $T \ln N^2$ in the free energies is due to a *difference in the entropy contributions* in the free energies: $\ln N^2$ has the typical form of an entropy if one identifies N^2 with the sum over the possible color configurations. More precisely, we expect $\Delta S_1(r \to 0, T) - \Delta S_{q\bar{q}}(r \to 0, T) = \ln 9$. Indeed this follows from standard thermal relations as in general the entropy (S) is related to the free energy (F) via $S = -\partial F/\partial T$. As we do not expect thermal modifications from the medium on the quark antiquark state at short distances, this difference in entropy is supposed to equal the difference in entropy of the quark antiquark state at zero temperature. A recent discussion of the entropies of quark states can be found in [109].

Before we analyze Eq. (2.22) with our lattice data for the free energies, let us also briefly comment on our expectations about the large distance behavior of $\Delta F_{q\bar{q}} - \Delta F_1$: As mentioned above, we do not expect that the different orientations of the charges in color space will influence the screening of the individual charges. Consequently, we expect that the *finite contributions* of the color singlet and color averaged free energies as well as of the color octet free energy will *coincide* at large separations of the color charges. In conclusion

we expect

$$\lim_{r\to\infty} \left(\Delta F_{q\bar{q}}(r,T) - \Delta F_1(r,T)\right) = 0 \tag{2.24}$$

at *all* temperatures. Note that a vanishing difference in free energy below T_c, implies that the color averaged, singlet and octet free energies signal confinement, too.

We have analyzed the relation (2.22) in Fig. 2.3 using $SU(3)$ lattice data for $\Delta F_{q\bar{q}}(r,T)/T - \Delta F_1(r,T)/T$ at distances $1/16 \lesssim rT \lesssim 2$ and temperatures close to the critical temperature (below and above T_c). As can be seen in that figure, the difference in free energy approaches zero values at large quark antiquark separations while in the short distance range we find a behavior as described in (2.22): The difference in free energies indeed approaches the value $\ln 9$, which indeed shows that the color averaged free energy is dominated by the contribution of the color singlet free energy at small rT. Thus the lattice data confirm our expectations formulated within (2.22) and (2.24). In fact, deviations from the asymptotic value $\ln 9$ are of less than 10% at $rT \lesssim 0.1$.

What are the consequences of our studies for the renormalization of the finite temperature heavy quark free energies? As we have stressed in our discussion above, the relations (2.22) and (2.24) equally well apply to the finite parts of the 2-point Polyakov loop correlation functions. In conclusion, the *relative normalization of the renormalized quantities* is such that $\Delta F_{q\bar{q}}(r,T)$, $\Delta F_1(r,T)$ and $\Delta F_8(r,T)$ coincide at large separations of the color sources while the different color structures will influence their properties in the short distance regime. Moreover, as the difference in the free energies turns out to be positive at all distances analyzed by us, $\Delta F_{q\bar{q}} - \Delta F_1 \gtrsim 0$, we conclude

$$\Delta F_1 \lesssim \Delta F_{q\bar{q}} \lesssim \Delta F_8 \qquad \forall T. \tag{2.25}$$

We stress again that this relation also implies a confining color octet free energy at temperatures below T_c.

Another instructive way to study the behavior of the finite temperature free energies at short distances was outlined in Sec. 1.3.3 by means of derivatives with respect to r, as undetermined additive renormalization constants cancel in this case. In fact, we separated from the finite temperature free energies the zero temperature part at small distances in terms of the effective coupling. In conclusion, temperature effects from the thermal medium on the color singlet quark antiquark free energies get suppressed in the limit of short distances. Actually, our finite temperature lattice data do not show significant dependencies on any other scale beside the distance scale r. Consequently, the renormalization group equation (2.14) is indeed fulfilled and thus the entropy contributions in the finite temperature free energies are supposed to vanish at small distances. This property suggests that the finite temperature color singlet free energies are given at small distances by the heavy quark potential at zero temperature.

In the following subsection we thus directly compare the finite temperature free energies with the heavy quark potential at short distances. This study will lead us to the formu-

lation of the renormalization prescription for the finite temperature quark antiquark free energies.

2.3.2 Renormalization prescription and continuum limit

In order to compare our lattice data with the heavy quark potential ($V_{q\bar{q}}(r)$) at zero temperature, we first have to specify $V_{q\bar{q}}(r)$. So far, we used the potential at zero temperature in terms of derivatives with respect to distance as undetermined renormalization constants cancel out by this way. In terms of the potential, however, we have to fix this constants. Using lattices with small lattice spacing $V_{q\bar{q}}(r)$ has recently been calculated for $SU(3)$ gauge theory for distances larger than 0.05 fm and the results have been extrapolated to the continuum limit [55]. At distances larger than r_0 (Sommer scale) which is defined through the slope of the heavy quark potential [110]

$$r_0^2 \left(\frac{dV_{q\bar{q}}(r)}{dr} \right)_{r=r_0} = 1.65, \tag{2.26}$$

it is known that $V_{q\bar{q}}(r)$ is well described by a simple linear confining potential corrected by a Coulomb-like term arising from string fluctuations,

$$V_{q\bar{q}}(r) = -\frac{\pi}{12r} + \sigma r \qquad \text{for } r > r_0 \quad \text{with } \sigma r_0^2 = 1.65 - \frac{\pi}{12}. \tag{2.27}$$

For distances smaller than $r_0 \simeq 0.5$ fm we use a polynomial interpolation of the lattice data of Ref. [55] normalized such that the resulting potential smoothly joins the confinement potential for $r > r_0$, i.e. we fix the free constant in the lattice results such that $r_0 V_{q\bar{q}}(r = r_0) = 1.65 - \pi/6$. In fact, this fixing results into the standard Cornell form (2.27). In some cases, however, we also need the potential at smaller distances than $r = 0.1 r_0 \simeq 0.05$ fm. Here we use the perturbative 3-loop calculation of the potential in the so-called qq scheme[6] [107] which agrees well with the lattice calculations up to distances $0.25 r_0$ [107]. For the following discussion we present the distance in physical units [fm] while sometimes we also will give the results in units of $\sqrt{\sigma}$, which is straightforward as both units are related through Eq. (2.27) (since $r_0 = 0.5$ fm). This zero temperature heavy quark potential is shown in Fig. 2.4 as the black line.

A comparison of free energies calculated at finite temperature and short distances with the heavy quark potential at zero temperature is shown in Fig. 2.4. In this figure we have normalized the color singlet quark antiquark free energy such that it lies on top of $V_{q\bar{q}}$ at the shortest distance which can be resolved on the lattice with temporal extent N_τ. From our discussion above it follows that rather than the color averaged free energy the color singlet free energy is supposed to become directly comparable to $V_{q\bar{q}}(r)$. Therefore in that figure we refer to lattice data for $\Delta F_1(r,T)$ at short distances and several temperatures below and above the critical temperature, for instance $0.9 \gtrsim T/T_c \gtrsim 12$. As can be seen in Fig. 2.4, the lattice data of the finite temperature color singlet quark antiquark free energies agree well in the range of short distances with the zero temperature heavy quark

[6] Specifying the scheme is necessary here as the 3-loop contribution is scheme dependent.

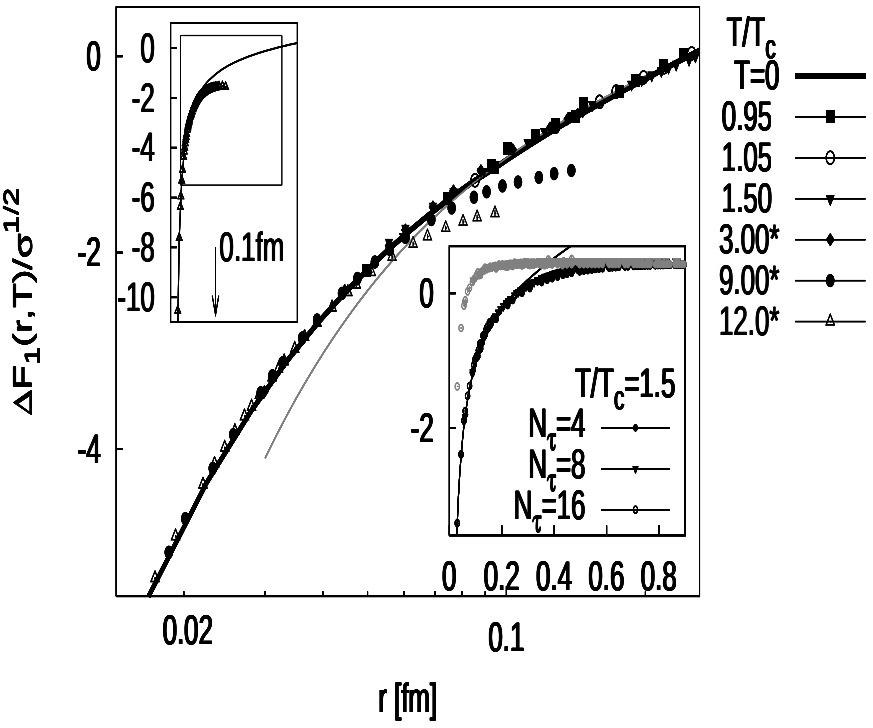

Figure 2.4: Comparison of the finite temperature quark antiquark free energy $\Delta F_1(r,T)$ to the heavy-quark potential at zero temperature. In this figure we have matched the finite temperature free energy at the shortest distance attainable on the lattice to the heavy quark potential at zero temperature, $V_{q\bar{q}}(r)$, from [55] (see the text). $V_{q\bar{q}}$ is shown through the black line. The distance scale r is set to logarithmic (in fm) while the free energy is given in units of the string tension. The grey line indicates the Cornell potential from the string picture [40]. The lattice data at temperatures which are indicated with a star do not contain all data we have calculated on the lattice. We have excluded data as they lie on top of $V_{q\bar{q}}$. The inserted figure at the top corner shows all data we have calculated at $T = 12T_c$. The other inserted figures is explained in the text (in these figures the distance is not logarithmically scaled).

potential once they are normalized to $V_{q\bar{q}}$ at $r = 1/TN_\tau$. We conclude from this that the finite temperature color singlet free energy can indeed be *renormalized* by matching the data at short distances to the heavy quark potential at zero temperature. As no additional divergences are introduced at finite temperature once the free energy is renormalized properly, all divergent self energy contributions are removed [92, 73]. We therefore infer that the *matching prescription* at small distances,

$$\Delta F_1^{\rm match}(r = 1/TN_\tau, T)\Big|_{N_\tau} \quad = \quad V_{q\bar{q}}(r = 1/TN_\tau) \tag{2.28}$$

provides a proper *renormalization prescription* for the finite temperature color singlet quark antiquark free energy. As this renormalization prescription fixes the difference $C \equiv \Delta F_1 - T\ln\langle {\rm Tr} L(\mathbf{x}) L^\dagger(\bar{\mathbf{x}})\rangle$, equally well the color octet and color averaged quark antiquark free energy are fixed at finite temperature. Moreover, the asymptotic large dis-

tance behaviors of the free energies are fixed, too, which leads to the renormalization of the Polyakov loop expectation value on the lattice through (2.19).

In general, a proper renormalization of some quantity on the lattice is equivalent to a well-behaved continuum limit of this quantity. In terms of the color singlet free energy, we expect that

$$\lim_{N_\tau \to \infty} \left(\Delta F_1^{\mathrm{match}}(r,T)\Big|_{N_\tau} \right) = \Delta F_1^{\mathrm{ren}}(r,T) \tag{2.29}$$

is well behaved. Actually, this limit defines the *continuum limit of the renormalized finite temperature free energy*. In order to analyze the behavior of the finite temperature free energy in the continuum limit, we have calculated the color singlet free energy at fixed physical temperatures on lattices with different temporal extensions. As an example we show in the insertion of Fig. 2.4 the free energy ΔF_1 (black symbols) and $\Delta F_{q\bar{q}}$ (grey symbols) at a fixed temperature $T/T_c = 1.5$ calculated on lattices with different temporal extensions, $N_\tau = 4, 8$ and 16. The color singlet free energy has been normalized to the zero temperature potential at $rT = 1/N_\tau$ for each N_τ separately. The resulting shift of the bare lattice free energy to the normalized one also normalizes the lattice data for the color averaged free energy shown in that figure. It can be seen from that figure that both, the color singlet and color averaged free energy, coincide separately for each channel at small and large distances although lattices with different N_τ were used. In fact, this implies a well-behaved continuum limit as $\beta = 1/T$ is fixed while N_τ grows.

For $N_\tau = 8$ we have studied the properties of ΔF_1 in the continuum limit more closely by varying the distance (r_{match}) at which the finite temperature color singlet free energy is matched to the heavy quark potential, for instance $r_{match}T = 1/N_\tau, \sqrt{2}/N_\tau, \sqrt{3}/N_\tau, 2/N_\tau, ...$ This is quite similar to calculating the renormalized free energy on lattices with different N_τ. For instance, the shortest distance that can be resolved on a lattice with $N_\tau = 4$ coincides with the distance at $rT = 2/N_\tau$ on a lattice with $N_\tau = 8$, and so on. We have analyzed the influence of the different matching conditions on the free energy at the largest distance that can be resolved on the lattice with spatial extent N_σ, $\Delta F_1(N_\sigma/2, T)$. From that kind of analysis we draw mainly two conclusions: First of all, calculations with $N_\tau = 4$ do not show significant deviations from calculations with $N_\tau = 8$ as the value $\Delta F_1(N_\sigma/2, T)$ stays unaffected from the variation of r_{match}. Indeed, the deviations of $\Delta F_1(N_\sigma/2, T)$, deduced by matching at $r_{match}T = 1/N_\tau, \sqrt{2}/N_\tau, \sqrt{3}/N_\tau, 2/N_\tau$ on the lattice with $N_\tau = 8$, from $\Delta F_1(N_\sigma/2, T)$ deduced from a matching at $rT = 1/N_\tau$ with $N_\tau = 4$ are smaller than the statistical errors on $\Delta F_1(N_\sigma/2, T)$ at a temperature $T = 1.5T_c$. Similar properties can be seen at all temperatures analyzed by us. Moreover, we note that the continuum limit is approached from above. This property follows from a comparison of the values $\Delta F_1(N_\sigma/2, T)$ on lattices with different N_τ and larger matching distances. In fact, a matching of the free energy at larger distances to the heavy quark potential in general leads to an enhancement of $\Delta F_1(N_\sigma/2, T)$. This property can indeed be deduced from Fig. 2.4. In other words, lattice calculations with smaller N_τ than 4 may result in an *enhancement* of the renormalized free energy in the temperature range covered by us.

In conclusion, a proper renormalization of the finite temperature free energy at high temperatures in general requires lattice calculations with lattices of large temporal extent, N_τ. This property is closely related to the renormalization condition $r \ll 1/T$, at which the thermal system effectively behaves zero temperature like. It follows from the discussion above that $N_\tau = 4$ is indeed close to this limit.

In the remaining three sections of this chapter we first discuss the renormalized 2-point Polyakov loop correlation functions below and above the critical temperature, present our lattice results for the renormalized Polyakov loop expectation value and generalize our approach to n-point functions. We furthermore deduce the corresponding effective renormalization constant as a function of the bare lattice coupling.

2.4 Renormalized quark antiquark free energy

It follows from our discussion in the last sections that the matching to the zero temperature heavy quark potential can be performed much easier with the color singlet free energies than with the color averaged ones. In particular, they allow to perform the matching to the heavy quark potential at zero temperature already with finite temperature free energies calculated on lattices with temporal extent $N_\tau = 4$. In this section, and if not explicitly noted differently throughout the whole thesis, we fix the free constant in the heavy quark potential as described above. It should be obvious that we refer from now to the renormalized free energies. Therefore, we will not explicitly indicate this in our notations.

2.4.1 A consistent picture of renormalized PLCs

Lattice results for the renormalized quark antiquark free energies in each color channel are shown in Fig. 2.5 as an example at one temperature below and one above T_c. Here we may distinguish three different distance regions characterized through different behaviors of the free energies at both temperatures [111]:

At *large quark antiquark distances*, i.e. for $r \gtrsim 4\sqrt{\sigma} \simeq 2$ fm, the renormalized color singlet (ΔF_1), the color octet (ΔF_8) and the color averaged ($\Delta F_{q\bar{q}}$) quark antiquark free energies coincide at both temperatures. This property of the renormalized free energies is consistent with our discussion presented above (see section 2.2). At the temperature below T_c, this figure once more shows that the quark antiquark free energies are dominated by one single, temperature dependent string tension for all color channels at large separations. In the *intermediate distance* regime, i.e. for $0.5 \lesssim r\sqrt{\sigma} \lesssim 4$ (0.25 fm $\lesssim r \lesssim 2$ fm), the different color structures of the free energies become visible. At temperatures below T_c we note that the renormalized free energies lead in all color channels to an enhancement compared to the heavy quark potential at zero temperature. This feature is consistent with the observations in current studies of the free energies in $SU(2)$ [23, 69]. At *small distances*, i.e. for $r\sqrt{\sigma} \lesssim 0.5 \simeq 0.25$ fm, the different color structures of the free energies begin to dominate the picture. In our renormalization prescription the color singlet free energy coincides with the potential at zero temperature at both temperatures while the

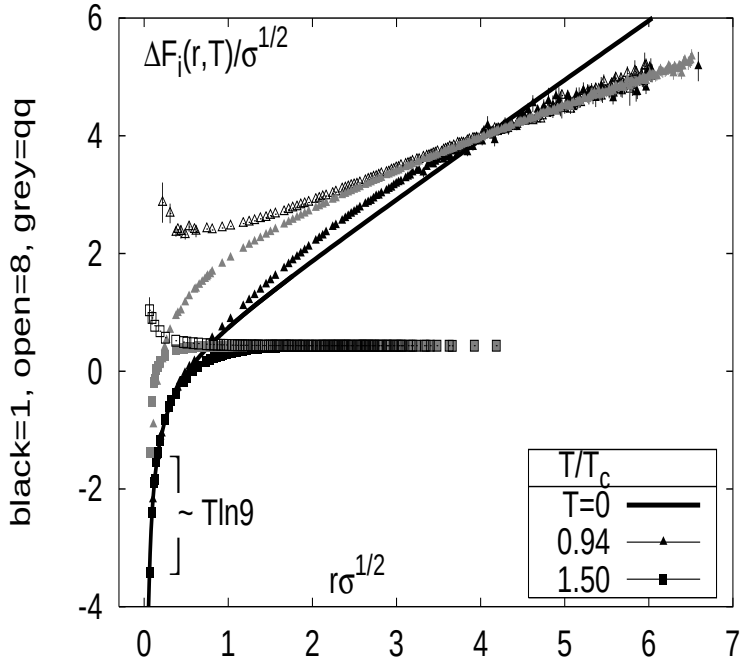

Figure 2.5: The renormalized quark antiquark free energies in $SU(3)$ as a function of $r\sigma^{1/2}$ (σ being the string tension at $T = 0$). The filled black symbols indicate the color singlet free energies and the open symbols the color octet ones. The color averaged free energies are given by the grey (filled) symbols. The black curve denotes the heavy quark potential; for the definition of $V_{q\bar{q}}(r)$ see the text. In this figure we summarize lattice data from simulations on lattices of size $32^3 \times 4, 8, 16$ and $64^3 \times 4$.

color octet free energy behaves repulsive. The latter property is in fact expected from leading order perturbation theory. The renormalized color averaged free energy respects the relation $\Delta F^R_{q\bar{q}} - \Delta F^R_1 = T \ln 9$ at short distances. In Fig. 2.5 we have indicated this property with the bracket shown at small distances.

In Fig. 2.5 we have selected temperatures which characterize the behavior of the free energies close to T_c. The fragmentation in the distance ranges presented above, however, depends substantially on the temperature ranges which are under consideration. In general, the limits given above will be shifted to larger distances at lower temperatures while they will be shifted to smaller values when analyzing higher temperatures.

Finally we note that the ordering of free energies suggested in Eq. (2.25) is indeed realized for the renormalized free energies: It can be seen from Fig. 2.5 that the color octet free energy provides an upper limit for the color averaged free energy which itself gives an upper boundary for the color singlet free energy at any finite T and r. This property can be observed at any temperature analyzed by us. In fact, in (2.25), the statement '$\gtrsim$' can be replaced with '=' in the asymptotic case, $r \to \infty$, while in the zero temperature limit, $T \to 0$, we expect $\Delta F_8(r, 0) > \Delta F_{q\bar{q}}(r, 0) = \Delta F_1(r, 0) = V_{q\bar{q}}(r)$ at any finite distance r.

2.4.2 More on renormalized PLCs

In order to analyze the influence of the thermal medium on the quark antiquark free energies in each color channel in more detail, we have plotted in Fig. 2.7 the free energies separated in the different color channels at several temperatures above and below T_c. We discuss first the thermal effects on the free energies below T_c (see the left column of that figure) and will then analyze the temperature effects above T_c (see the right column of this figure).

We discuss the color singlet (A), the color octet (B) and the color averaged free energy (C) at temperatures *below the deconfinement phase transition temperature*: At short distances, the temperature dependence of the color singlet free energy appears to be much smaller than in the case of the color octet and color averaged free energies. In fact, the influence of the thermal medium on $\Delta F_1(r,T)$ almost vanishes at separations $r\sqrt{\sigma}$ smaller than 1.5, while at such small distances $\Delta F_8(r,T)$ still shows a strong temperature dependence. We argue, however, that these effects at small distances result from the finite temperature averaging involved through Eq. (1.32). In fact, we have noted in Sec. 1.3.3 that the finite temperature color octet free energies (in terms of derivatives with respect to distance) do not show temperature effects at small distances. Thus, the observed temperature dependencies at small distances are specific to our matching condition. Actually, we also expect to find a temperature dependence in the color averaged free energy arising from the constant shift, $T\ln 9$ (see (2.22)). This effect, however, appears to be rather small at small distances at the temperatures below T_c. This can be explained by the fact that the difference in the temperatures of the shown free energies is small, $0.9 \gtrsim T/T_c \gtrsim 0.98$. We analyze the color averaged free energies separately in the next subsection with Fig. 2.6 in more detail.

At intermediate distances we realize that the enhancement in the finite temperature free energy compared to the heavy quark potential is visible in all color channels and at all temperatures analyzed by us. Moreover, while the color singlet free energy shows an almost temperature independent enhancement up to $r\sqrt{\sigma} \gtrsim 2$, the enhancement[7] of the color octet and color averaged free energies show strong temperature dependencies. When going to large distances, however, the free energies cross the zero temperature heavy quark potential and the differences in the different color channels vanish. In fact, at such large distances, i.e. for $r\sqrt{\sigma} \gtrsim 2$, the *naively expected temperature ordering* of the free energies,

$$\Delta F_i(r,T_1) \;>\; \Delta F_i(r,T_2) \qquad \text{for } T_1 \;<\; T_2 \qquad (i=1,8,q\bar{q}), \tag{2.30}$$

is found for the temperatures below T_c.

Lattice results for the renormalized color singlet, color octet and color averaged free energies at temperatures *above the phase transition temperature* are shown in Fig. 2.7 (D), (E) and (F), respectively. From our studies in the last sections it follows that the color

[7] Again this is due to the small temperature interval covered below T_c. Of course we expect ΔF_1 to approach the $T=0$ potential at all distances in the small T limit.

Estimate of the screening radius r_{screen}				
T/T_c	β	$\Delta F_{q\bar{q}}(r \to \infty, T)/T$	$r_{screen}T$	r_{screen}[fm]
1.03	4.5592	1.460 (42)	0.77 (1)	0.56 (1)
1.20	4.6605	0.914 (16)	0.74 (1)	0.46 (1)
1.50	4.8393	0.506 (24)	0.77 (1)	0.39 (1)
3.00	5.4261	-0.030 (10)	0.94 (2)	0.24 (1)
6.00	6.0434	-0.184 (16)	1.05 (5)	0.13 (3)
9.00	6.3910	-0.200 (06)	1.12 (2)	0.09 (1)
12.0	6.6450	-0.202 (08)	1.14 (3)	0.07 (2)

Table 2.1: Change in free energy due to the presence of a heavy quark antiquark pair in a thermal heat bath. The table gives results for $\Delta F_{q\bar{q}}(r \to \infty, T)/T$ obtained in calculations on a $32^3 \times 8$ lattice and the screening radius r_{screen} defined through (2.31). In order to set the physical scale we used $T_c/\sqrt{\sigma} = 0.635$ [86] and $\sqrt{\sigma} \simeq 420$ MeV.

singlet free energy is temperature independent at short distances and coincides with the heavy quark potential $V_{q\bar{q}}(r)$. This feature can be seen in (D). It can also clearly be seen from Fig. 2.7 (E) that the color octet free energies at short distances show temperature effects. This is, however, in main parts due to the matching condition in our renormalization scheme. From the same argument it follows that also temperature effects in the color averaged free energy are expected at short distances. These effects are clearly seen in Fig. 2.7 (F).

At intermediate distance we note the break-away of the color singlet free energy from $V_{q\bar{q}}$. In contrast to this, the color averaged and color octet free energy show an enhancement compared to the heavy quark potential. In the case of the color octet free energy this results from its repulsive behavior at short and intermediate distances. In the case of the color averaged free energy this is due to the shift by $T \ln 9$.

On the other hand, at large quark antiquark separations, the color sources get screened by the medium which leads to the finite values $\Delta F_i(r \to \infty)$, $i = 1, 8, q\bar{q}$. As can be seen in Fig. 2.7 (D, E, F), at asymptotic large distances the free energies in the different color channels coincide defining an only temperature dependent finite value $\Delta F^{\infty}_{q\bar{q}}(T)$. We note that the temperature ordering of this value is unique, i.e. $\Delta F^{\infty}_{q\bar{q}}(T_1) > \Delta F^{\infty}_{q\bar{q}}(T_2)$ for $T_1 < T_2$.

Let us finally pay attention to a quite different aspect that can be studied in terms of the renormalized free energy above T_c. In [92] we have argued that the study of free energies can be used to give a rough estimate of the onset radius r_{screen} for color screening. As can be seen in Fig. 2.7, the color singlet quark antiquark free energy changes rapidly from the zero temperature pure Coulomb like behavior at short distances to the constant behavior at large distances. This property reflects the exponential suppression of the free energy due to screening of the two static charges. As this change is so rapid, we suggest to use $\Delta F_{q\bar{q}}(r \to \infty, T)/T$ to define a screening radius r_{screen}, which characterizes the onset of

the screening through the relation

$$\frac{V_{q\bar{q}}(r_{screen})}{T} \equiv \frac{\Delta F_{q\bar{q}}(r \to \infty, T)}{T}. \tag{2.31}$$

Clearly, the values of the free energies in the infinite distance limit do not depend on the color structures. The values of r_{screen} defined in this way are listed in Tab. 2.1. As can be seen, $r_{screen} \simeq 0.5$ fm in the vicinity of the critical temperature, $T_c \simeq 270$ MeV, while r_{screen} drops to 0.1 fm at $T/T_c = 9$. In fact, we expect that the screening radius r_{screen} will drop asymptotically like the inverse Debye mass, i.e. $r_{screen} \sim 1/g(T)T$.

2.4.3 Short distance properties of the color averaged $q\bar{q}$ free energy

We have stressed in the previous sections that the renormalized *color averaged* quark antiquark free energy still shows temperature effects in the short distance limit although the color singlet and color octet free energies will not show temperature dependencies. In the following discussion we pay detailed attention to this property. From Eq. (2.22) we concluded that the color averaged free energy will show a Coulomb-like behavior at short distances, and moreover, that the temperature effect in the color averaged free energy will be given by $T \ln 9$. In order to analyze both properties we *subtract the expected temperature effect* $T \ln 9$ from the renormalized color averaged free energies. In the following we thus study the quantity

$$\Delta\tilde{F}_{q\bar{q}}(r,T) = \Delta F_{q\bar{q}}(r,T) - T \ln 9. \tag{2.32}$$

rather than the renormalized color averaged free energy. This quantity is shown in Fig. 2.6 at several temperatures below and above T_c. We also show in that figure the heavy quark potential, $V_{q\bar{q}}(r)$ (black line). From that figure it can be seen that the subtraction of $T \ln 9$ from the renormalized color averaged free energy indeed compensates the temperature effects at small distances as the data for $\Delta\tilde{F}_{q\bar{q}}(r,T)$ lie on top of each other at short distances although they are calculated at different temperatures. Moreover, a comparison of this finite temperature quark antiquark free energy defined in this way with the heavy quark potential at short distances shows that the shortest distances that can be resolved in our lattice studies lie indeed on top of $V_{q\bar{q}}(r)$. It thus follows that the color averaged finite temperature free energy shows the pure (unscreened) Coulomb-like behavior in the short distance limit. It is worth noting that the drop of the color averaged free energy at such small distances is thus not related to screening. In fact, the quantity defined in (2.32) will stay comparable with the heavy quark potential in the asymptotic limit $r \to 0$. In conclusion, the temperature effects in the renormalized color averaged free energy, $\Delta F_{q\bar{q}}(r,T)$, can be absorbed at small r in a simple term given by $T \ln 9$.

Finally we note that the free energy $\Delta\tilde{F}_{q\bar{q}}(r,T)$ defined in (2.32) does not show an enhancement compared to the heavy quark potential at temperatures below T_c and intermediate distances. Moreover, the temperature ordering of this quantity, $\Delta\tilde{F}_{q\bar{q}}(r,T)$, is quite simple at *all* temperatures and distances:

$$V_{q\bar{q}}(r) \gtrsim \Delta\tilde{F}_{q\bar{q}}(r,T_1) \gtrsim \Delta\tilde{F}_{q\bar{q}}(r,T_2) \qquad \text{for } T_1 < T_2. \tag{2.33}$$

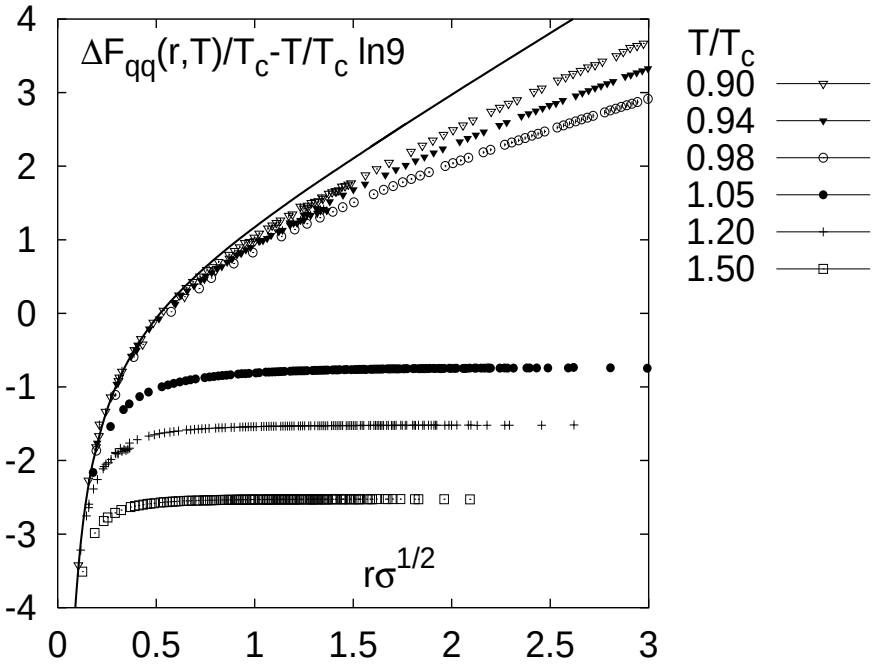

Figure 2.6: The shifted color averaged free energy $\Delta\tilde{F}_{q\bar{q}} = \Delta F_{q\bar{q}} - T\ln 9$ at temperatures below and above the phase transition temperature compared to the heavy quark potential (line). In this figure we utilize data from lattice simulations with lattices of size $32^3 \times N_\tau$ with $N_\tau = 4, 8$ and 16.

In conclusion, the temperature effect in the color averaged free energy becomes trivial at small distances, although it is quite complex at intermediate and large distances.

From our discussion it follows that the matching of the finite temperature free energy to the heavy quark potential can also be performed using the color averaged free energies. In order to get the relative normalization of the different color channels right when doing the matching with these free energies instead of using the color singlet free energy, one has to refer to (2.22). It follows, however, that the matching with the color singlet free energy can be performed much easier than with the color averaged free energy, as ΔF_1 shows a proper Coulomb-like behavior even at larger distances than the color averaged free energies. Indeed, it can be seen in Fig. 2.6 that the finite temperature color averaged free energy breaks away from the heavy quark potential at relatively small distances. Nonetheless it should be conceptually satisfying that the renormalization process discussed here in terms of the color singlet free energy could be equally well be performed in terms of an observable, $\Delta F_{q\bar{q}}(r,T)$, which is given in terms of a manifestly gauge invariant operator.

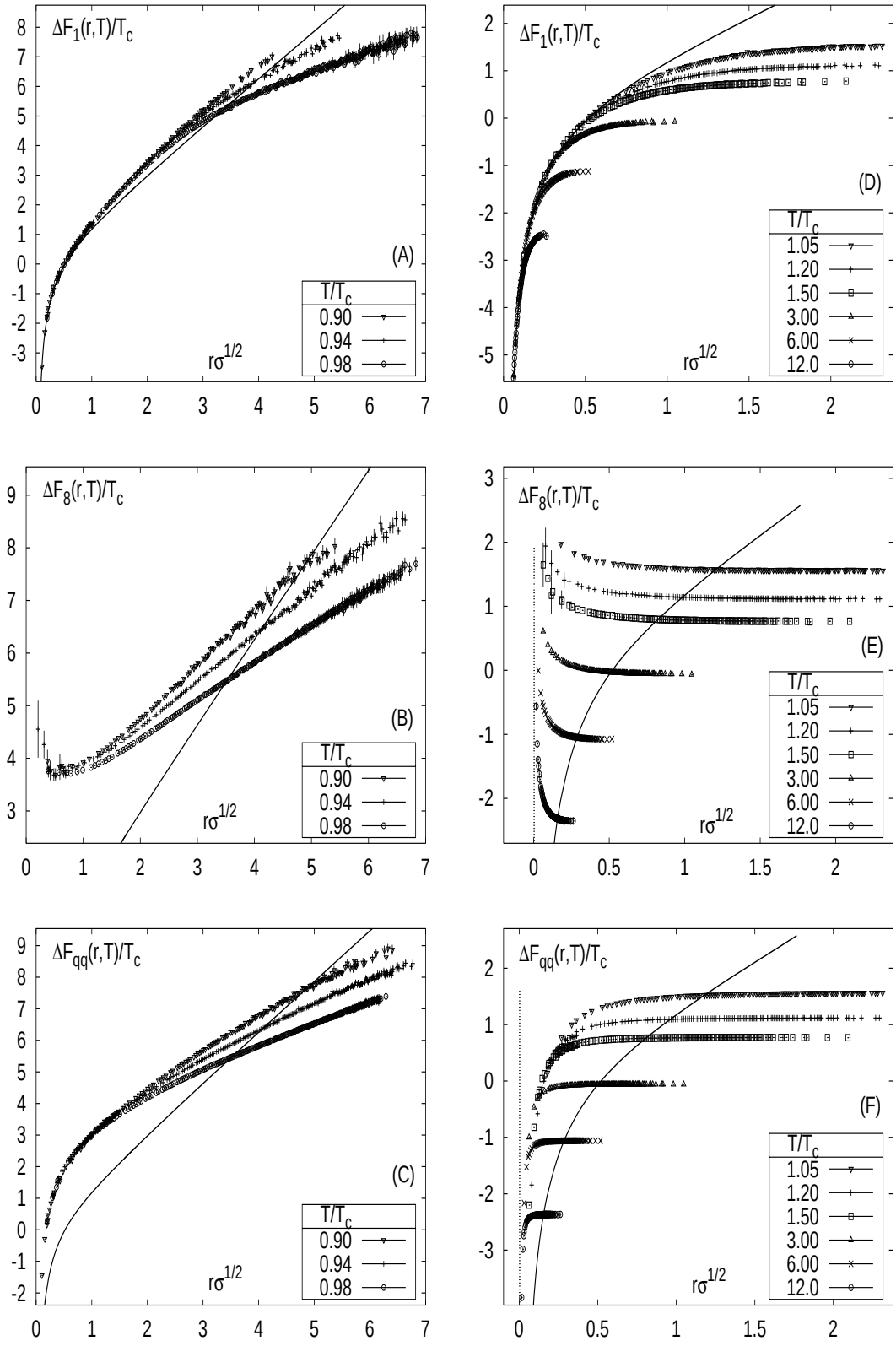

Figure 2.7: The renormalized quark antiquark free energies in the color singlet (A, D), color octet (B, E) and the color averaged channels (C, F) below and above T_c compared to $V_{q\bar{q}}(r)$.

2.5 Towards renormalized n-point PLCs

The analysis of the quark antiquark free energies presented in the previous sections shows that all three, the color singlet, the color octet as well as the color averaged free energies can be renormalized by matching $\Delta F_1(r,T)$ at small quark antiquark separations to the heavy quark potential at zero temperature. In this way all divergent self energy contributions can be removed. Moreover, we have argued that at asymptotic large distances the free energies yield the value $\Delta F^\infty(T)$ defined in (2.18). This value, now only a function of the temperature, leads to a proper estimate of the renormalized Polyakov loop via (2.19), as no additional divergences get introduced at finite temperature once the renormalization has been performed at short distances, i.e. at zero temperature. In order to determine the asymptotic value $\Delta F_{q\bar{q}}(r\to\infty,T)$ we have used the property that all free energies coincide at asymptotic large separations of the color sources. We have used $\Delta F_1(r\to\infty,T)$ rather than the color averaged free energy to determine the asymptotic value at several temperatures above T_c using lattices with different temporal extent, $N_\tau = 4, 8$ and 16. In order to avoid any fits, we have, in fact, used the value of $\Delta F_1(r,T)$ at maximal on-axis separation of the color sources on a lattice with spatial extent N_σ. We thus define $\Delta F^\infty(T) \equiv \lim_{N_\sigma\to\infty} \Delta F_1(N_\sigma/2,T)$. In order to estimate systematic errors on the renormalized free energies we have performed the matching at $rT = 1/N_\tau$ as well as at $rT = \sqrt{2}/N_\tau$. In fact, in this way cut-off effects arising from broken rotational symmetry at non-zero lattice spacing are taken into account as a systematic error and $|\langle \mathrm{Tr} L^R\rangle|$ should allow to estimate the convergence to the continuum limit value within statistical as well as systematic errors.

2.5.1 The renormalized Polyakov loop

Lattice results for the renormalized Polyakov loop calculated from lattices with the different temporal extents N_τ are shown in Fig. 2.8 and listed in Tab. 2.2. From the figure it can be seen that the expectation value of the renormalized Polyakov loop does not show any systematic effects arising from the different finite lattices although lattices with different temporal extent were used. Indeed, the lattice data form a smooth function of the physical temperature. It follows that the renormalized Polyakov loop expectation value defined through our renormalization prescription is well behaved in the continuum limit. This property is of course closely related to the behavior of the 2-point Polyakov loop correlation functions in the continuum limit. Thus a well-behaved $|\langle \mathrm{Tr} L^R\rangle|$ in the $a\to 0$ limit once more shows that the renormalization prescription for the 2-point correlation functions works well at short distances. Indeed, as also the data from the smallest lattice ($N_\tau = 4$) lie on the curve, this property shows that the matching of these data works well in the temperature range analyzed by us. In other words, the values for $|\langle \mathrm{Tr} L^R\rangle|$ deduced at finite a for $N_\tau = 4$ show no significant deviations from the continuum limit values extracted on larger lattices.

It also follows from that figure that the expectation value of the renormalized Polyakov loop acts as an order parameter for the confinement deconfinement phase transition as $|\langle \mathrm{Tr} L^R\rangle|$ is zero below T_c, where the free energy signals confinement, but approaches finite values

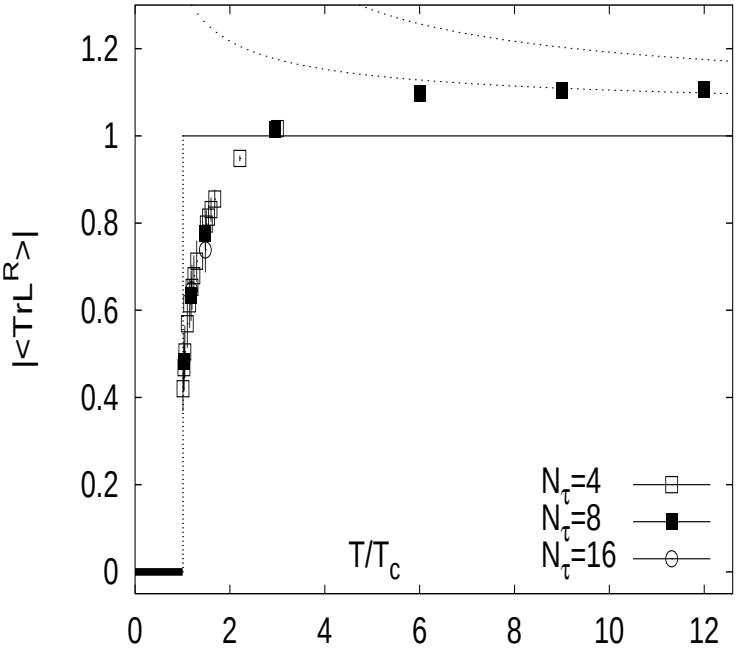

Figure 2.8: The renormalized Polyakov loop expectation value $|\langle \mathrm{Tr} L^R \rangle|$ defined in (2.18) calculated on lattices of size $32^3 \times 4, 8, 16$. The matching to the zero temperature potential utilizes the standard Cornell form. The dotted lines give the perturbative result from Eq. (2.12) where we have promoted the coupling to a 1-loop running coupling with $T_c/\Lambda_{\overline{MS}} = 1.14(4)$ [87, 86]. The scale is set by the low Matsubara frequencies, $\pi T, ..., 4\pi T$.

above T_c. We have indicated a vanishing Polyakov loop expectation value below T_c with the thick black line in that figure; it follows directly from (2.19). Moreover, the renormalized order parameter is related to the difference in free energy arising from the presence of a single colored test charge in the gluonic heat bath, $|\langle \mathrm{Tr} L^R \rangle| \equiv \exp(-\Delta F_q/T)$. In this sense, the renormalized Polyakov loop expectation value works as an order parameter which indeed has a physical meaning. Finally we note that approaching T_c from above the renormalized Polyakov loop expectation value approaches a finite value. This property signals a (weakly) first order phase transition. We note that the discontinuity of $|\langle \mathrm{Tr} L^R \rangle|$ at T_c is about 0.4 which indeed is much larger than the jump at T_c which the bare lattice data show (see Fig. 2.2). We thus find $\Delta F_q \simeq 0.9 T_c \simeq 240$ MeV.

The (free) energies are defined only up to an additive normalization which has been fixed at zero temperature. In fact, the renormalized Polyakov loop is only fixed up to a multiplicative constant that results from the arbitrary fixing of the zero temperature heavy quark potential, *i.e.* through the convention of not including a non-zero constant in the Cornell potential.

At high temperatures, $T \gtrsim 3T_c$, we note that the free energy $\Delta F_q(T)$ gets negative and correspondingly $|\langle \mathrm{Tr} L^R \rangle|$ attains values larger than unity (see also Tab. 2.2). At asymptotically high temperatures, perturbation theory suggests $\lim_{T\to\infty} |\langle \mathrm{Tr} L^R \rangle| = 1$ (see Eq. (2.12)

The renormalized Polyakov loop expectation value ($T > T_c$)					
$N_\tau = 4$			$N_\tau = 8$		
T/T_c	$\Delta F_q/T$	$\lvert\langle \mathrm{Tr} L^R\rangle\rvert$	T/T_c	$\Delta F_q/T$	$\lvert\langle \mathrm{Tr} L^R\rangle\rvert$
1.01	0.867 (34)	0.420 (51)	1.03	0.730 (21)	0.482 (68)
1.03	0.759 (32)	0.468 (53)	1.18	0.457 (08)	0.633 (58)
1.05	0.684 (37)	0.504 (61)	1.48	0.253 (12)	0.776 (38)
1.10	0.564 (30)	0.569 (56)	3.00	-0.015 (05)	1.015 (18)
1.15	0.486 (31)	0.615 (57)	6.00	-0.092 (08)	1.096 (08)
1.20	0.427 (29)	0.653 (52)	9.00	-0.100 (03)	1.105 (07)
1.24	0.387 (26)	0.679 (48)	12.0	-0.101 (04)	1.106 (07)
1.30	0.339 (28)	0.713 (47)			
1.50	0.226 (19)	0.798 (32)			
1.55	0.206 (16)	0.814 (28)			
1.60	0.185 (17)	0.831 (28)			
1.68	0.157 (12)	0.855 (22)			
2.21	0.053 (01)	0.948 (07)			
3.00	-0.02 (01)	1.017 (11)			

Table 2.2: The heavy quark free energy $\Delta F_q/T$ of a single test quark and the renormalized Polyakov loop expectation value $\langle \mathrm{Tr} L\rangle$ calculated from lattices $32^3 \times N_\tau$ with $N_\tau = 4, 8$. The error of $|\langle \mathrm{Tr} L^R\rangle|$ includes the systematic error as described in the text.

with $g \to 0$).

We have analyzed the dependence of $|\langle \mathrm{Tr} L^R\rangle|$ on the overall fixing of the zero temperature heavy quark potential in [93]. In order to do so, we performed a constant shift (c) on the heavy quark potential, $V_{q\bar{q}} + c$, where $V_{q\bar{q}}$ is defined in Sec. 2.3.2. We then also extracted the renormalized Polyakov loop, $|\langle \mathrm{Tr} L^R_{(c)}\rangle|$, from a matching of the free energy to this potential in the same way as described above. A comparison of both renormalized Polyakov loops, $|\langle \mathrm{Tr} L^R_{(c=0)}\rangle|$, which is the original value, and $|\langle \mathrm{Tr} L^R_{(c=-T_c)}\rangle|$, which refers to a shift of the energy scale by $c = -T_c$, is shown in Fig. 1 of Ref. [93] (inserted figure). We have also included in that figure the (continuum) perturbative estimate of $\langle \mathrm{Tr} L^R\rangle$ presented in [96] (see also Eq. (2.12)), where we have promoted the coupling g to a 1-loop running (renormalized) coupling $g_R(T)$ (see the dotted line in that figure). First of all we note that in the language of continuum perturbation theory the high temperature limit 1 is approached from above (see also the discussion in [96]). In fact, this behavior can also be seen in the shifted data, $|\langle \mathrm{Tr} L^R_{(c=-T_c)}\rangle|$, which in the temperature regime analyzed by us decrease with increasing temperatures. We note, however, that a constant shift of the zero temperature heavy quark potential results in a non-perturbative multiplicative constant in the renormalized Polyakov loop expectation value, *i.e.* $|\langle \mathrm{Tr} L^R_{(c\neq 0}\rangle| = \exp(-c/T)|\langle \mathrm{Tr} L^R_{(c=0)}\rangle|$, which nonetheless approaches unity in the large temperature limit. In fact, although the renormalized Polyakov loop expectation value at finite temperatures is only fixed up to an arbitrary multiplicative renormalization, it will approach a universal value at infinite

temperature, as

$$\lim_{T\to\infty} |\langle \mathrm{Tr} L^R_{(c\neq 0)}\rangle| = \lim_{T\to\infty} \exp(-c/T)|\langle \mathrm{Tr} L^R_{(0)}\rangle| = \lim_{T\to\infty} |\langle \mathrm{Tr} L^R_{(0)}\rangle|. \tag{2.34}$$

We therefore expect that contact with perturbation theory can be established unambiguously at high temperatures where the magnitude of the renormalized Polyakov loop (defined in our renormalization scheme) is unaffected by a shift of $V_{q\bar{q}}(r)$. Strictly speaking, this is, however, the case only at infinitely high temperatures where we expect $\lim_{T\to\infty} |\langle \mathrm{Tr} L^R_{(c)}\rangle| = 1$.

In the other limit, for instance at temperatures close to T_c, a constant shift will indeed affect the magnitude of $|\langle \mathrm{Tr} L^R\rangle|$. However, once the value of $|\langle \mathrm{Tr} L^R\rangle|$ is non-zero in a representation (c), the renormalized Polyakov loop expectation value will remain finite for all finite shifts. We thus conclude that the renormalized Polyakov loop expectation value works as an order parameter in $SU(3)$.

In conclusion, $|\langle \mathrm{Tr} L\rangle|$ signals not only the confinement deconfinement phase transition, but is indeed also sensible to the order of the phase transition. Moreover, it approaches a universal value (which we expect to be 1) in the infinite temperature limit. Both properties are independent of the normalization of the heavy quark potential at zero temperature.

2.5.2 The effective renormalization constant $Z^R(g^2)$

We are now in the position to discuss the renormalization constant which corresponds to our renormalization prescription. It is given through $(|\langle \mathrm{Tr} L^R\rangle|/|\langle \mathrm{Tr} L\rangle|)^{N_\tau}$ or can alternatively be estimated from (2.20). However, it follows from the discussion above that the renormalization constant $Z^R(g^2)$ can be more suitably extracted from the color singlet free energy than from $\Delta F_{q\bar{q}}$. In contrast to (2.20) we thus determine $Z^R(g^2)$ from

$$Z^R(g^2) \;=\; \exp\left(-\frac{\Delta F_1(r,T) - T\ln\langle \mathrm{Tr} L(\mathbf{x}) L^\dagger(\bar{\mathbf{x}})\rangle}{2TN_\tau}\right). \tag{2.35}$$

$Z^R(g^2)$ is related to the shift C which relates the bare Polyakov loop correlation functions to the renormalized quantities, *i.e.* $C \equiv \Delta F_i^R(r,T) - \Delta F_i(r,T) = -2TN_\tau \ln Z^R(g^2)$, $i = 1, 8, q\bar{q}$. This definition allows us to give a renormalization prescription for the free energies and the Polyakov loop.

Our lattice results for $Z^R(g^2)$ (at temperatures above T_c) are shown in Fig. 2.9 as a function of the bare coupling $g^2 = 6/\beta$, where β denotes the lattice coupling (see Tab. A.1). Our results obtained on lattices with temporal extent $N_\tau = 4$ and $N_\tau = 8$ are listed in Tab. 2.3 and Tab. 2.4. As the discussion of the renormalization constant is closely related to the discussion of the renormalized Polyakov loop given above, we present here only some brief comments.

First of all we note that the (non-perturbative) values for the effective renormalization constant shown in Fig. 2.9 are indeed independent of the temporal lattice extent. In fact, the data from lattice calculations with different N_τ show a common behavior as a function of the bare coupling g^2. It can be seen that the renormalization constants $Z^R(g^2)$ decrease

The renormalization constant ($T > T_c$)					
$N_\tau = 4$			$N_\tau = 8$		
β	g^2	Z^R	β	g^2	Z^R
4.080	1.471	1.3725 (54)	4.5592	1.316	1.3583 (28)
4.090	1.467	1.3717 (71)	4.5600	1.315	1.3585 (26)
4.100	1.463	1.3715 (79)	4.5951	1.306	1.3553 (28)
4.127	1.454	1.3721 (88)	4.6290	1.296	1.3523 (29)
4.154	1.444	1.3724 (87)	4.6605	1.287	1.3496 (31)
4.179	1.436	1.3730 (81)	4.6619	1.286	1.3495 (34)
4.200	1.429	1.3734 (74)	4.6874	1.280	1.3473 (33)
4.229	1.419	1.3734 (68)	4.7246	1.270	1.3441 (36)
4.321	1.389	1.3717 (47)	4.8393	1.240	1.3344 (24)
4.343	1.384	1.3708 (41)	4.8661	1.233	1.3319 (23)
4.365	1.375	1.3700 (39)	4.8921	1.227	1.3297 (21)
4.400	1.364	1.3685 (34)	5.4261	1.106	1.2863 (10)
4.600	1.304	1.3531 (09)	6.0434	0.993	1.2438 (04)
4.839	1.240	1.3330 (13)	6.3910	0.939	1.2238 (03)
			6.6450	0.903	1.2108 (02)

Table 2.3: The renormalization constant $Z^R(g^2)$ at various lattice couplings β obtained from lattice calculations with lattices of size $32^3 \times 4, 8$. Listed are the lattice couplings β and the bare coupling g^2 defined through $g^2 = 2N/\beta$. The values of $Z^R(g^2)$ were estimated from a matching to the zero temperature heavy quark potential fixed to the standard Cornell form ($c \equiv 0$). All couplings correspond to temperatures above T_c.

The renormalization constant ($T < T_c$)					
$N_\tau = 4$			$N_\tau = 8$		
β	g^2	Z^R	β	g^2	Z^R
4.000	1.500	1.3748 (72)	4.3212	1.389	1.3767 (22)
4.020	1.493	1.3771 (66)	4.4231	1.357	1.3711 (16)
4.040	1.485	1.3788 (61)	4.4472	1.349	1.3696 (23)
4.050	1.482	1.3792 (58)	4.4551	1.347	1.3692 (19)
4.060	1.478	1.3798 (54)	4.4784	1.340	1.3675 (18)
4.070	1.474	1.3777 (19)	4.4862	1.337	1.3667 (15)
			4.4937	1.335	1.3661 (11)

Table 2.4: Same as in Tab. 2.3: The renormalization constant $Z^R(g^2)$ at lattice couplings β below T_c calculated on lattices of size $32^3 \times 4, 8$. Also given are the bare couplings $g^2 = 6/\beta$.

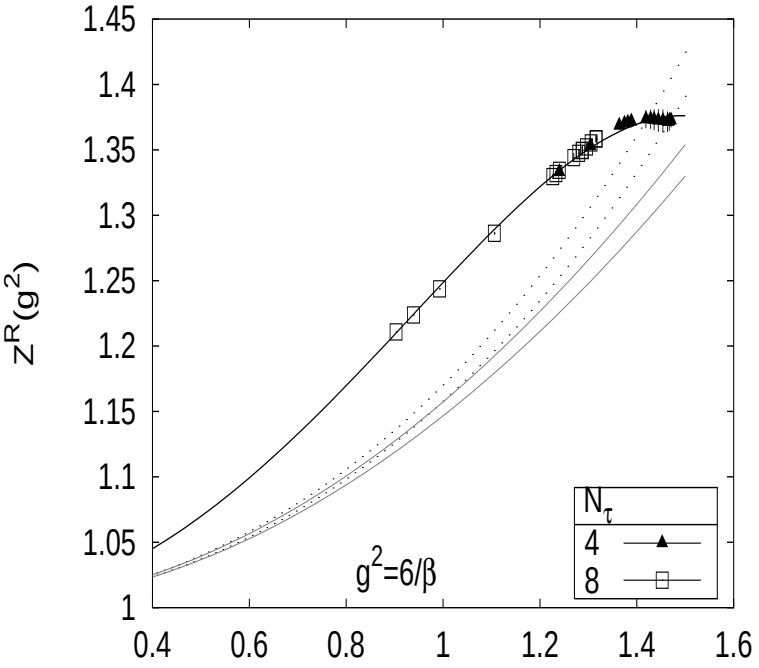

Figure 2.9: The renormalization constant $Z^R(g^2)$ from $SU(3)$ MC studies as a function of the bare lattice coupling $g^2 = 6/\beta$ from lattices of size $32^3 \times N_\tau$ with $N_\tau = 4$ (triangles) and 8 (squares). The lines in this figure are different estimates of $Z^R(g^2)$ in spirit of (2.13). They are explained in the text. The non-perturbative values of the renormalization constant shown in this figure are listed in Tab. 2.3.

with decreasing coupling. This behavior is indeed expected from lattice perturbation theory [102]. As the renormalization constant $Z^R(g^2)$ calculated by us is supposed to cancel the divergence in (2.10), we expect from (2.13) a leading order perturbative behavior like

$$Z^R(g^2) \simeq 1 + g^2 \frac{N^2-1}{N} Q^{(2)} + \mathcal{O}(g^4), \tag{2.36}$$

where we take $Q^{(2)}/N_\tau = 0.057(2)$ [102] in our case. This estimate (including the error on $Q^{(2)}/N_\tau$) is shown in Fig. 2.9 as black dotted lines. As can be seen from that figure, the data cannot be described by this estimate in the coupling regime analyzed by us. Moreover we note that the non-perturbative renormalized lattice data show a weakening of its increase with increasing g^2 at large couplings. This property cannot be described by leading order lattice perturbation theory.

As it stands, (2.13) describes only the first few terms of an infinite series which (may) reconstruct the exponential function in (2.10). In spirit of the leading order term in (2.13) one will thus rather think of

$$\langle \mathrm{Tr} L \rangle \simeq \exp(g^2(N^2-1)/N Q^{(2)} + \mathcal{O}(g^4)) \tag{2.37}$$

than of (2.36). This estimate is shown in Fig. 2.9 as grey lines. However, it can be seen

from the figure that the re-exponentiation of the 1-loop term does not change much the values of $\langle \mathrm{Tr}L \rangle$ in the coupling regime analyzed by us. In conclusion, the leading order term in (2.13), although it is re-exponentiated in spirit of (2.10), does not fit the data on $Z^R(g^2)$ in the coupling range analyzed by us. It follows that higher order contributions to the renormalized Polyakov loop - and consequently to the renormalization constant - are still important in the perturbative series in this coupling regime.

On the other hand, using the parametric form of the re-exponentiated leading order expression as an ansatz for a fit to our lattice data leads to a quite different value for $Q^{(2)}/N_\tau$ from the value deduced in [102]. Actually, from a best fit analysis we find that the lattice data can be described with $Q^{(2)}_{fit}/N_\tau = 0.107(1)$ and a pre-factor of the $\mathcal{O}(g^4)$-term $-0.065(3)$. The fit result is shown in Fig. 2.9 with the single black line which matches the data. Note that the value $Q^{(2)}_{fit}/N_\tau$ is roughly two times larger than the value deduced from lattice perturbation theory [102].

In conclusion - and in accordance with our discussion of the renormalized Polyakov loop - we expect contact with perturbation theory at smaller couplings than analyzed by us.

2.5.3 Essay on the divergence structure in n-point PLCs

Let us consider a Polyakov loop correlation function which involves more than two Polyakov loops. For example, we consider the renormalization of the n-point Polyakov loop correlation functions,

$$\left\langle \prod_{i=1}^{n} \mathrm{Tr}L(\mathbf{x}_i) \prod_{i=1}^{\bar{n}} \mathrm{Tr}L^\dagger(\bar{\mathbf{x}}_i) \right\rangle \simeq \exp\left(-\Delta F_{nq,\bar{n}\bar{q}}(T, \mathbf{x}_1, ..., \mathbf{x}_n, \bar{\mathbf{x}}_1, ..., \bar{\mathbf{x}}_{\bar{n}})/T\right). \quad (2.38)$$

It follows[8] that also higher correlation functions than those estimated in the previous sections require renormalization. However, as we have introduced the effective renormalization constant multiplicatively for the Polyakov loop, the renormalization program can easily be generalized to renormalize any n-point Polyakov loop correlation function. Indeed, Eq. (2.17) suggests [93]

$$\begin{aligned} \left\langle \prod_{i=1}^{n} \mathrm{Tr}L^R(\mathbf{x}_i) \prod_{i=1}^{\bar{n}} \mathrm{Tr}L^{R\dagger}(\bar{\mathbf{x}}_i) \right\rangle &= \left(Z^R(g^2)\right)^{(n+\bar{n})N_\tau} \left\langle \prod_{i=1}^{n} \mathrm{Tr}L(\mathbf{x}_i) \prod_{i=1}^{\bar{n}} \mathrm{Tr}L^\dagger(\bar{\mathbf{x}}_i) \right\rangle \\ &= \exp\left(-\Delta F_{nq,\bar{n}\bar{q}}(T, \mathbf{x}_1, ..., \mathbf{x}_n, \bar{\mathbf{x}}_1, ..., \bar{\mathbf{x}}_{\bar{n}})/T\right). \quad (2.39) \end{aligned}$$

In conclusion, it is enough to calculate only 2-point Polyakov loop correlation functions on the lattice to extract the renormalization constant as *all n-point Polyakov loop correlation functions* are fixed through $Z^R(g^2)$. In fact, the shift which is needed to yield the renormalized free energy from the bare lattice data, $C_{nq,\bar{n}\bar{q}} = \Delta F_{nq,\bar{n}\bar{q}} - \Delta F^{bare}_{nq\bar{n}\bar{q}}$, can be written in terms of the renormalization constant as

$$C_{nq,\bar{n}\bar{q}} = -(n+\bar{n})TN_\tau \ln Z^R(g^2) \qquad (\forall T). \quad (2.40)$$

[8] For instance, in leading order perturbation theory the n-point correlation functions are directly related to the 2-point functions which are divergent. 3-point correlation functions, which are related to the qqq free energy after renormalization, are subject of [112, 113].

This is the more general formulation of the renormalization prescription for the free energy we have given in (2.21). Thus, in spirit of (2.39), the divergence structure in the Polyakov loop correlation functions has indeed a *hierarchic* structure.

We should clarify, however, that our renormalization prescription is restricted to the case that the Polyakov loops in the correlation functions appear at some distance $\mathbf{x}$ only with power one. Otherwise, for instance constructions like L^2, L^3, ..., will introduce additional divergences which will *not cancel out* in the renormalization scheme introduced by us. This can be seen from the following argument: Such kind of divergences are usually discussed in the framework of the operator product expansion (OPE) [114, 115, 94]. Following the structure which is suggested by the OPE, for instance in terms of L^2, one finds

$$L(\mathbf{x}+\xi)L(\mathbf{x}-\xi) \quad \stackrel{\xi\to\mathbf{0}}{=} \quad \sum_i C_i(\xi)\; O_i\left(L^2(\mathbf{x})\right), \tag{2.41}$$

where $O_i(L^2)$ is a complete set of *local* composite operators. The crucial difference of the renormalization process for objects like (2.41) from the renormalization process analyzed by us is that on the right hand side of (2.41) (after performing the limit $\xi \to 0$) one has a *local composite* operator while on the left hand side of (2.41) (before doing the limit) one has a *non-local composite* operator. Consequently, the renormalization of local composite operators deals with a set of *new* divergences which are not subject of our discussion. In fact, due to this fatal property of $\langle \mathrm{Tr}L(\mathbf{x})\mathrm{Tr}L^\dagger(\bar{\mathbf{x}})\rangle$ in the limit $\mathbf{x} \to \bar{\mathbf{x}}$, we have explicitly imposed the boundary condition, $\mathbf{x} \neq \bar{\mathbf{x}}$, in (2.17). A discussion of the renormalization of the Polyakov loop in higher powers than one can be found in Ref. [99] (a related note is given in footnote 2 of this chapter).

Let us finally allow for the question whether we have calculated a renormalization constant which is specific to the Polyakov loop or not. For this discussion let us assume that we were also interested in the renormalization of the more general Green's function, G, which introduce mixtures of the Polyakov loop *and* the elementary fields U (lattice link variable),

$$G(\mathrm{Tr}L, L, U_0, U_i). \tag{2.42}$$

For instance, the *cyclic Wilson loop* [57] is *an example* for a correlation function which mixes the Polyakov loop, L, with the link variables U. Indeed, also such kind of objects need renormalization as the counter terms, which are present in the Lagrangian in order to renormalize the Green's functions which involve only the elementary fields, are in general not enough (only the gauge links in time direction (U_0) should require renormalization, *i.e.* a multiplication with $Z_U(g^2)$). As the Polyakov loop does not mix under renormalization, the renormalized Polyakov loop can be obtained from (2.16), $L^R = Z_L(Z_U)^{N_\tau}L$. In the following discussion we show that most likely $Z_L = 1$.

A convenient way to consider the divergence structure of objects like (2.38) or (2.42) is to do so in terms of the generating functional formalism. The usual formalism can be extended to generate the n-point Polyakov loop correlation functions on the lattice by introducing appropriate sources η_L and $\eta_L^\dagger$ (here for $N > 2$) which couple to the composite (untraced) operators L and $L^\dagger$. As usual, functional derivatives with respect to these

sources lead to the higher Green's functions (on the lattice) and one can then set the sources to zero[9]. We are now interested in the counter terms which have to be included in such a generating functional in order to ensure a proper renormalization of *all higher correlation functions*, including also the usual Green's functions which involve only the elementary fields U and $U^\dagger$. In order to analyze the counter terms, we may assume that the generating functional, W, is already properly renormalized from the beginning, $W \to W^R$. Excluding local composite operators from the following discussion the renormalization of W can be achieved by introducing the renormalization constant $(\tilde{Z}^R)^{N_\tau} = \tilde{Z}_L(\tilde{Z}_U)^{N_\tau}$ for the Polyakov loop in addition to the usual renormalization constants $\tilde{Z}_U$ for the gauge link variable and $\tilde{Z}_g$, which is associated with the coupling renormalization. Let us now consider $\langle \mathrm{Tr} L^R \rangle_R$ obtained from the generating functional in the renormalized language, W^R. It can be generated in two different ways, once in terms of one single functional derivative with respect to $\eta_L^\dagger$, but it can equally well be generated from N_τ derivatives with respect to the sources which couple to the elementary gauge links. In fact, the Polyakov loop can be considered as an N_τ-point $U(x)$ field correlation function, which indeed is not supposed to require extra renormalization. Moreover, any correlation function which involves the Polyakov loop, for instance the n-point Polyakov loop correlation function, can be obtained from W^R in these two different ways. On the other hand, any Green's function which does not introduce the Polyakov loop is definitely generated from W^R. By construction *all* Green's functions are renormalized as we started from the renormalized

[9] In order to be more precisely consider

$$W[J, J^\dagger, \eta_L, \eta_L^\dagger] \;=\; \frac{1}{W_0} \int \prod_{x_\mu} dU_\mu \exp\left(-S[U] - \sum_x \left(J_\mu^\dagger U_\mu + U_\mu^\dagger J_\mu + \eta_L^\dagger L + L^\dagger \eta_L \right) \right), \tag{2.43}$$

which is supposed to generate the new (bare) Green's functions on the lattice. The connected Green's functions follow from $\ln W$ while the 1PI Green's functions follow from the Legendre transformation of the (original) sources J and $J^\dagger$ of $\ln W$ with respect to their associated fields, U and $U^\dagger$. Moreover, Feynman rules for the original field (U_μ) which interacts between the composite operators L and $L^\dagger$ can be obtained from that expression. As usual, functional derivatives with respect to the sources lead to the higher Green's functions. For example

$$\begin{aligned} \mathrm{Tr}\frac{\delta}{\delta \eta_L^\dagger(\mathbf{x})} \mathrm{Tr}\frac{\delta}{\delta \eta_L(\bar{\mathbf{x}})} W[J, J^\dagger, \eta_L, \eta\dagger_L]\Big|_{J=\ldots=\eta_L^\dagger=0} &= \langle \mathrm{Tr} L(\mathbf{x}) \mathrm{Tr} L^\dagger(\bar{\mathbf{x}}) \rangle, \\ \mathrm{Tr}\frac{\delta^2}{\delta \eta_L^\dagger(\mathbf{x}) \delta \eta_L(\bar{\mathbf{x}})} W[J, J^\dagger, \eta_L, \eta\dagger_L]\Big|_{J=\ldots=\eta_L^\dagger=0} &= \langle \mathrm{Tr} L(\mathbf{x}) L^\dagger(\bar{\mathbf{x}}) \rangle \end{aligned} \tag{2.44}$$

generate the well-known 2-point Polyakov loop correlation functions which are related to the color averaged and color singlet $q\bar{q}$ free energies. But also the general thermal Wilson line as well as the n-point Polyakov loop correlation function (2.38) can be obtained from (2.43). Any Green's function, however, which contains the Polyakov loop L can be obtained from (2.43) in two different ways. The simplest case is

$$\langle \mathrm{Tr} L \rangle \;=\; -\mathrm{Tr}\frac{\delta W}{\delta \eta_L^\dagger}\Big|_{J=\ldots=0} = \mathrm{Tr}\frac{\delta^{N_\tau} W}{\delta J^\dagger \ldots \delta J^\dagger}\Big|_{J=\ldots=0}. \tag{2.45}$$

(Assume N_τ to be an even number.)

generating functional. This shows that the introduction of the source terms $\eta_L L^\dagger$ and $\eta_L^\dagger L$ in the generating functional is *gratuitous* for the renormalization of L. In fact, explicitly comparing the counter term structure of the Green's functions which is obtained by introducing the Polyakov loop in the two ways discussed above, one finds

$$\begin{aligned}\left\langle \prod_{i=1}^{n} \mathrm{Tr} L^R(\mathbf{x}_i) \prod_{i=1}^{\bar{n}} \mathrm{Tr} L^{R\dagger}(\bar{\mathbf{x}}_i) \right\rangle_R &= \left(\tilde{Z}^R(g^2)\right)^{(n+\bar{n})N_\tau} \left\langle \prod_{i=1}^{n} \mathrm{Tr} L(\mathbf{x}_i) \prod_{i=1}^{\bar{n}} \mathrm{Tr} L^\dagger(\bar{\mathbf{x}}_i) \right\rangle_R \\ &= \left(\tilde{Z}_U\right)^{(n+\bar{n})N_\tau} \left\langle \prod_{i=1}^{n} \mathrm{Tr} L(\mathbf{x}_i) \prod_{i=1}^{\bar{n}} \mathrm{Tr} L^\dagger(\bar{\mathbf{x}}_i) \right\rangle_R .\end{aligned}$$

This indeed leads to the identification $\tilde{Z}^R(g^2) = \tilde{Z}_U$. Like in the continuum, on the lattice L has a privileged status, too: Its renormalization only requires the renormalization of the coupling and (elementary) gauge field, *i.e.* $\tilde{Z}_U \simeq \exp(\tilde{Z}_g \sum_{i=1}^{N^2-1} \tilde{Z}_A)$. More importantly, however, this identification shows that it is most likely that we have calculated $\tilde{Z}_U$ rather than some renormalization constant which is specific to the Polyakov loop. In fact, we have checked with our lattice data that the 2-point Polyakov loop correlation functions and the cyclic Wilson loop have the same divergence structure.

Unfortunately, we point out here, that the renormalization constants introduced here ($\tilde{Z}_L$, $\tilde{Z}_U$, $\tilde{Z}^R$), are related to the effective renormalization constant we calculated on the lattice (Z^R) via a rather non-trivial equation: The expectation value $\langle ... \rangle_R$ respects the fact that in this case also the *gauge action* is renormalized, $\langle ... \rangle_R \equiv \prod_x U_x ... \exp(S^R)$, with S^R being the renormalized gauge action. In contrast in the MC approach we applied on the lattice, this is not the case and therefore Z^R and $\tilde{Z}^R$ are related via

$$|\langle Z^R \mathrm{Tr} L \rangle| = |\langle \tilde{Z}^R \mathrm{Tr} L \rangle_R|. \tag{2.46}$$

This relation, however, is indeed far from trivial. The knowledge, however, of a solution of (2.46), for instance $\tilde{Z}^R = f(Z^R)$, would lead to a powerful tool in lattice MC methods as it would open the possibility to perform MC simulations with a *non-perturbatively renormalized lattice gauge action*. For instance, lattice operators (in pure gauge theory), which do not require extra renormalization, would become calculable renormalized from the beginning by simply rescaling the lattice link variable U with $\tilde{Z}_U$.

We add that research on renormalized lattice gauge actions is not new and the present knowledge on this research field is summarized and reviewed regularly at lattice conferences. Nonetheless we note that most investigations so far use perturbative relations. A related discussion of an equation like (2.46) can be found in [116]. At this level, we have to leave further details concerning a solution of (2.46) open for future studies.

We close this chapter with a discussion of the things done so far and relate the renormalized Polyakov loop to present problems which are subject of current investigations in the field.

2.6 Further remarks on renormalization

The study of the renormalized Polyakov loop correlation functions at small distances has led us to a proper renormalization prescription for the Polyakov loop expectation value. In

fact, the concept we followed is not new and has already been anticipated in the discussion of the heavy quark antiquark free energies presented in [117]. Nonetheless the question arises why this concept of the renormalization leads to success. In order to analyze this question it appears helpful to point out parallels of our non-perturbative concept to the renormalization of TrL in the continuum perturbative approach.

The renormalizability of the finite temperature field theory, in the perturbative approach in the continuum, in general requires the renormalizability of the theory at zero temperature. For instance, the usual renormalization of objects at finite temperature takes place in the zero temperature limit as at finite temperature *no additional* divergences get introduced. In fact, a proper renormalization of finite temperature quantities requires a proper separation of the zero temperature part from the matter contribution as only the $T = 0$ piece is supposed to contain the UV divergences. In the case of the Polyakov loop correlation function we have shown that this separation can be performed at short distances, $r \ll 1/T$, where the finite temperature free energy is much less affected by the thermal medium. Indeed, from a heuristic point of view one will not expect thermal modifications of the finite temperature quark antiquark free energy at distances which are small compared to the length scale defined through the thermal gluon wave length. This property led us indeed to the separation of the heavy quark potential at zero temperature from the finite temperature free energy at short distances (see Fig. 1.8). The separation of the zero temperature part from the finite temperature free energy thus is closely related to the usual separation of the UV divergence in continuum perturbation theory. Nonetheless, this is only the *separation* of the divergence - we still have to remove it.

The cancellation of the divergence is defined in our renormalization prescription by simply *matching* the finite temperature free energy to the heavy quark potential at short distances. The zero temperature potential is fixed by the definition of the overall constant in the energy scale. For a proper cancellation of the divergence it is mandatory to use the perturbative estimate for the heavy quark potential as it contains the *r-running* of the coupling at small distances. We note that this statement is quite similar to *Polyakov's suggestion*, as it claims that the renormalization of the Polyakov loop will follow from the usual coupling renormalization.

Finally we gave some insights into the Polyakov loop as a composite operator on the lattice. We showed that it is most likely that - once more in accordance with Polyakov's suggestion - the Polyakov loop on the lattice will not require extra renormalization. Indeed, in our renormalization scheme the renormalization of the Polyakov loop on the lattice appears to be similar to the renormalization prescription which is proven to work in perturbation theory in the continuum. Thus the renormalization prescription suggested by us is quite similar to the standard renormalization program of continuum perturbation theory at finite temperature, implemented on the lattice and solved with non-perturbative methods.

We note that our renormalization prescription is different from the *normalization* condition we have frequently used in the first chapter,

$$\delta F_{q\bar{q}}(r,T) \quad = \quad -T \ln \frac{\langle \mathrm{Tr}L \mathrm{Tr}L^\dagger \rangle}{|\langle \mathrm{Tr}L \rangle|^2}. \tag{2.47}$$

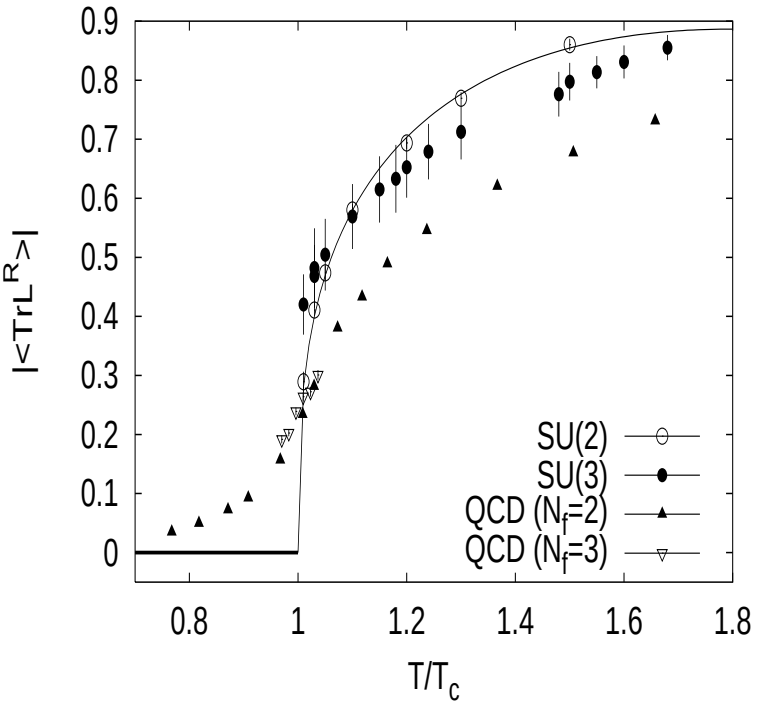

Figure 2.10: A comparison of the renormalized Polyakov loop expectation value $|\langle \mathrm{Tr} L^R \rangle|$ calculated in different thermal heat bathes. The open symbols show results in $SU(2)$ from [118], the closed black circles are our data and the triangles show a first estimate of full QCD (from [119, 120]). The closed triangles correspond to 2-flavor QCD and the open triangles to the 3-flavor case. More details are given in the text.

While within this normalization (at temperatures above T_c) the linear divergence cancels out in Eq. (2.10), a proper renormalization of the finite parts is still missing. The use of this condition on the lattice is somewhat similar to the use of a dimensional regularization scheme in the continuum perturbative approach without renormalization of the finite parts.

It should be obvious that the renormalization concept analyzed by us can easily be generalized to any $SU(N)$ gauge theory and to full QCD, for instance to QCD with light dynamical quarks. It will be of even greater interest in the latter case as the renormalized quark antiquark free energies at temperatures below T_c will show string breaking free energy. In fact, our renormalization prescription has recently been applied in $SU(2)$ [69] and investigations of full QCD [120] are currently being performed. In order to compare results from these studies with the renormalized Polyakov loop in $SU(3)$ we show in Fig. 2.10 the lattice results from investigations in $SU(2)$, $SU(3)$ and full QCD (2- and 3-flavor QCD) at temperatures close to T_c[10].

[10]It is well-known, that the Polyakov loop expectation value acts as an order parameter for the confinement deconfinement phase transition in the case of $SU(N)$ while it does not in the case of full QCD. The confinement phase transition in $SU(2)$ is found to be second order [65, 121], while in the case of $SU(3)$ it

In fact, a well behaved scaling behavior for the case of $SU(2)$ is expected at criticality and is indeed observed [69]. The line in Fig. 2.10 shows the scaling behavior with a critical exponent $\beta = 0.3265$ (see also the discussion in [69]). One can see from that figure that the confinement deconfinement phase transition in terms of the renormalized Polyakov loop in $SU(2)$ indeed appears as a second order one, while in the case of $SU(3)$ the data points cannot be described with this scaling behavior. Rather than critical behavior the $SU(3)$-values show a discontinuity at T_c which indeed is expected from the first order transition. The situation changes when one includs dynamical quarks into the theory. In this case the global $Z(3)$ symmetry is broken through the mass term in the QCD-Lagrangian and string breaking takes place at temperatures below T_c. One therefore does not expect that $\langle \mathrm{Tr} L^R \rangle$ will act as an order parameter in the strict sense, but still is expected to indicate the transition to the high temperature phase as it is supposed to change from small values below T_c to larger values above the deconfinement point. From the data points of full QCD calculations shown in Fig. 2.10 it can clearly be seen that the renormalized Polyakov loop in this case changes *continuously* from small to large values. Due to string breaking, the value of the renormalized Polyakov loop does, however, not vanish below T_c. In fact, only in the limit $T \to 0$ we expect a vanishing value for the renormalized Polyakov loop as $\lim_{T\to 0} e^{-\Delta F_q/T} = 0$.

Finally we note that having solved the problem of a proper renormalization of the Polyakov loop on the lattice opens the possibility to analyze various aspects of finite temperature QCD which are considered to be related to properties of the Polyakov loop. These are, for instance, the pressure and the free energy of the plasma [125] where perturbative calculations fail, at least at temperatures close to T_c. Different Polyakov loop models [27, 25] have been investigated and it is argued that 'Polyakov loop condensation' can overcome these problems. In these models the renormalized Polyakov loop is an important input parameter. In fact, a detailed analysis along the spirit of these models using the renormalized Polyakov loop will lead to a better understanding of the thermodynamics close to T_c. Such kind of studies do not exist but can be developed now on the basis of our analysis. In the following we turn, however, to a quite different aspect of the renormalized free energies which is supposed to be important for the understanding of confining forces in finite temperature QCD. The separation of the potential energy and entropy from the finite temperature free energies is subject of the following chapter.

is a weakly first order transition [122, 123] and it is an ordinary first order transition for $N > 3$ (see [124]). The renormalized Polyakov loop expectation value should mirror the order of the phase transition.

Chapter 3

From free energy to the QCD force at finite T

The investigation of medium effects on the color averaged quark antiquark free energies, calculated from the Polyakov loop correlation functions, has become an important topic in the analysis of the thermal properties of hadrons [18], as such kind of investigations have been utilized to analyze the temperature dependence of bound state problems in heavy quarkonium physics at temperatures below and above T_c. For instance, the suppression of charmonium production has been proposed as a probe for the creation of the quark gluon plasma in high energy nucleus-nucleus collisions [31]. Thus, these studies are of importance not only for the confirmation of theoretical models through experimental findings on the quark gluon plasma, but also for an understanding of the different plasma signals in current experiments (see for instance Ref. [7]). Consequently, many different theoretical studies in this field have been performed since the early work on charmonium suppression [31, 126, 32].

One essential input in most of these considerations is the behavior of quarkonium states in a deconfined medium. This problem can in principle be addressed directly in finite temperature lattice QCD. Until quite recently, however, computer performance and techniques did not allow such studies, as the expected small size of quarkonium requires very small lattice spacings. One therefore resorted to *potential theory*, starting from the Schrödinger equation,

$$\mathcal{H}\psi_i \;=\; E_i\psi_i \;, \tag{3.1}$$

with the Hamiltonian

$$\mathcal{H} \;\equiv\; 2m_i - \frac{\bigtriangledown^2}{m_i} + V(r) \;, \tag{3.2}$$

where ψ_i specifies the wave function of the bound state under consideration, E_i its mass, and $V(r)$ the heavy quark potential [126]. In absence of a thermal medium ($T = 0$), the potential between the heavy quark pair is known to be of standard Cornell form at large distances while this parameterization needs perturbative corrections at short distances due

to the weakening of the coupling. The presence of the thermal medium, however, modifies the potential, so that we now have $V(r,T)$ in Eq. (3.1). Actually, however, the present studies make use of the thermal properties of the quark antiquark *free energies* in order to define an appropriate finite temperature potential. Moreover, most of these studies concentrate on the thermal modifications of the *color averaged* free energies at rather *large distances*.

The conclusions we draw are thus threefold: Firstly, of even greater relevance than the quark antiquark free energy for heavy quark physics is the quark antiquark *potential energy* at finite temperature, as this quantity appears in the quantum mechanical and field theoretical relations of the potential models. Secondly, in order to analyze thermal properties of bound state problems it appears to be more appropriate to do so in terms of the *color singlet* and *color octet* channels rather than utilizing the color averaged free energies. In fact, these color channels are supposed to be related to the properties of real, physical hadrons. Finally one should analyze the finite temperature potential energies in the *full distance and temperature range* as the potential at small distances and temperatures close to T_c is of importance in the heavy quark physics.

The difficulty of a proper separation of the potential energies (E) and entropies (S) from the Polyakov loop correlation functions arises from the fact that the r-dependence of the quark antiquark free energies results from the r-dependence of E and S [73, 92]. Actually, the r-dependence in the free energy is given by

$$\Delta F_i(r,T) \;=\; \Delta E_i(r,T) - T\Delta S_i(r,T), \tag{3.3}$$

with $i = 1, 8, q\bar{q}$. The feature that also the entropies are r-dependent quantities makes this relation quite non-trivial. Unfortunately, over the years it has become customary to denote the logarithm of the Polyakov loop correlation functions itself as the *heavy quark potential at finite temperature*. Thus the role of any additional entropy contribution in the Polyakov loop correlation functions has been ignored at finite temperature, so far. It is thus mandatory for the further analysis of the thermal properties of bound states via potential models to get control over the entropy contributions in the Polyakov loop correlation functions from short to large distances. The non-trivial r-dependence of the free energies in (3.3) shows that it may be misleading to use the thermal properties of the free energies in potential models.

In this chapter we will analyze (3.3) in terms of *thermodynamic relations* which are well-known from Statistical Mechanics. Indeed, these relations allow us to extract $\Delta E_i(r,T)$ and $\Delta S_i(r,T)$ *non-perturbatively* from the *renormalized* free energies [92, 93]. As it stands, these relations do not depend on the color structure. We suggest to use these new finite temperature potentials (in future) in potential models for an analysis of the thermal properties of the heavy quarkonium spectra in finite temperature QCD.

3.1 A new look at the QCD potential and force at finite T

We discuss here the thermodynamic properties of the *renormalized* heavy quark free energies in more detail. In fact, having fixed the free energies through renormalization is equivalent to having fixed the partition functions for the thermal system. For instance, we have

$$\Delta F_{nq,\bar{n}\bar{q}} = -T \ln \frac{Z_{nq,\bar{n}\bar{q}}(V,T,\mathbf{x}_1,...,\bar{\mathbf{x}}_{\bar{n}})}{Z(V,T)}. \tag{3.4}$$

In contrast to (1.15) the free energies are now directly related to the corresponding partition functions. Consequently, all thermodynamic information about the system is fixed and can be deduced from the renormalized free energies. Our study thus opens the possibility to refer to thermal relations in order to separate the excess energies (potentials) and excess entropies from the renormalized free energies. We suggest that this can be done through

$$\Delta E_{nq,\bar{n}\bar{q}}(T,\mathbf{x}_1,...,\bar{\mathbf{x}}_{\bar{n}}) = -T^2 \frac{\partial \Delta F_{nq,\bar{n}\bar{q}}(T,\mathbf{x}_1,...,\bar{\mathbf{x}}_{\bar{n}})/T}{\partial T}, \tag{3.5}$$

$$\Delta S_{nq,\bar{n}\bar{q}}(T,\mathbf{x}_1,...,\bar{\mathbf{x}}_{\bar{n}}) = -\frac{\partial \Delta F_{nq,\bar{n}\bar{q}}(T,\mathbf{x}_1,...,\bar{\mathbf{x}}_{\bar{n}})}{\partial T}. \tag{3.6}$$

As it stands, these thermodynamic relations are neither bound to some specific temperature nor to some specific distance range. In fact, they allow us to study the finite temperature potential energies and entropies *non-perturbatively in all color channels*. In this section we are interested in analyzing the thermal relations (3.5) and (3.6) using the renormalized heavy quark antiquark free energies $\Delta F_1(r,T)$, $\Delta F_8(r,T)$, $\Delta F_{q\bar{q}}(r,T)$ as well as $\Delta F_q(T)$.

From the definitions above it follows that ΔE_i and ΔS_i determine the *difference in energy* and the *difference in entropy* due to the presence of static charges which are put into the thermal heat bath. They thus also contain the potentials and entropies of the thermal heat bath alone. These quantities have been calculated in Ref. [127] and could be subtracted from the renormalized free energies. We note, however, that they do not show any r-dependence and therefore the r-dependencies of the finite temperature potentials and entropies are indeed given by E_i and S_i in ΔE_i and ΔS_i. It thus follows that also the finite temperature force, $K_i(r,T)$, can be calculated from these finite temperature potentials,

$$K_i(r,T) = -\frac{d\Delta E_i(r,T)}{dr}. \tag{3.7}$$

In terms of forces, confinement is supposed to lead to non-vanishing $K_i(r,T)$ at large distances while deconfinement should yield a vanishing force at large distances. In vacuum physics the force is thus often used to analyze the coupling as undetermined constants get removed in the force. At finite temperature, however, the force defined in Eq. (3.7) is complicated through screening effects. As the finite temperature force is not affected from the arbitrary overall fixing of the zero temperature potential we expect that (3.7) can similarly be used to estimate the running coupling. Hence we expect that the finite

temperature force defined in Eq. (3.7) will not change its sign, *i.e.* $K_1(r,T) \geq 0$.

The approach we suggested above can easily be generalized to full QCD. In fact, as the renormalization concept we refer to is supposed to work also in this case [128, 119], and as the thermal relations are not specific to the choice of action S, the program we outline is supposed to lead to the finite temperature potential and to the entropy also in QCD. It will be of even greater importance in this case as these potentials will reflect the string breaking energy. In this thesis, however, we are interested in the analysis of the finite temperature potential energies and entropies which are contained in the free energies of the pure $SU(3)$ gauge theory. In the following we discuss this issue in more detail.

3.1.1 Thermodynamics with heavy quark free energies

For the discussion of the thermal properties of the renormalized free energies it appears convenient to reanalyze the r- and T-dependence of the renormalized quark antiquark free energies defined in the r-T-plane. In Fig. 3.1 we show an illustrative example of the functional dependencies of the renormalized color singlet free energies. In that figure we try to indicate that the finite temperature color singlet free energies become temperature independent at small distances while the explicit temperature dependence becomes visible at large distances. The free energies below T_c signal confinement and the free energies above T_c show the color screening property as they approach finite values at large distances. At T_c we have included in that figure the feature that the free energies will show the first order phase transition. This kind of phase transition is supposed to lead to a discontinuity in the free energies at T_c. We have indicated this property with the hatched plane at the critical temperature. For instance, unlike in $SU(2)$, it follows that for the $SU(3)$-case there does not exist a definite choice for the free energies at the critical temperature. Note, however, that the specific fine structure of the renormalized color singlet free energies is not shown in Fig. 3.1. For instance, the color singlet free energies below T_c in this figure do not illustrate the enhancement compared to the heavy quark potential at zero temperature and intermediate distances which we noted in the previous chapter.

Fig. 3.1 also illustrates that the entropy contributions to the free energy are r-dependent quantities. This property can easily be deduced from the thermal relations as follows: Since the color singlet quark antiquark free energy at asymptotically small quark antiquark separations becomes temperature independent, $dF_1(r \to 0,T)/dT = 0$, this relation also implies via (3.6) that the entropy contribution ΔS_1 vanishes in this limit. However, for large separations, the color singlet free energy is temperature dependent and it thus follows that $\Delta S_1 \neq 0$ at large distances. The other color channels (octet, averaged[1]) show similar

[1]In order to be precise we note here that the argument presented does strictly speaking not apply to the color averaged free energy, as we have stressed before that $\Delta F_{q\bar{q}}(r,T)$ will not become temperature independent at small r. Consequently, the argument given does not apply to this case. Therefore it might be possible that the r-dependencies of the entropy contributions to ΔF_1 and ΔF_8 compensate each other, which may result in $\Delta S_{q\bar{q}} \neq \Delta S_{q\bar{q}}(r)$. In the following we will, however, provide evidence that this is not the case. In fact, the relation $\Delta F_{q\bar{q}} - \Delta F_1 = T \ln 9$ indeed tells us that $\Delta S_{q\bar{q}}(r \to 0,T) = -\ln 9$ instead of

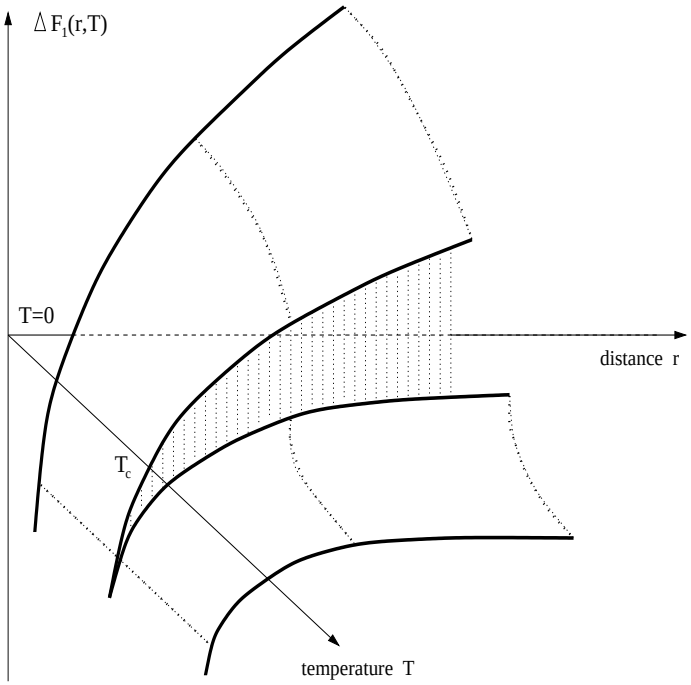

Figure 3.1: A schematic figure of the renormalized static quark antiquark free energies in the color singlet channel at finite temperatures. We show here the free energies ΔF_1 as a function of r and T over the r-T-plane. This figure only shows the basic properties of the renormalized singlet free energies, *i.e.* the temperature independence at small r, the confinement signal below T_c, the first order phase transition at T_c and the deconfinement signal above T_c. Details like the enhancement of the finite temperature color singlet free energies at temperatures below T_c compared to the heavy quark potential at intermediate distance, are not explicit shown here. In this figure we consider ΔF_1 rather than $\Delta F_1/T$, the change in free energy with temperature at fixed distance r is related to the entropy. For further discussions of this figure see the text.

behavior.

Let us discuss the *physical meaning* of the excess finite temperature entropies as we have seen that they will play an important role in the free energies. In general, entropies are given by the sum over all possible thermal configurations of the system. In our case we expect that the zero temperature statistical contributions [109] as well as the thermal properties of the medium, for instance the gluon density in the heat bath, are supposed to modify these entropies. As the entropies defined through (3.6) refer to the *difference* of the entropies in the presence and absence of static charges in the thermal bath, it follows that in general the positivity of entropies, $\Delta S_i \gtrsim 0$, is not required. The differences in entropies is related to a destruction or generation of thermal configurations when the quarks get introduced into the heat bath. In general one can say that large absolute values ($|\Delta S_i|$) indicate that the configuration of the thermal system changes much when color charges get introduced into the heat bath.

Nonetheless, the questions remain how to understand an r-dependent potential and en-

$\Delta S_{q\bar{q}}(r \to 0) = 0$, *i.e.* it turns out to approach a T-independent constant.

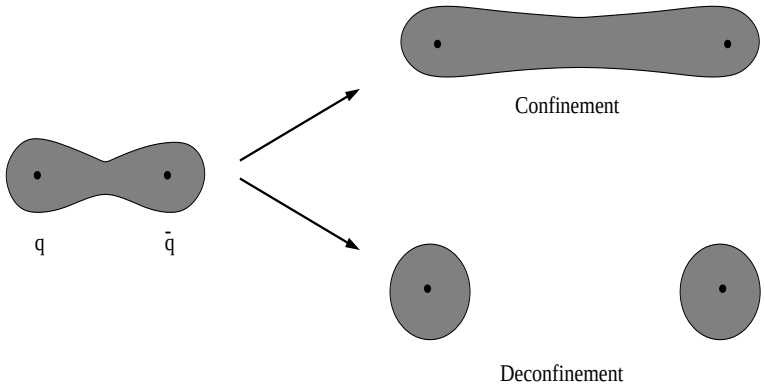

Figure 3.2: A schematic figure that illustrates the possibility of the r-dependence of the energies and entropies at finite temperature. The grey clouds represent a higher gluon density around the quarks (black points) compared to the rest frame of the gluon density in the pure gluonic heat bath. In the confinement phase the gluon density is supposed to form a thin flux tube [53] while in the deconfinement phase the clouds can be separated through screening. We suggest that the geometric structures of these gluon clouds are related to the values of $\Delta E_i(r,T)$ and $\Delta S_i(r,T)$ in the free energies.

tropy contribution and what causes this property in the free energies. We may resort here to a well-known *heuristic picture* in which this r-dependence gets more transparent: The potentials and entropies in the free energies estimate the difference in the configurations due to the presence of the static quarks. In general, placing the quarks into the thermal heat bath will lead a polarization of gluons which will surround the color charges. From this rather heuristic view there will be a kind of gluon cloud which screens the color charges of the quarks. In conclusion, placing the static color charges into the thermal heat bath will change the configuration of the system and thus will change the entropy and energy compared to the entropy and energy of the pure thermal heat bath. Thus, in this heuristic figure, the value of ΔE_i and ΔS_i is, though not closer specified, somehow related to the geometric structure of the gluon density (clouds) in the thermal heat bath. It follows, that these gluon clouds will overlap at short distances while at large distances the geometric structure of these clouds depends on the screening properties of the thermal medium in the different phases. For instance, at temperatures below T_c it is well-known that the gluons form a thin flux tube between the two color charges [53] while at temperatures above T_c the clouds of both charges can be separated from each other. This property is shown in Fig. 3.2. It can be seen in this figure that we expect the values of the entropies at temperatures below T_c to change continuously with increasing distances as the flux tube enlarges while in the case of a deconfined medium the change in entropy will stop at some value as the clouds get separated at some distance. As at large separations the relative orientation of the different color charges in the color space do not influence the screening properties we indeed expect that the potentials and entropies in the different color channels will coincide.

At short distances the gluon clouds wash out as the color charges screen each other. This is expected to take place at distances which are smaller than the thermal wave length

of the gluons. At such small distances the difference in potential energy is not modified from the heat bath and the entropy is supposed to vanish or will approach finite values. We do not expect that the entropy is modified by the temperature and thus is supposed to be given through the statistical formulation at zero temperature. A related discussion of these entropies has recently been given [109]. They calculated the quantum statistical entropy of one single quark to be $S_q^{\rm stat} = \ln 3$. This suggests that the vacuum entropy of a quark antiquark pair is given by $S_{q\bar{q}}^{\rm stat} = \ln 9$.

3.1.2 On expectations and uncertainties

As this is the first time that a non-perturbative analysis of the finite temperature potential energies and entropies is performed, the present knowledge on the thermal properties of these quantities is quite limited. We thus concentrate in this section on the expectations and uncertainties which follow from the use of the *renormalized free energies* in thermodynamic relations for E_i and S_i. We first discuss consequences for the r-dependence of the potentials and entropies at large distances in both phases and then turn to a discussion of their short distance properties. Finally we remark on thermal properties of the potentials and entropies at asymptotically large distances in the deconfinement phase. This will also be the starting point of our discussions of the lattice results.

The (asymptotic) string pictures are supposed to describe the r-dependence of the quark antiquark free energies at large distances, for instance, at distances where the free energies in the different color channels approximately coincide. Following Eq. (1.5), the r-dependence of the finite temperature potentials and entropies at low temperatures is given by ($r \gg 1/T \gg 1/T_c$)

$$\Delta E_i(r,T) \simeq \sigma_E(T) r - T + \mathcal{O}(T^2), \tag{3.8}$$

$$\Delta S_i(r,T) \simeq \sigma_S(T) r - \ln 2rT - 1 + \mathcal{O}(T), \tag{3.9}$$

where we have used '$\simeq$' in these relations in order to indicate that these relations are supposed to describe the finite temperature potentials and entropies *up to additive renormalization*. The temperature dependencies of the string tensions $\sigma_E(T)$ and $\sigma_S(T)$ are defined through

$$\sigma_E(T) = \sigma + \frac{\pi}{3} T^2 + \mathcal{O}(T^3), \tag{3.10}$$

$$\sigma_S(T) = 2\frac{\pi}{3} T + \mathcal{O}(T^2). \tag{3.11}$$

It follows that the finite temperature potentials signal confinement at large distances as $\sigma_E(T)$ is positive. Moreover, as this string tension is *increasing with increasing temperatures*, the finite temperature potentials appear to increase with increasing temperature at large distances. As σ in (3.10) denotes the string tension of the heavy quark potential at zero temperature it follows that the finite temperature potentials are supposed to be larger than $V_{q\bar{q}}$ at large distances. It is worth noting that the string tensions of the finite temperature potentials smoothly approach the zero temperature value in the limit

$T \to 0$[2]. We also note that (3.8) suggests a linear potential at finite temperatures at this level. Actually, approximations of the string fluctuations to higher accuracy are expected to add r-dependent corrections with powers lower than one. A similar statement is proven for the heavy quark potential at zero temperature [129] by using a mathematically more rigorous argument. Both properties are indeed quite different from the thermal features that the quark antiquark free energies show. For instance, the temperature dependence of the string tension in the free energies is in contrast to (3.10) decreasing with increasing temperatures and the typical logarithmic corrections to the linear term in the free energies disappear in the potential.

The finite temperature entropies are supposed to increase with increasing distance, too. This property is indeed conform with the statement we gave in the discussion of Fig. 3.2 as we noted that the entropies below T_c will continuously change with changing distances as the geometric structure of the flux tube changes continuously. We note that the string tension of the heavy quark potential at zero temperature is missing in (3.11). This indicates that confinement indeed originates from potential energy rather than from entropy. Note, that the typical logarithmic correction to the finite temperature free energies appear here as entropy contributions. They originate from the transverse fluctuations of the finite temperature string. Actually, these fluctuations turn out to *reduce* the difference in entropy. Nonetheless, as $rT \gg 1$, the linear term in (3.9) is the leading term at large distances. Consequently, the entropy *reduces the confining signal*, *i.e.* the effective string tension in the free energies.

The approximation of the string fluctuations given above for the free energies cannot be applied when going to higher temperatures [46, 130]. Instead of this approximation, at temperatures close to T_c, a large D-expansion is supposed to lead to the temperature dependence of the string tension in the free energies [46, 130] (see for instance Eq. (1.6)). Following this expression, one finds

$$\Delta E_i(r,T) \simeq \tilde{\sigma}_E(T) r, \tag{3.12}$$

$$\Delta S_i(r,T) \simeq \tilde{\sigma}_S(T) r, \tag{3.13}$$

where in this case the string tensions $\tilde{\sigma}_{E,S}(T)$ are given by

$$\tilde{\sigma}_E(T) = \sigma \left(\sqrt{1 - \left(\frac{T}{T_c}\right)^2} + \left(\frac{T}{T_c}\right)^2 \frac{1}{\sqrt{1 - \left(\frac{T}{T_c}\right)^2}} \right), \tag{3.14}$$

$$\tilde{\sigma}_S(T) = \sigma \frac{T}{T_c^2} \frac{1}{\sqrt{1 - \left(\frac{T}{T_c}\right)^2}}. \tag{3.15}$$

Actually, both string tensions are divergent[3] in the limit $T \to T_c$. Clearly, the temperature dependence of the string tensions in the potentials characterize the temperature

[2]The limit $T \to 0$ in this string picture is ill-defined as $rT \gg 1$ is required. Moreover, (3.5) cannot be applied in this limit as $\Delta F_i/T$ diverges.

[3]Such a divergent behavior of the entropy (and potential energy) in the case of the string picture in the limit $T \to T_c$ should not be confused with the so-called *roughening transition* which is known from the *solid-*

dependence of the color forces. Consequently the asymptotic string picture suggests an increasing force with increasing temperatures at large distances which may diverge at T_c.

At small distances the different color structures lead to a different behavior of the potentials and entropies in the different color channels. We discuss here only the case of the color singlet potentials and entropies. At small distances the color singlet free energy is given by the heavy quark potential at zero temperatures. It thus follows

$$\Delta S_1(r \to 0, T) \simeq 0 \qquad \text{and} \quad \Delta E_1(r \to 0, T) \simeq V_{q\bar{q}}(r). \tag{3.16}$$

From our discussion above it follows that these relations are expected to be true at *all* temperatures. Indeed, similar relations can be deduced for the other color channels.

Let us turn to the finite temperature potentials and entropies in the *deconfined phase*. Although we have seen in the first chapter that leading order perturbation theory is most likely not applicable for the description of the color averaged free energies at temperatures a few times the critical temperature, more reliable information seems to be given by perturbation theory for the color singlet and color octet free energies at large distances. We thus mainly discuss here the r- and T-dependencies of the potentials and entropies in these two color channels.

At large distances, one expects that the color singlet and color octet free energies are of color screened Coulomb form. From leading order high temperature perturbation theory ($r \gg 1/T$) one thus expects (up to renormalization)

$$\Delta E_{1,8}(r,T) \simeq C_{1,8}\frac{\alpha(T)e^{-m(T)r}}{r}\left(1 + rT\frac{dm(T)}{dT} - \frac{T}{\alpha(T)}\frac{d\alpha(T)}{dT}\right), \tag{3.17}$$

$$\Delta S_{1,8}(r,T) \simeq C_{1,8}\frac{\alpha(T)e^{-m(T)r}}{r}\left(r\frac{dm(T)}{dT} - \frac{1}{\alpha(T)}\frac{d\alpha(T)}{dT}\right). \tag{3.18}$$

From these relations it follows that the finite temperature potentials and entropies signal deconfinement as both approach finite values at large distances. This property is consistent with our discussion of the r-dependence of the entropies given above, for instance with the feature that the gluon clouds which screen the static color charges can be separated at high temperatures. We organized the relations (3.17) and (3.18) in a way that the prefactors in both relations give the leading order perturbative estimate for the free energies, i.e. $\Delta E_{1,8} \simeq \Delta F_{1,8}(1 + ...)$ and $\Delta S_{1,8} \simeq \Delta F_{1,8}(...)$. This simplifies a comparison of the behavior of the free energies with the behavior suggested by these relations for the potentials and entropies.

on-solid (SOS) models or from the more general random surface models [131] (see also [46]). Actually, although this kind of phase transition is indeed observed to take place in the strong coupling range of $SU(N)$ gauge theories [132, 41], and has been studied in detail in terms of the string tension [52, 133, 134], it is well-known that the roughening transition provides a potential barrier for extrapolations of strong coupling expansions in $SU(N)$ down to the weak coupling regime as there appears a singularity of the string tension as a function of the bare lattice coupling [18]. The lattice results we analyze in the context of our present studies, which are quite close to T_c, are supposed to have just undergone this transition [46]. Moreover, the roughening transitions does not imply deconfinement as the string tension is not vanishing after this kind of phase transition (when going from strong to rather weak couplings).

The differentiation of the Debye-mass $m(T) \simeq gT$ and the coupling $\alpha(T) = g^2/4\pi$ is given by the β-function which in leading order perturbation theory is supposed to be *negative*. Consequently, in leading order perturbation theory the change of these quantities with a change in temperature is given by

$$\frac{dm(T)}{dT} \simeq \sqrt{\frac{N}{3}}\left(g + \beta(g)\right) \simeq \sqrt{\frac{N}{3}}\left(g - \beta_0 g^3\right) \simeq +\sqrt{\frac{N}{3}}g, \tag{3.19}$$

$$\frac{d\alpha(T)}{dT} \simeq \frac{1}{T}\frac{1}{2\pi}g\beta(g) \simeq -\frac{1}{T}\frac{1}{2\pi}\beta_0 g^4. \tag{3.20}$$

This shows that the r- and T-dependence of the potentials and entropies is quite complex. In general, however, we expect that the terms in brackets in Eqs. (3.17) and (3.18) are positive at large distances as we expect that the sign of the screened Coulombic behavior is given by the Casimirs, $C_{1,8}$. Indeed, in this approach the influence of the different color structures on the potentials and entropies only enters through C_i. It should be obvious, however, that the behavior of the potentials and entropies at intermediate and small distances will deviate from (3.17) and (3.18) as, for instance, the entropy given (3.18) is supposed to show a color screened Coulombic behavior at small distances (see Eq. (3.16)). This cannot be correct as we have deduced on quite general grounds that $\Delta S_1(r,T)$ will vanish at small distances. This also shows that it is mandatory for an analysis of the color singlet and octet potentials and entropies to respect the r-running of the coupling at intermediate and small distances.

Let us finally discuss the properties of the potentials and entropies at asymptotically large quark separations in the deconfinement phase. In fact, as we have seen that they are supposed to approach finite values at temperatures above T_c, it is of interest to analyze their behavior in the high temperature limit ($T \to \infty$). From perturbation theory it follows that the finite temperature free energies at large distances are supposed to become describable by $\Delta F_{q\bar{q}}(r \to \infty, T) \simeq -g^2 T$. While $\Delta E_q/T_c$ at the temperatures analyzed by us seems to vanish at high temperatures, high temperature perturbation theory predicts negative values for the internal energy, too. Indeed, assuming $\Delta F_q \simeq -g^2 T$ from high temperature perturbation theory, it follows

$$\Delta E_q \simeq -2\beta_0 T g^4 \qquad \text{while} \qquad \Delta S_q \simeq g^2 - 2\beta_0 g^4, \tag{3.21}$$

where β_0 is the first coefficient in the perturbative β-function, $\beta(g) = \beta_0 g^3 + \mathcal{O}(g^5)$[4]. Leading order perturbation theory would suggest $\lim_{T\to\infty} \Delta E_q/T = 0$ and $\lim_{T\to\infty} \Delta E_q/T_c = -\infty$. Note that the leading order coefficient in the entropy in this perturbation theory inspired approach is positive. In conclusion, we expect $\Delta S_q \gtrsim 0$ at high temperatures.

The situation described above will change when referring to full QCD. Although the behavior of the finite temperature potentials and entropies in the high temperature, deconfined

[4] An arbitrary power in the coupling, which may result in perturbation theory from resummation techniques, will not influence the general properties of our statement. For instance, the ansatz $\Delta F_q \simeq g^n T$ (with an arbitrary power n) leads to similar relations like (3.21).

phase is supposed to be quite similar to that of corresponding quantities in $SU(3)$, qualitative changes will occur. In particular, in the presence of dynamic quarks (full QCD) at temperatures below the deconfinement point string breaking will appear. While it should be obvious that in this case the finite temperature potentials will indeed signal the string breaking energy as they are flattening at large separations, it is a quite interesting and so far unanswered question whether these energies will increase with temperature similar to the case of $SU(3)$. In fact, our studies in Ref. [119] indicate that the string breaking energy will increase with increasing temperatures.

3.2 The asymptotic behavior of ΔF_q, ΔE_q and ΔS_q

In order to analyze the temperature dependence of the potential energies and entropies at asymptoticly large distances ($r \to \infty$), it is convenient to study first the asymptotic properties of the renormalized free energies. For instance, this can be done in terms of the simplest free energy given by

$$\Delta F_q \equiv \lim_{r\to\infty} \Delta F_{q\bar{q}}(r,T)/2 \qquad (T > T_c)\ . \tag{3.22}$$

Moreover, the discussion of ΔF_q is closely related to the discussion of the renormalized Polyakov loop expectation value. While ΔF_q defined in this way is finite above T_c, it is infinite below T_c due to confinement. In order to include in our discussion also the free energies in the low temperature phase, instead of (3.22) we will estimate

$$\Delta F_q(r\sqrt{\sigma}=2,T) \quad \equiv \quad \Delta F_{q\bar{q}}(r\sqrt{\sigma}=2,T)/2 \qquad (T < T_c) \tag{3.23}$$

at temperatures *smaller than* T_c where $r\sqrt{\sigma} = 2$ ($r \simeq 1$ fm) is supposed to be close to the physical extent of heavy quarkonium [135]. The free energies ΔF_q defined in this way are shown in Fig. 3.3 as function of temperature. In this figure we estimate both, the values for $\Delta F_q/T_c$, as they are related to the single quark entropies (ΔS_q), and the values for $\Delta F_q/T$, since the change of this quantity with a change in temperature reflects the single quark potential energies (ΔE_q) (see Eqs. (3.5) and (3.6)).

3.2.1 Temperature dependence of the asymptotic free energy ΔF_q

Let us first comment on the *temperature dependence* of the single quark free energies at temperatures close to T_c. It can clearly be seen from Fig. 3.3 that the free energy changes monotonic with temperature in both phases, $\Delta F_q(T_1) \gtrsim \Delta F_q(T_2)$ for $T_1 \lesssim T_2$. This statement, however, is true only for the data shown in this figure. We will see that it will be different in certain distance and temperature intervals. In addition we note that the free energy is not only discontinuous at T_c but also exhibits some kind of *inflection point* as function of temperature at T_c. It thus follows that the entropies and also the potential energies will show a more complicated temperature dependence at temperatures close to T_c.

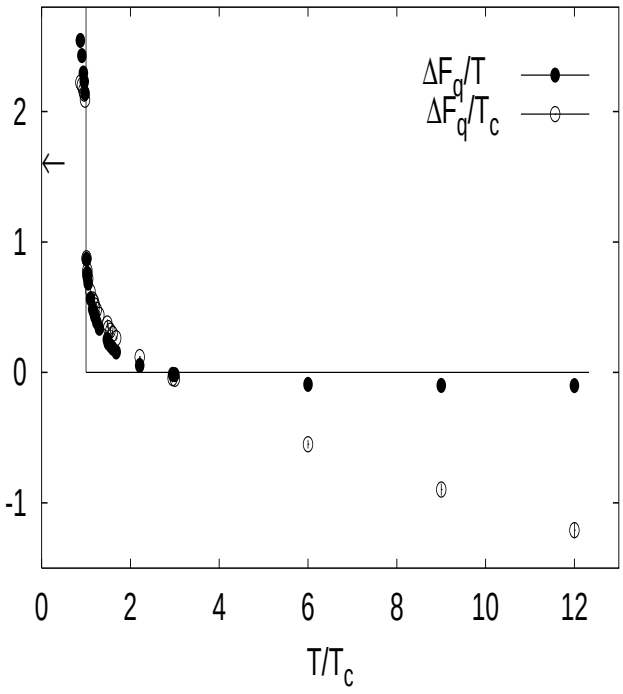

Figure 3.3: The behavior of $\Delta F_q/T_c$ (open symbols) and $\Delta F_q/T$ (filled symbols) as function of T/T_c in the high and low temperature phase. The definitions of ΔF_q we used here are given in Eqs. (3.22) and (3.23). The arrow in this figure points at the heavy quark potential for a single quark, $V_q \equiv V_{q\bar{q}}/2$, given in units of T_c at distance $r\sqrt{\sigma} = 2$. In this figure we summarize results from calculations on lattices with sizes $32^3 \times N_\tau = 4$ and 8.

At *temperatures below* T_c the values for $\Delta F_q/T$ and $\Delta F_q/T_c$ decrease with increasing temperature in the temperature range analyzed by us. However, the corresponding value of the heavy quark potential at zero temperature, $V_{q\bar{q}}(r\sqrt{\sigma} = 2)/2T_c \simeq 1.6$, lies significantly below the values for $\Delta F_q/T_c$ shown in Fig. 3.3 (the arrow at the left frame in that figure points at $V_{q\bar{q}}(r\sqrt{\sigma} = 2)/2T_c$). As we expect the finite temperature quark antiquark free energies in the color singlet and color averaged channels to approach the heavy quark potential smoothly in the limit of vanishing temperature, *i.e.* $\lim_{T\to 0} F_{1,q\bar{q}}(r,T) = V_{q\bar{q}}(r)$, this property indicates that ΔF_q will exhibit a *maximum* at some temperature. In fact, this property is closely related to the enhancement of the renormalized finite temperature quark antiquark free energies compared to the heavy quark potential which we have noticed at *intermediate distances* in Sec. 2.4.1. Consequently, a maximum in free energy as function of temperature will lead to a *change in sign* of the entropy. It is worth noting that this statement is restricted to the entropy as the behavior of $\Delta F_q/T_c$ is quite different from the behavior of $\Delta F_q/T$ in the limit $T \to 0$: While $\Delta F_q/T_c$ will stay well-defined and finite at some finite distance and is supposed to approach smoothly the corresponding zero temperature heavy quark potential in this limit, $\Delta F_q/T$ will diverge in this limit. Correspondingly, the behavior of ΔS_q will be quite different from that of ΔE_q in the low

temperature phase. We note, however, that in the limit of vanishing temperatures the term $T\Delta S_i$ in Eq. (3.3) will vanish, and we thus expect $\Delta E_q = V_q$ at $T = 0$ although (3.5) cannot be applied.

Let us finally turn to the free energies in the *high temperature phase* ($T > T_c$). It can be seen from Fig. 3.3 that the free energy indeed changes rapidly with temperature close to T_c. This rapid change in free energy will lead to quite large potential energies and entropies in the temperature range close to T_c. We also note that both, $\Delta F_q/T$ and $\Delta F_q/T_c$, change their sign from positive to negative values at some temperature close to $3T_c$. In fact, $\Delta F_q/T_c$ seems to decrease continuously at high temperatures, while the values for $\Delta F_q/T$ remain close below zero. In fact, from high temperature perturbation theory one would expect $\Delta F_q \simeq -g^2 T$. Consequently, in the high temperature limit one would expect $\Delta F_q/T_c \to -\infty$ and $\Delta F_q/T \simeq -g^2 \to 0$. In fact, if $\Delta F_q \simeq -g^2 T$ turns out to be correct, the data shown in Fig. 3.3 suggest a *change in sign of the potential energies*. This, however, would show up only at temperatures larger than those analyzed by us. In contrast to this, the entropies would not change their sign at high temperatures.

We note, however, that the behavior of $\Delta F_q/T$ in the temperature range shown in Fig. 3.3 is still consistent with $\Delta F_q \simeq -cT$, where c is some small (positive) constant. In fact, a running of the coupling with the temperature, $g = g(T)$, would become visible in Fig. 3.3 in terms of vanishing values for $\Delta F_q/T$ at higher temperatures than analyzed by us. Following our discussion of the high temperature limit of the renormalized Polyakov loop, we indeed expect $\lim_{T\to\infty} \Delta F_q/T = 0$ rather than $\lim_{T\to\infty} \Delta F_q/T = -c$.

Let us finally comment on the properties of the free energies at *small distances*. In this limit the enhancement in the free energies over the heavy quark potential which we noticed above is expected to develop differently in different color channels. In fact, we do not expect this enhancement in the limit of asymptotic small distances in the case of the color singlet free energy, as ΔF_1 will approach the heavy quark potential, while the enhancement will persist at $r \to 0$ in the color averaged and color octet channels. In the latter channels we rather expect $\Delta F_8 \to \infty$ as it is repulsive, and the enhancement in the color averaged free energy over $V_{q\bar{q}}$ is given by $T \ln 9$ according to (2.22).

We thus find that the behavior of the free energies as *function of temperature* is quite complex at short and intermediate distances. Correspondingly, the properties of the finite temperature potential energies and entropies are expected to be quite complex, too. It is worth noting that this statement is not limited to some temperature range and thus equally well applies to quantities below the deconfinement point.

3.2.2 The asymptotic behavior of ΔE_q and ΔS_q

We discuss now the asymptotic behavior ($r \to \infty$) of the single quark entropies (ΔS_q) and potential energies (ΔE_q). We have calculated ΔS_q and ΔE_q separately from each other applying Eqs. (3.6) and (3.5) to the renormalized free energies defined through Eqs.

(3.22) and (3.23). The derivatives in these relations are approximated by finite differences. The statistical error of these differences is calculated via the Jack-knife analysis. Further details on our calculations will be presented in the next section. Our results are listed in Tab. 3.1 in terms of $\Delta E_q/T_c$ and ΔS versus the temperature scale, T/T_c. We have checked that the recombination of the values for $\Delta E_q/T_c$ and for ΔS_q to the free energies, for instance the values $T_c/T(\Delta E_q/T_c - (T/T_c) \times \Delta S_q)$, match to the initial free energies given in Tab. 2.2 at all temperatures, although both, ΔE_q and ΔS_q, are calculated separately from the free energies. Our results are summarized in Fig. 3.4 in terms of ΔS_q (open circles) and $\Delta E_q/T_c$ (filled circles) as function of temperature below and above T_c.

We first discuss our results at temperatures *close to* T_c on both sides of the phase transition. It can be seen from Fig. 3.4 that the potential energies and entropies indeed approach surprisingly large values on both sides of the phase transition. For instance, at temperature about $0.97T_c$, the finite temperature potential energy $\Delta E_q/T_c$ is about three times larger than the corresponding value for the heavy quark potential (defined for a single quark, $V_q(r) \equiv V_{q\bar{q}}(r)/2$). This value is indicated in the figure through the arrow on the left hand side. The enhancement of the finite temperature potential energies compared to the heavy quark potential (V_q) is caused by the rapid change in free energy with a change in temperature close to T_c. Moreover, despite the discontinuity in free energy at T_c, we also observed that the free energies exhibit some kind of inflection point as function of temperature located at T_c which leads to a maximum in energy and entropy at T_c[5].

We now concentrate on the properties of the *entropies at temperatures below* T_c. From Fig. 3.4 it can be seen that the entropies drop quite rapidly when going from the phase transition temperature down to smaller temperatures. For instance, $\Delta S_q \simeq 2.7$ at $T \simeq 0.97T_c$, while it is indeed smaller than one at $0.9T_c$. Actually, from our discussion of Fig. 3.3 we deduced that $\Delta F_q/T_c$ will have a maximum as function of temperature (if taking the value from $\Delta F_{q\bar{q}}(r,T)$ at intermediate distances). This feature will indeed lead to a change in sign of ΔS_q as function of temperature below T_c. It follows that ΔS_q will be *negative* at smaller temperatures than analyzed by us. We stress again, that ΔS_q refers to the difference in entropies due to the presence of the static charge, *i.e.* $\Delta S_q = S_q - S$. It thus follows that the relevant thermodynamic configuration of the system changes a lot when a static quark is placed into the heat bath at temperatures close to T_c where ΔS_q is quite large.

[5]The question which indeed arises now is, whether the potential energies and entropies will diverge in the limit $T \to T_c$ or not (see our discussions in Sec. 3.1.2). We have analyzed this question for the color averaged entropies as they are statistically better determined and, moreover, the temperature dependence of the string tension in the entropies is expected to be less complicated than in the potentials. We have analyzed whether

$$\lim_{T\to T_c} \frac{\Delta S_{q\bar{q}}(r,T)}{r} \quad \simeq \quad -\lim_{T\to T_c} \frac{d\tilde{\sigma}_S(T)}{dT} \tag{3.24}$$

is finite or not. At the temperatures and distances analyzed by us we could not find a signal for a divergent behavior at T_c. Unfortunately, however, we could not go to large enough distances and temperatures close to T_c to demonstrate this clearly. However, deviations from a divergent behavior are clearly expected [33].

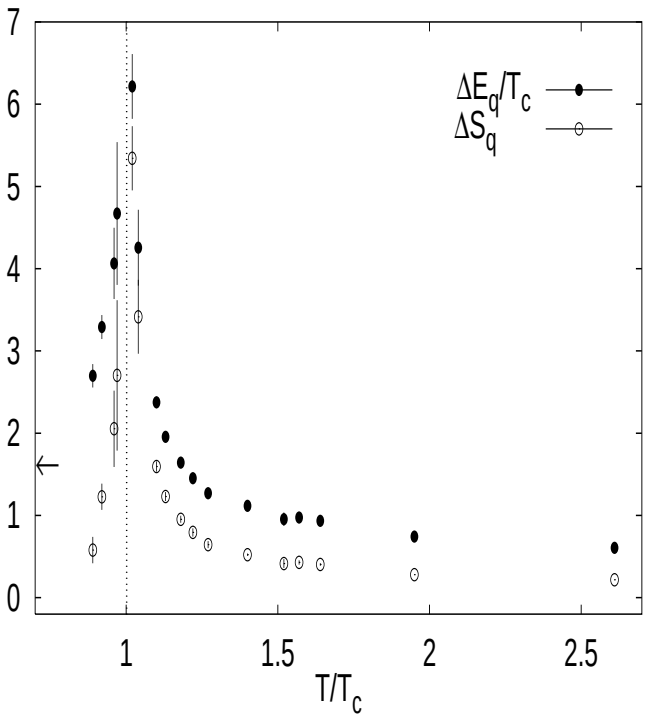

Figure 3.4: The asymptotic values of $\Delta E_q/T_c$ (filled symbols) and ΔS_q (open symbols) as function of T/T_c in the high and low temperature phase. ΔE_q and ΔS_q are estimated from the thermal relations (see Eqs. (3.5) and (3.6)) applied to the single quark free energies ΔF_q defined in Eqs. (3.22) and (3.23). The arrow points at the value for the heavy quark potential defined on $V_{q\bar{q}}(r\sqrt{\sigma} = 2)/2$. The values shown in this figure are also summarized in Tab. 3.1.

We also note here, that there are no particular boundary conditions on the entropies which require $\Delta S_q(T = 0) = 0$. The fact that the free energies at zero temperature will coincide with the heavy quark potential rather follows from the vanishing term $T\Delta S_q$ in the free energies at $T = 0$.

We finally turn to the properties of ΔS_q and $\Delta E_q/T_c$ in the *high temperature phase*. First of all, it can be seen from Fig. 3.4 that, although the entropies start with large values at temperatures close to T_c, they rapidly decrease with increasing temperatures. In fact, the entropy decreases by a factor 5 from its value close to T_c when increasing the temperature by about 15%. This rapid change of ΔS_q from large to small values reflects the rapid change in free energy with increasing temperatures close to T_c. We note, however, that at high temperatures a weakening in the decrease of $\Delta F_q/T$ was observed by us which may result from a weakening of the coupling $g(T)$. Indeed, in the limit of infinitely high temperatures we expect a vanishing entropy contribution, $\lim_{T\to\infty} \Delta S_q = 0$. In view of our discussions in Sec. 3.1, vanishing entropies at high temperatures indicate that the thermodynamic configuration of the system does not change much at high temperatures although color charges get introduced into the heat bath. Note that we have deduced a

The asymptotic values ΔE_q and ΔS_q					
T/T_c	$\Delta E_q/T_c$	ΔS_q	T/T_c	$\Delta E_q/T_c$	ΔS_q
0.89	2.70 (14)	0.58 (16)	1.02	6.22 (39)	5.34 (39)
0.92	3.29 (15)	1.23 (16)	1.04	4.26 (46)	3.42 (45)
0.96	4.06 (43)	2.05 (46)	1.10	2.37 (07)	1.59 (06)
0.97	4.67 (87)	2.70 (91)	1.13	1.96 (06)	1.23 (05)
			1.18	1.64 (05)	0.95 (04)
			1.22	1.45 (06)	0.79 (05)
			1.27	1.27 (05)	0.64 (04)
			1.40	1.12 (02)	0.52 (01)
			1.52	0.95 (08)	0.42 (05)
			1.57	0.97 (04)	0.43 (03)
			1.64	0.94 (03)	0.40 (02)
			1.95	0.74 (01)	0.28 (01)
			2.61	0.61 (01)	0.22 (01)

Table 3.1: The asymptotic values for the potential energies, $\Delta E_q/T_c$, and the entropies, ΔS_q, at several temperatures in the low and high temperature phase. The data which are given for the low temperature phase are calculated from the free energies at fixed finite distance, $r\sqrt{\sigma} = 2$. The values we present here are calculated within the method described in Sec. 3.3 on lattices of size $32^3 \times 4$.

similar property in Sec. 2.4.2 where we have studied the extent of the gluon clouds which surround and screen the color charges. In analogy to a vanishing entropy, we claimed that the screening radius (r_{screen}) will vanish in the high temperature limit.

As one would expect from Fig. 3.3, the behavior of $\Delta E_q/T_c$ at high temperatures is supposed to be more complicated. While $\Delta E_q/T_c$ at the temperatures analyzed by us seems to vanish at high temperatures, high temperature perturbation theory suggests negative values for the internal energy, too.

3.3 The r- and T-dependence of the potential energies

We are now interested in an appropriate formulation of (3.5) and (3.6) in terms of lattice data at arbitrary distances. The differentiation with respect to the temperature in the continuum, d/dT, will be replaced by us with the difference quotient,

$$\frac{df(\tilde{T})}{dT} \quad \rightarrow \quad D_{\tilde{T}}(f) \equiv \frac{f(T_1) - f(T_2)}{T_1 - T_2} \quad \text{with} \;\; \tilde{T} = (T_1 + T_2)/2 \; . \tag{3.25}$$

This approximation is natural for small temperature steps, $\Delta T = T_1 - T_2$. In order to realize small temperature steps, we calculated the color averaged, color singlet and color octet (renormalized) free energies on the lattice using temperature steps about $\Delta T \simeq 0.05 T_c$ at temperatures close to T_c, as in this temperature range the change in free energies is large already for small changes in temperature. At high temperatures we used appropriate

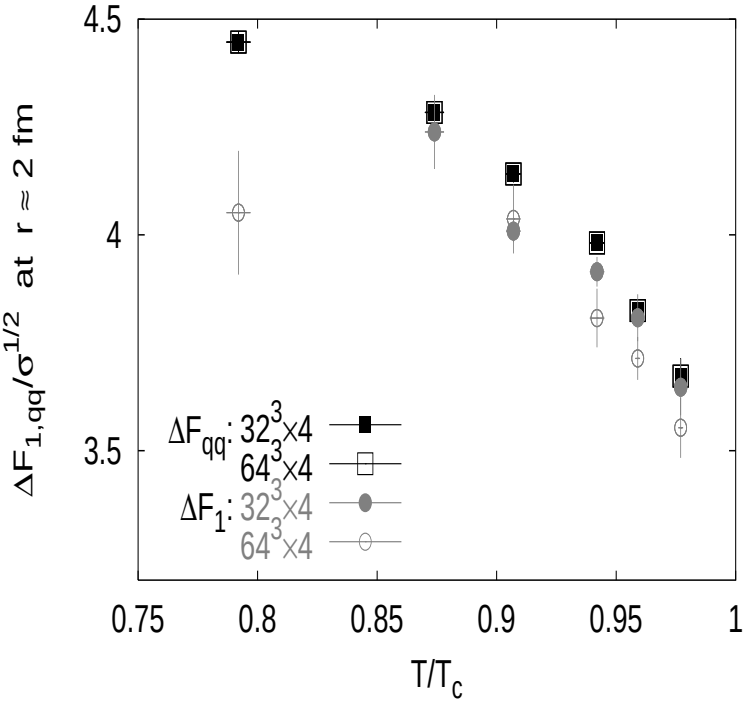

Figure 3.5: The influence of the finite spatial lattice volume on the (renormalized) free energies. We show here the color averaged (squares) and color singlet (circles) free energies at fixed distance $r = 2$ fm as function of temperature. The open symbols denote our results from simulations on lattices of size $64^3 \times 4$ and the filled symbols show results from lattices of size $32^3 \times 4$.

larger temperature steps at high temperatures. The grid we used for the discretization of the free energies in the temperature direction is given in Tab. A.1.

More difficult to control, however, are the systematic errors which arise from the uncertainty of the temperature scale and from the finite volume effects on the lattice. Especially the latter has to be handled with care as (3.5) and (3.6) require the infinite volume limit. In general one expects that the dependence of spatial correlation functions on the finite lattice volume are stronger at large separations of the correlated operators than at small separations. In order to get an estimate for the dependence on the finite lattice volume we used MC simulations on lattices of size $32^3 \times 4$ (in the following we call the data from this lattice *set I*) and of size $64^3 \times 4$ (*set II*). We run the simulations on both lattices at several lattice couplings below and above T_c and compared the renormalized quark antiquark free energies from both lattices.

In Fig. 3.5 we compare the finite temperature quark antiquark free energies from set I with the results from set II at fixed distance, $r \simeq 2$ fm, at several temperatures below T_c. At large distances the free energies below T_c will be more strongly influenced by the finite lattice volume as they signal confinement than the free energies above T_c which are controlled by deconfinement. In this figure we show results for the color singlet (grey symbols) and for the color averaged quark antiquark free energies (black symbols). Re-

sults from set I ($32^3 \times 4$-lattice) are denote by closed symbols and the results from set II ($64^3 \times 4$-lattice) are shown with open symbols. Unfortunately, the statistical significance of the color singlet free energies is about ten times lower than the significance of the color averaged free energies. Consequently, the results for the color singlet free energies still have large statistical errors. This can be seen from the data in Fig. 3.5. While the data for the color singlet free energies from set I and set II show deviations from each other they still agree within statistical errors and, moreover, the data for the color averaged free energies indeed coincide from both sets. We thus draw the conclusion that finite volume effects are negligible in our data at the distances considered by us. However, the low statistical significance of the color singlet free energies will affect the predictive power of the derivatives calculated through Eq. (3.25). Fortunately, the statistical significance of the color singlet data is much better at shorter distances. Thus we restrict our present analysis to distances $r \lesssim 1.5$ fm. In fact, in this distance regime we do not expect significant finite volume effects and the statistical errors allow for reliable results for Eq. (3.25). This can indeed be followed from the data we presented in Sec. 3.2 as data at 'asymptotic', large distances.

The calculation of the potential energies and the entropies from Eqs. (3.5) and (3.6) at arbitrary distances needs interpolation of the free energies in the r-direction as the thermal relations require a comparison of free energies at different temperatures but fixed *physical* distances. In order to avoid any fit[6] to the complicated structure of the heavy quark antiquark free energies, we used a cubic spline which interpolates between the lattice data in the r-direction. We divided the lattice data at each temperature into subsamples and calculated the spline interpolations on each of these subsamples. The error estimate of the spline interpolation at a given distance is calculated by using the Jack-knife analysis on the subsamples. The differentiation with respect to the temperature is approximated by the difference quotient (3.25) defined on the spline approximations. In order to minimize the systematic error involved in the spline approximation, we calculated (3.25) at the distance sample $\{r_i\}$ which is given by the input data of the free energy with the lower temperature. This means, that only the r-dependence of the free energy with the correspondingly higher temperature is interpolated by the spline. Finally we note that we also calculate the derivatives at short distances where the free energy is less influenced by the temperature and consequently the values of $\mathcal{D}_T$ are supposed to vanish. In order to get reasonable results at short distances we thus have partly set by hand the values of $\mathcal{D}_T$ to zero. It is worth noting that the analysis described above can be performed in each

[6] A different calculation method from ours could be to perform a best-fit analysis of the renormalized free energies and to calculate Eqs. (3.6) and (3.5) with respect to the temperature dependence of the fit parameters. This method could allow to calculate the potentials and entropies at arbitrary temperature. It is, however, mandatory for such analysis to find an appropriate fit-function which respects the complicated r-dependence of the free energies from short to large distances. From our discussions in the first chapter it follows that a parameterization of the free energies, however, is not that easy to find. Moreover, it is still quite unclear whether the temperature dependencies of the fit parameters will in parts lead to a divergent temperature dependence at T_c or not. The ansatz suggested in Eq. (1.51) (with appropriate modifications) maybe a reasonable candidate for such studies. A similar analysis in full QCD, however, indeed requires the fit method as the general experience shows that these free energies behave quite noisy.

color channel.

In the following discussions we refer to data for the finite temperature potentials and entropies calculated with these methods. For instance, we have calculated the potentials and entropies from the finite temperature free energies by using (3.5) and (3.6) *separately from each other* in all three color channels. We have checked that the potentials and entropies calculated in this way recombine to reasonable corresponding free energies which, for instance, match well the originate (renormalized) finite temperature free energies. In parts we also checked our results with a fit method (similar to the method described in the footnote below). We do not find significant deviations from our results. In conclusion we expect that our lattice data for the potentials and entropies yield statistically significant values up to distances about $r \lesssim 1.5$ fm (corresponding to $r\sqrt{\sigma} \lesssim 3$).

3.3.1 The finite temperature quark antiquark potential energies

We discuss here the general properties of the finite temperature quark antiquark potential energies in the different color channels below and above T_c. As an example we summarize our results in Fig. 3.6 for the color singlet, color octet and color averaged potential energies at $T = 0.92T_c$ and $T = 1.4T_c$. The filled symbols indicate the color singlet potential energies while the open symbols refer to the color octet and the grey symbols to the color averaged potentials. The black line shows the heavy quark potential at zero temperature.

We first consider the finite temperature potentials in the *confined medium* (given by the triangles): It can clearly be seen that the large distance behavior of the potential energies in each color channel is controlled by confinement as the potential energies increase continuously with increasing distances. Moreover, at large separations the finite temperature potentials approach values which are significantly larger than the heavy quark potential at zero temperature. We have discussed this property in the last section. We note here, however, that in contrast to the color octet and color averaged potentials, the finite temperature color singlet potential energy still stays close to the heavy quark potential at relatively large distances. In fact, the finite temperature color singlet potential below T_c is comparable to the zero temperature potential up to distances about $r\sqrt{\sigma} \lesssim 1.7$. The enhancement of the finite temperature color singlet free energies compared to the heavy quark potential thus vanishes in terms of the singlet potential (at intermediate distances). At larger distances, however, the singlet potential clearly breaks away from $V_{q\bar{q}}(r)$. In fact, it follows from our discussions of the string picture in Sec. 3.1.2 that the potential energies will coincide at large distances and will show a unique r-dependence. At distances about $r\sqrt{\sigma} \gtrsim 2.5$ the color averaged and color octet potential energies indeed coincide within statistical errors. Indeed, at such distances we have observed (in chapter 1) that the free energies start to show unique behavior. The color singlet quark antiquark potential energy in Fig. 3.6 is still below the color octet and averaged potentials. In terms of the color singlet potential, however, we could not go to such large distances to demonstrate clearly that also the color singlet potential will coincide with them. We also note that

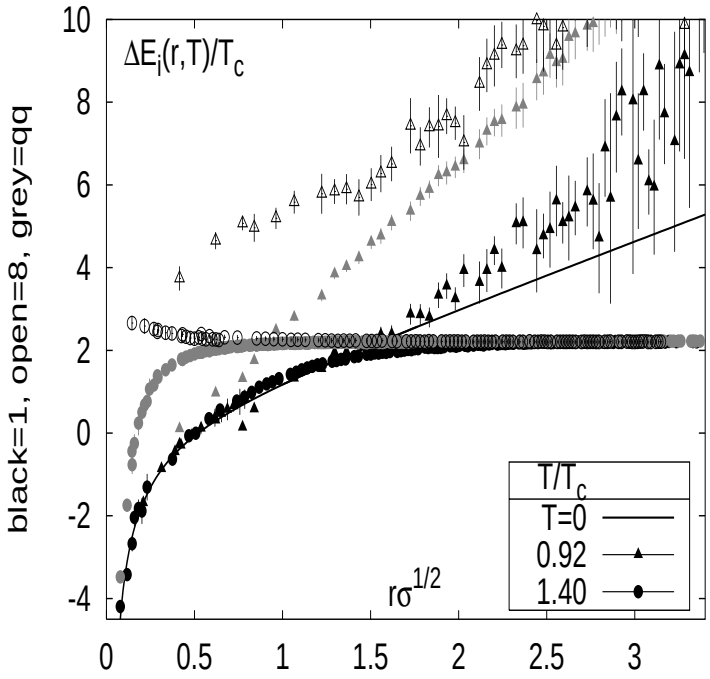

Figure 3.6: The potential energies at $0.92T_c$ and at $1.40T_c$ defined on (3.5) in the color singlet, octet and averaged channel as function of the distance $r\sqrt{\sigma}$. The black filled symbols summarize the color singlet potentials and the open symbols the color octet ones. The grey filled symbols show the color averaged finite temperature potentials.

within statistical errors the color averaged potential energy can be described as linearly increasing with increasing distances. This property is consistent with Eq. (3.8) and also with our observation that the color averaged free energies in general fit into the string picture at smaller distances than the singlet and octet free energies.

At short distances the different color structures control the behavior of the finite temperature potential energies (below T_c). The color singlet potential energy remains comparable to the heavy quark potential and also the color averaged potential approaches $V_{q\bar{q}}(r)$ in this limit. This property signals that the difference in color singlet and color averaged free energies is indeed given by the difference in the entropy contributions in both free energies. This feature is suggested from Eq. (2.22). The color octet internal energy, however, stays significantly above the zero temperature potential. In fact, in the short distance limit we expect that the color octet potential will be repulsive. However, we could not go to short enough distances in order to demonstrate this property clearly in Fig. 3.6.

The finite temperature potentials in the *deconfined medium* are also summarized in Fig. 3.6 using circles as symbols. The potentials in this phase indeed coincide in all color channels at large distances and, more importantly, they signal the deconfinement feature. Both properties are consistent with our discussions in Sec. 3.1.2, for instance with Eq. (3.17). Moreover, it can clearly be seen from Fig. 3.6 that the finite temperature potential energies

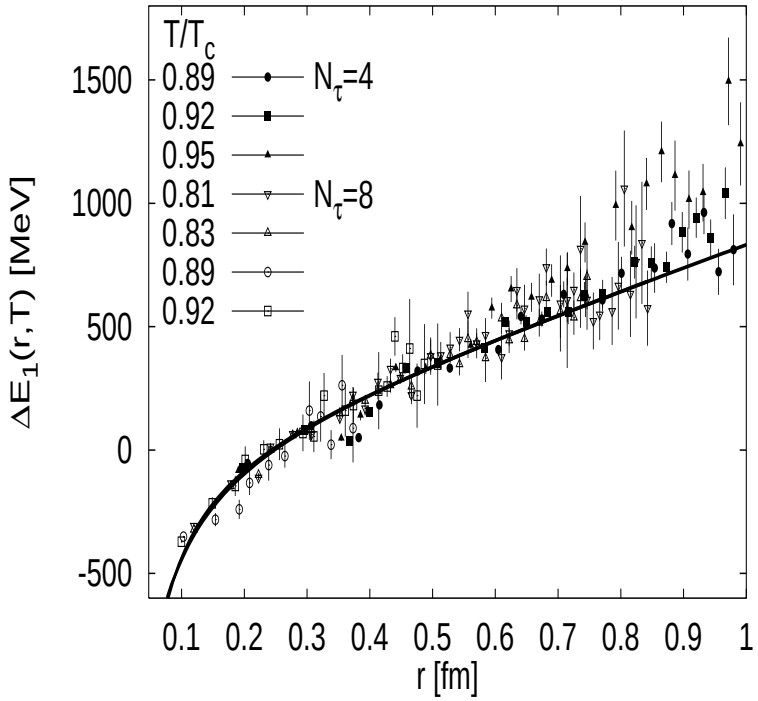

Figure 3.7: The color singlet potentials $\Delta E_1(r,T)$ in physical units [MeV] as a function of the physical distance r [fm] at temperatures below T_c. This figure contains results from lattice MC simulations on lattices of size $32^3 \times N_\tau$ with $N_\tau = 4, 8$. The black line is the heavy quark potential at zero temperature.

do not vanish in the limit of large distances. We have discussed this quite important property in the sections above. At small distances the finite temperature color singlet quark antiquark potential as well as the color averaged potential approach the zero temperature heavy quark potential. Moreover, we can indeed find evidence that the color octet potential energy signals a repulsive behavior at small r. At intermediate distances we observe a small enhancement of the finite temperature color singlet potential compared to $V_{q\bar{q}}(r)$.

3.3.2 Thermal properties of the potential energies

We show in Fig. 3.7 our non-perturbative results for the color singlet potentials at several temperatures below T_c in physical units (MeV) as function of the distance r in fm. We summarize here our data of $\Delta E_1(r,T)$ from lattice MC calculations with $N_\tau = 4$ and 8 at small distances, $r \lesssim 1$ fm. We have noted above that the statistical significance of our potential energies at larger distances is strongly decreasing in this color channel. We thus note here only two properties which follow from this figure: With respect to the statistical uncertainties which still dominate the potentials we do not see evidence for (strong) temperature dependencies at distances $r \lesssim 0.7$ fm and the temperatures

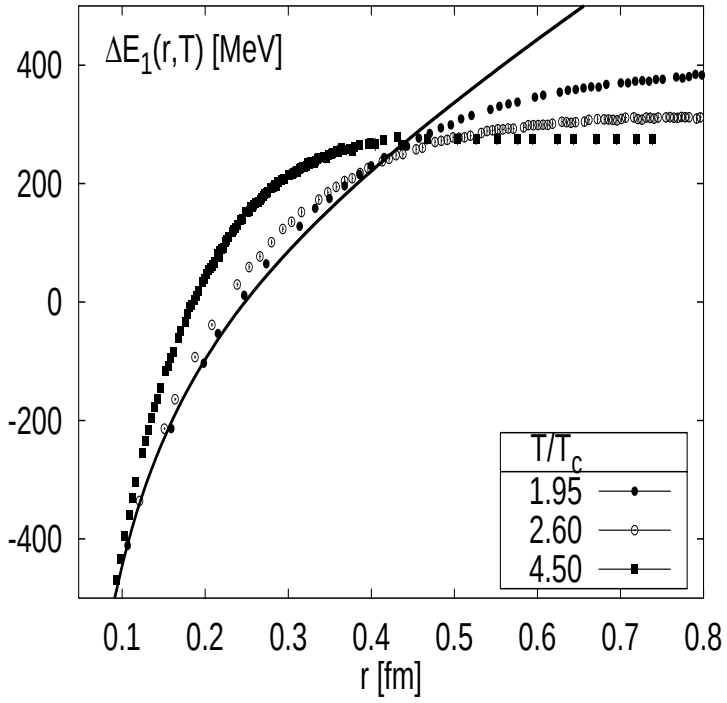

Figure 3.8: Similar to Fig. 3.7, however, here we show the color singlet potentials in a deconfined medium ($T > T_c$).

analyzed in that figure, $T \lesssim 0.95T_c$. In fact, at small distances the finite temperature color singlet potentials become comparable to the heavy quark potential. However, temperature effects become important at larger distances. In fact, the data in Fig. 3.7 and Fig. 3.6 clearly indicate that the finite temperature color singlet energies will break away from the heavy quark potential at $r \gtrsim 0.7$ fm. Moreover, it can be deduced from Fig. 3.7 and the discussions in Sec. 3.1.2 that the potentials will increase with increasing temperatures at large distances.

This property implies that the finite temperature color singlet force defined in (3.7) will be stronger the higher the temperature. As the slopes of the finite temperature potentials is increasing with increasing temperatures this property indeed implies confinement, $K_1(r,T) > 0$. Correspondingly the force has no zeros at temperatures below T_c. This important feature was discussed in Sec. 3.1.2. In the small distance regime it can be followed from Fig. 3.7, however, the finite temperature forces will become comparable to the confining force at zero temperature.

In Fig. 3.8 we summarize our lattice data for the color singlet potentials in the deconfined medium. In this figure we mainly discuss the thermal properties of the finite temperature potentials at intermediate and small distances, $r \lesssim 0.8$ fm. First of all we note that the color singlet internal energies at finite temperature indeed approach the heavy quark

potential at small distances while at large distances they signal deconfinement, but they do not vanish. In fact, the asymptotic ($r \to \infty$) values of the potential energies are indeed quite large, *i.e.* $\Delta E_1 \gtrsim 250$ MeV at the temperatures shown in Fig. 3.8. These values depend strongly on the temperature, for instance $\Delta E_1(r, T_1) \gtrsim \Delta E_1(r, T_2)$ for $T_1 < T_2$. This property was discussed in detail by us in the sections above.

This temperature ordering at large distances, however, changes when going to small distances. It can clearly be seen from Fig. 3.8 that the potential energies approach $V_{q\bar{q}}(r)$ from above. In fact, this property is seen at all temperatures analyzed by us. Consequently, the finite temperature internal energies show an enhancement at short distances compared to the heavy quark potential. In fact, at short distances, for instance at $r \simeq 0.25$ fm, the potential energies show a temperature dependence like

$$\Delta E_1(r, T_1) \quad \gtrsim \quad \Delta E_1(r, T_2) \qquad \text{for } \; 1.9 T_c \lesssim T_1 < T_2 \lesssim 5 T_c \; , \;\; r \simeq 0.25 \text{ fm} \; . \quad (3.26)$$

In conclusion, the color singlet potential energies above T_c show strong temperature dependencies at quite small distances. This may indicate that the color singlet potential energies get modified due to color screening as the r-dependence of the potentials changes strongly in the short distance regime.

Consequently, also the finite temperature color singlet force will show a complicated r- and T-dependence at small distances. While at quite small distances the finite temperature forces will coincide with the force at zero temperature, the enhancement of the color singlet potentials at intermediate distances compared to the heavy quark potential will lead to an enhancement of the forces at finite temperatures. In fact, as the slope in the potentials at small distances is increasing with increasing temperatures also the force at small distances will increase with increasing temperatures. At large distances, however, the finite temperature forces will vanish as the potentials flatten. This property is consistent with deconfinement. It can be followed from Fig. 3.8 that the finite temperature forces will signal deconfinement at smaller distances the higher the temperatures. This property, however, in general does not imply that it will be favorable to separate the static color charges at some high temperature rather than at a lower deconfining temperature.

Further finite temperature potentials at several temperatures below and above the deconfinement point are summarized in Fig. 3.9. In these figures we also show the color averaged potentials at several temperatures. We will not elaborate here any further on a discussion of the potential energies as the thermal properties discussed above can clearly be seen these figures. In conclusion, the basic properties of the finite temperature potentials above T_c are indeed in accordance with our discussions outlined in Sec. 3.1.2. We finally turn to a discussion of the finite temperature entropies.

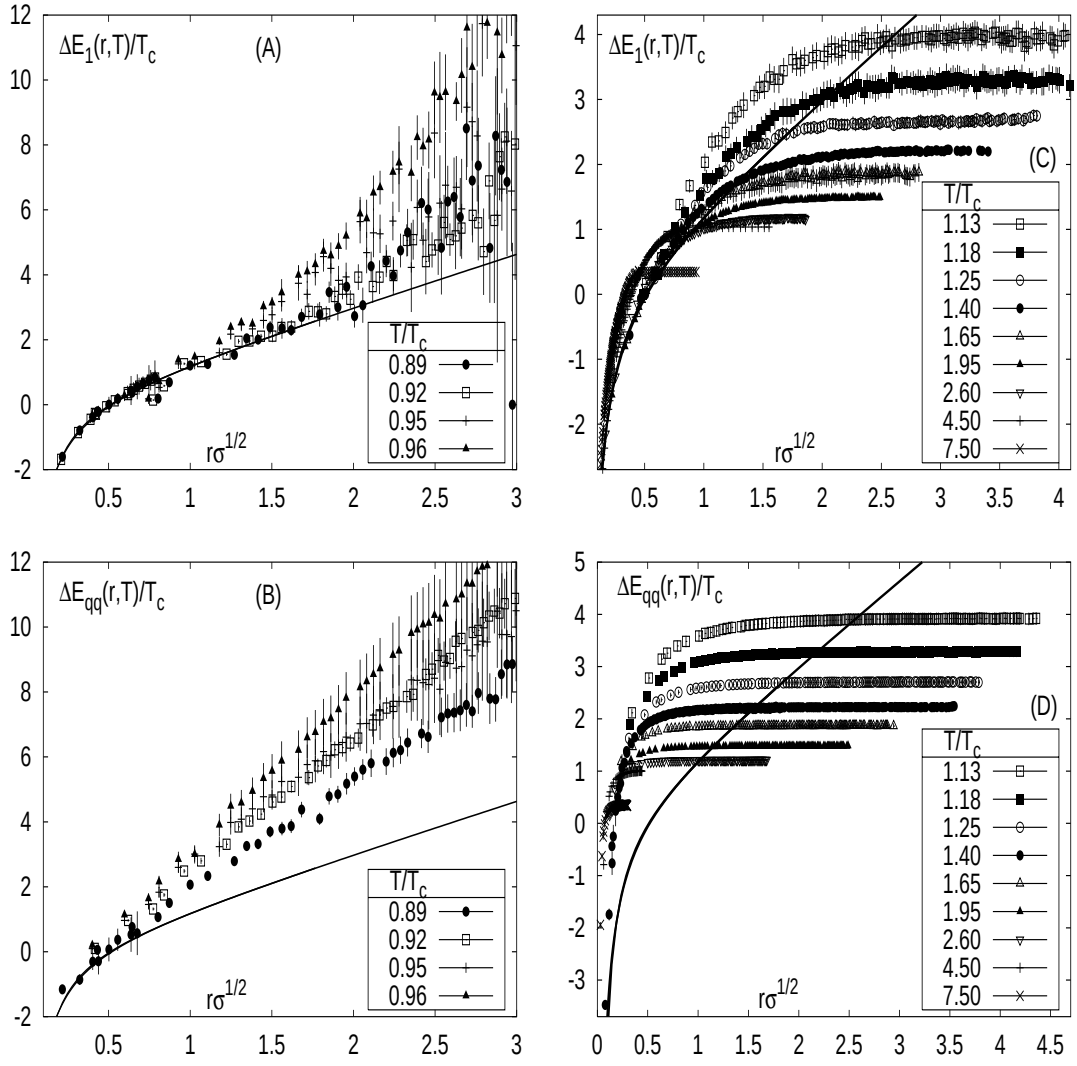

Figure 3.9: The finite temperature potential energies obtained from (3.5) using the renormalized free energies in the color singlet (A, C), and color averaged (B, D) channels at temperatures below and above T_c. The black line indicates in each figure the heavy quark potential.

3.4 Remarks on the entropy contributions in Polyakov loop correlation functions

We have calculated the finite temperature entropies separately independently from the potentials from (3.6) using the methods discussed above. We present here results for the color singlet and color averaged entropies at temperatures below and above the deconfinement point. Similarly to the data for the color octet potentials also the data for the octet entropies are still too noisy for a proper discussion.

In this section we first discuss the thermal properties of the entropies and verify, for example the relation $\Delta S_1 - \Delta S_{q\bar{q}} = -\ln 9$ at short distances predicted from Eq. (2.22). The physical meaning of the entropies we discuss in the following was discussed in Sec. 3.2.

The lattice results for the finite temperature entropies calculated from the thermal relation (3.6) are summarized in Fig. 3.10. In theses figures we show the dimensionless quantities $\Delta S_{1,q\bar{q}}(r,T)$ as a function of the distance in units of the square root of the string tension, $r\sqrt{\sigma}$. Each of these figures shows separately the different color channels at temperatures below and above T_c. In the left column of that figure we show the results at several temperatures in the confinement phase while the figures on the right show our results in the deconfinement phase.

We first discuss the excess entropies at temperatures *below* T_c. Fig. 3.10 (A) shows lattice results for the finite temperature entropies in the color singlet channel. It can be seen from that figure that the entropy contributions in this color channel indeed vanish in the short distance range while at large distances the entropies increase with increasing distances. A vanishing entropy $\Delta S_1(r,T)$ at short distances is consistent with the property we deduced in the last chapter, as at small r the finite temperature free energy is dominated by the potential energy. We note that the entropy contributions increase with increasing temperatures at large distances. This feature was predicted in Sec. 3.1.2 and was verified with our analysis in Sec. 3.2.

The finite temperature entropies in the color averaged channel are shown in Fig. 3.10 (B) at temperatures below T_c. It can be seen that these entropies approach negative values at small distances. Actually, relation (2.22) in combination with the renormalization group equation (2.14) predicts $\ln 9$ at short distances for the color averaged finite temperature entropies, *i.e.* $\lim_{r\to 0} \Delta S_{q\bar{q}}(r,T) = -\ln 9$ (for all temperatures). This limit is indicated in that figure with a black line. It can be seen from that figure that the lattice data seem to approach this limit at small r. Unfortunately, however, we could not go to small enough distances in order to demonstrate this rigorously. From our discussions in Sec. 3.1.2 it follows that the entropies in this channel are supposed to diverge linear with increasing distances. The data in this figure approximately show this behavior.

Let us now discuss the results for the entropies at *temperatures above* T_c. They are shown in the right column of Fig. 3.10 sorted with the different color channels. Lattice results of our investigations of the entropies in the color singlet channel are shown in figure (C). It can be seen from that figure that the finite temperature color singlet entropies do indeed

approach zero values at small distances. This property is consistent with our discussions above. At intermediate distances, however, the entropies increase with increasing distances and approach finite values at large distances. We note that the plateau values at large distances decrease with increasing temperatures. Actually, we have suggested this behavior in Sec. 3.2. From that discussion it follows that we expect a vanishing entropy in the limit of high temperatures. Our results thus confirm this property.

Lattice results for the finite temperature color averaged entropies are summarized in Fig. 3.10 (D). Here we note that the entropies approach indeed negative values at small distances. This property is in accordance with our remarks made above. Actually we expect that the finite temperature color averaged entropies approach $-\ln 9$ in the limit of small r. This limit is indicated with a black line in that figure. At large distances the entropies approach finite values. From a comparison of Fig. 3.10 (C) and (D) it clearly follows that the plateau values of ΔS_1 indeed equal the values of $\Delta S_{q\bar{q}}$ for each temperature.

In general one can say that the finite temperature entropies behave in the way we have deduced in the previous sections. From our discussion of the physical interpretation of the finite temperature entropies in Sec. 3.2 we concluded that the thermal configuration of the system does not change much when a color singlet quark antiquark pair is introduced in the heat bath close to each other. This property is observed by us at all temperatures as ΔS_1 vanishes at small distances. Otherwise, when placing the quark antiquark pair separated with large distances from each other into the thermal heat bath, the thermal configuration gets strongly affected due to the presence of these quarks. Moreover, at temperatures below T_c, the values of the difference in entropy due to the presence of the static charges approach large values and indeed diverges at infinite quark antiquark separations. This feature signals confinement. In contrast to this, at temperatures above the phase transition temperature the difference in entropy due to the presence of the charges approaches finite values which are supposed to vanish at (infinitely) high temperatures. The screening property of the thermal gluons thus allows to separate the quark antiquark pair and consequently, this property is consistent with deconfinement.

Taking the relation between the color screening property and the entropies at finite temperature seriously, the behavior of the r-dependence of the entropies can be used to analyze the physical extent of the gluon clouds which surround the color charges. For instance, from the figures in Fig. 3.10 it follows that the plateau values of the entropies at temperatures above T_c are approached at smaller distances the higher the temperature is. This property suggests that the radius of this clouds decreases with increasing temperatures. A similar quantity (r_{screen}) was deduced by us in the previous chapter. We note, however, that by construction r_{screen} estimates the beginning of screening effects at small distances while the plateau value of entropies rather estimates the extent of the gluon clouds.

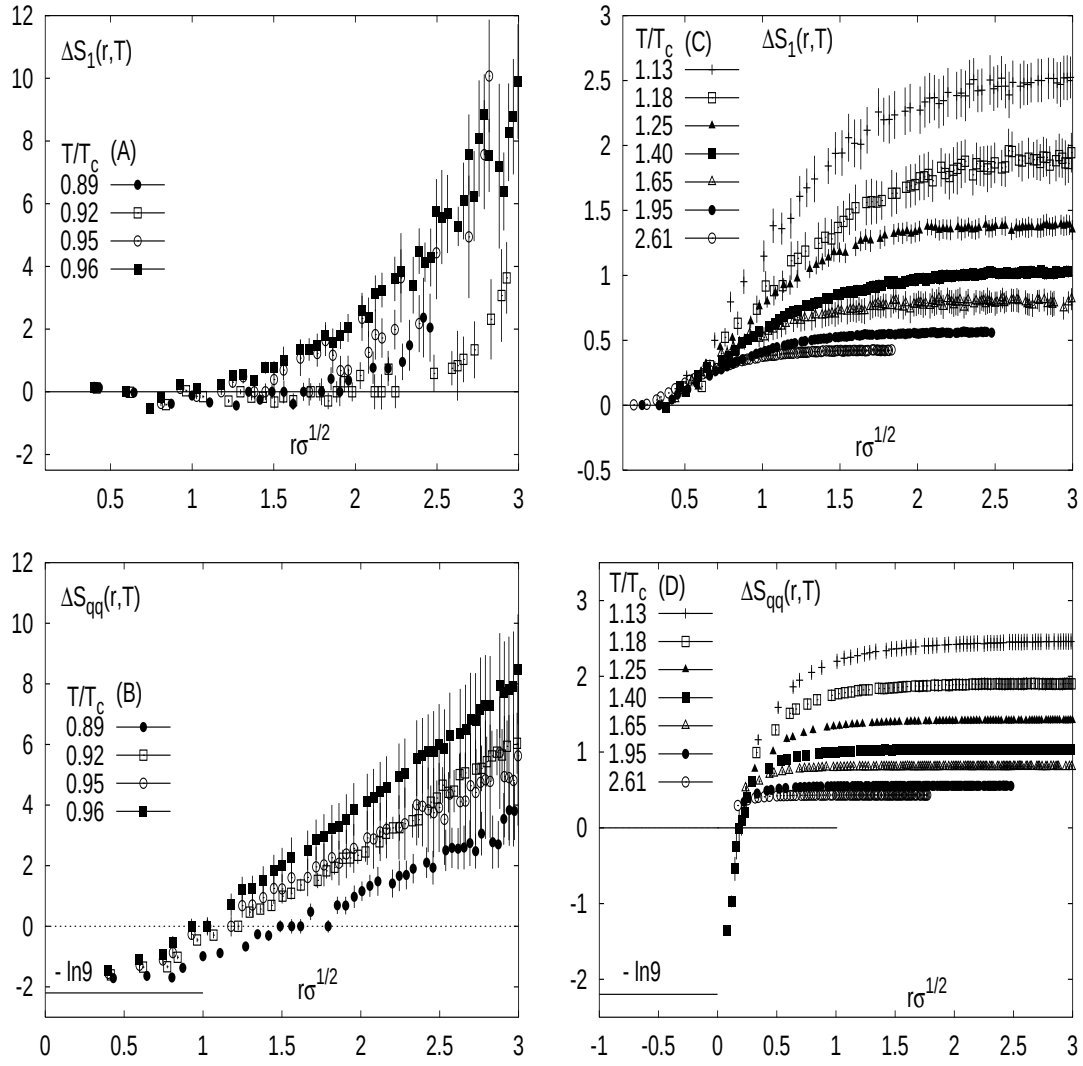

Figure 3.10: The r- and T-dependence of the finite temperature entropy contributions in Polyakov loop correlation functions at several temperatures below and above the deconfinement point. In these figures we show $\Delta S_{1,q\bar{q}}(r,T)$ as functions of the distance $r\sqrt{\sigma}$ separately for the color singlet and color averaged channels.

Summary and outlook

Throughout this thesis we have analyzed the thermal properties of the static quark antiquark free energies in the $SU(3)$ gauge theory at finite temperatures. While the color averaged free energies are well-known from various earlier studies at large distances [33], we presented here a detailed analysis of the finite temperature free energies in the color singlet, color octet ($N = 3$) and color averaged channels from large to rather short distances. Especially the short distance properties of the free energies were analyzed in detail in this thesis. In order to go to small distances, $r \simeq 0.01$ fm, it was mandatory to use lattices of quite large temporal extent (N_τ). We therefore used in our calculations lattices of size $32^3 \times N_\tau$ with $N_\tau = 4, 8$ and 16. In some cases we were also interested in the thermal properties of the free energies at rather large distances. We thus also used lattices of size $N_\sigma^3 \times 4$ with $N_\sigma = 32, 48$ and 64. Actually, this allowed us not only to analyze the free energies at quite short distances ($rT \gtrsim 1/N_\tau$) but also at large distances ($rT \lesssim N_\sigma/(2N_\tau)$). In fact, the shortest distances analyzed by us were about 5 times smaller than those used in calculations of the free energies in other existing studies at finite temperatures and about 10 times smaller than those used in corresponding lattice studies of the heavy quark potential at zero temperature [55, 54]. We used in our lattice simulations the tree level improved Symanzik gauge action and corrected our data for lattice artifacts by using the gluon propagator method [55]. By minimizing lattice artifacts in our analysis of the free energies we extracted continuum properties from our lattice data even at distances of the order of the lattice spacing, $r \simeq a$.

For our analysis of the free energies we used lattice simulations at several lattice spacings covering the temperature range from $T \simeq 0.85T_c$ up to temperatures several times the deconfinement point. For instance, the highest temperature resolved by us is about $12T_c$. We should note here that the analysis in chapter 3 required derivatives of the free energies with respect to temperature and thus the knowledge of the free energies in small temperature steps in the whole temperature range was needed. In parts we calculated the free energies in temperature steps of about $\Delta T \simeq 0.05T_c$.

The data for the color singlet and color octet free energies were calculated from gauge dependent correlation functions and thus required gauge fixing. However, it has recently been shown that the free energies from correlation functions we used coincide with a gauge independent formulation of the free energies when fixing the Coulomb gauge [23]. By fixing this gauge we indeed presented a first gauge independent analysis of the color $SU(3)$ singlet and octet free energies.

In the first chapter we analyzed the free energies from large to short distances. In the spirit of high temperature perturbation theory we defined the so-called screening functions [74] for the color singlet free energies which were used by us to separate the large distance behavior ($rT \gg 1$) of the free energies from their short distance behavior ($rT \ll 1$). We used this separation for the analysis of non-perturbative effects related to screening at large distances. In fact, we found evidence that the large distance high temperature behavior of the color singlet free energies are dominated by one gluon exchange predicted from high temperature perturbation theory. This allowed us to extract the screening masses from the color singlet free energies in terms of correlated fits. The temperature dependence of the masses (m_D) we obtained from these studies can be well described by $m_D/m_{\rm pert} \simeq 1.5(1)$ at temperatures down to $T \gtrsim 2T_c$, where $m_{\rm pert}$ was defined in spirit of high temperature perturbation theory, *i.e.* $m_{\rm pert}(T) = g(T)T$.

For our analysis of the short distance properties of the free energies we resorted to methods frequently used at zero temperature [55, 54]. In order to cancel undetermined constants from the free energies at small distances we calculated the effective coupling from the color singlet free energies, *i.e.* $\alpha_{\rm eff(1)} \equiv d\Delta F_1/dr$. We compared this quantity to the force at zero temperature. We concluded that at short distances the color singlet free energies become comparable to the heavy quark potential (at zero temperature) in terms of the effective coupling.

We closed the first chapter with notes on the free energies below the deconfinement point. We observed that the different free energies signal confinement and behave uniquely at large distances, *i.e.* also the color octet free energies signal confinement. Similar findings have been reported in earlier studies by us [82] and for $SU(2)$ in Refs. [23, 69]. At small distances we found evidence for a repulsive color octet free energy. This is expected from high temperature perturbation theory.

In the second chapter we turned to the renormalization of the Polyakov loop and its correlation functions on the lattice. A well suited starting point for that discussion was the observation of dominant vacuum physics in the 2-point Polyakov loop correlation functions at small distances. We concluded that a proper renormalization could be obtained by matching the free energies at small distances to the heavy quark potential. This renormalization prescription fixes some effective renormalization constant, $Z^R(g^2)$, in the Polyakov loop, *i.e.*

$$L^R(\mathbf{x}) \;\equiv\; Z_L \prod_{x_0=1}^{N_\tau} Z_U U_0(x_0,\mathbf{x}) \;=\; \left(Z^R(g^2)\right)^{N_\tau} L(\mathbf{x}).$$

We have shown that the 2-point Polyakov loop correlation functions for the color singlet, octet and averaged free energies can be fixed through renormalization with one single renormalization constant. In fact, we showed that the relative normalization of the free energies is such that they coincide at large distances while in the intermediate and short distance regime the color structure dominates the behavior of the free energies. At short distances, we have shown that the difference in color singlet and averaged free energy is determined by some entropy-like, temperature dependent constant, which for color $SU(N)$

is given by $T \ln N^2$. This shows that the color averaged free energies are indeed quite different from a two gluon exchange dominated contribution at small distances.

Our renormalization prescription indeed cancels the linear divergence on the lattice and the renormalized Polyakov loop and its correlation functions do not show any dependences from the finite temporal lattice extent. This property has been investigated by us with using lattices of different temporal extent. For instance, we showed that in this way the Polyakov loop expectation values deduced from simulations with $N_\tau = 4, 8$ and 16 lie on a universal, temperature dependent curve. The renormalized Polyakov loop is thus well-behaved in the continuum limit and can be used as an order parameter for the confinement deconfinement phase transition.

Having fixed the Polyakov loop on the lattice through renormalization, *i.e.* having fixed the renormalization constant $Z^R(g^2)$, opens the possibility for different studies of related problems. A quite interesting study in future will be to analyze the relation of the effective renormalization constant with renormalization constants which are specific to the gauge field and coupling renormalization, as this could lead to a strictly non-perturbative renormalized lattice gauge action. A discussion of Polyakov loops models [25, 26] and the equation of state [27, 28] with renormalized Polyakov loops can now be performed. Moreover, the renormalization constant $Z^R(g^2)$ fixes any n-point Polyakov loop correlation function. An analysis of the renormalized 3-point functions based on the the constants deduced by us is subject of present and future studies (see for instance [112, 113]).

In the last chapter we suggested that the renormalized free energies could be used to calculate the finite temperature potentials and entropies. We calculated these quantities using thermodynamic relations, *i.e.* we extracted $\Delta E_i(r,T)$ and $\Delta S_i(r,T)$ non-perturbatively from

$$\Delta E_{1,8,q\bar{q}}(r,T) \;=\; -T^2 \frac{\partial \Delta F_{1,8,q\bar{q}}(r,T)/T}{\partial T} \quad \text{and} \quad \Delta S_{1,8,q\bar{q}}(r,T) \;=\; -\frac{\partial \Delta F_{1,8,q\bar{q}}(r,T)}{\partial T}\,.$$

The properties of these potentials (and entropies) are quite complex and in parts different from the usual expectations. Although we have shown that the potentials below T_c signal confinement in the different color channels, we observed that the effective string tension in the confining potentials increases with increasing temperatures. However, the temperature dependence of the color singlet confining potentials turns out to be small, *i.e.* they are comparable to the heavy quark potential at distances of about $r \lesssim 0.7$ fm and $T \lesssim 0.95 T_c$. This property, however, may change when going to higher temperatures. Our calculations of the potentials in the deconfined medium also show new properties. For instance, in contrast to a vanishing potential in the deconfined medium at large distances we have quantified a non-vanishing, however clearly deconfining potential. Only in the high temperature limit we expect a vanishing potential at large distances. Moreover, the behavior of the potentials at small distances is quite complex and is different in different color channels. For instance, the color singlet potentials approach the heavy quark potentials at small r while the color octet potentials signal a repulsive behavior.

The physical relevance of the finite temperature potentials determined by us is evidently

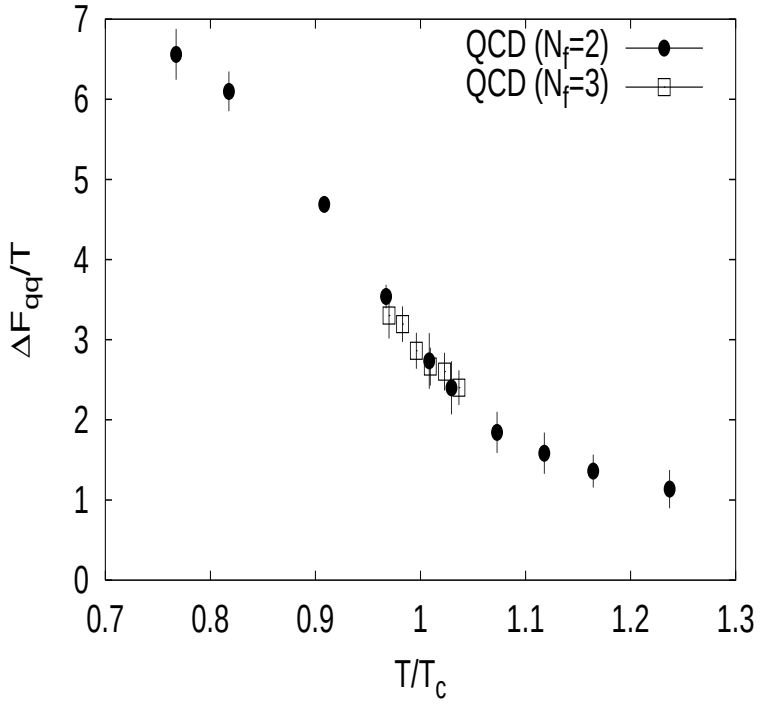

Figure 3.11: The (renormalized) free energy in full QCD at asymptotic large distances ($\Delta F_{q\bar{q}}(T)/T \equiv \lim_{r\to\infty} \frac{\Delta F_{q\bar{q}}(r,T)}{T}$) as function of the temperature. This figure summarizes first (preliminary) lattice results for light dynamic fermions in color $SU(3)$-QCD with 2 (closed circles) and 3 (open squares) flavors.

large as model calculations allow to discuss binding properties of heavy quark bound states. Up to now only phenomenologically inspired potentials could be used in such analyses to define potentials at finite temperature. We suggest here to use these new potentials in model calculations in future. Such kind of analyses are in progress by us (see Ref. [136]). Of even greater relevance than the potentials in $SU(3)$ are, however, the finite temperature potentials in full QCD. Their calculation can follow from now on. Indeed, the conceptual approach we developed in this thesis is subject of several different investigations in full QCD at finite temperature (see Fig. 3.11 and Ref. [119]) and is also in progress at finite densities [128]. In conclusion, the study of thermal properties of renormalized Polyakov loop correlation functions has opened many new directions for future studies.

Appendix A

Lattice simulation parameters and results

This appendix is organized as follows:

A1. Lattice gauge action
A2. Temperature scale and the string tension
A3. Tables of simulation parameters and results

A1. Lattice gauge action

We refer to the tree level improved Symanzik lattice gauge action [81, 79] consisting of 1×1 and 2×1 loops given by

$$S^{(2,1)} = \beta \sum_{x,\nu>\mu} \frac{5}{3}\Big(1 - \frac{1}{N}\,\mathrm{Re\ Tr}\ \square_{\mu\nu}(n)\Big) - \frac{1}{6}\Big(1 - \frac{1}{2N}\mathrm{Re\ Tr}\Big(\square_{\mu\nu}(n) + \square_{\mu\nu}(n)\Big)\Big). \qquad \text{(A.1)}$$

This reconstruction of the continuum gauge action on the lattice is known to correct for the ultra-violet properties of the action in the continuum limit. In our simulation we used a pseudo heat bath algorithm with FHKP updating [137, 138] in the $SU(2)$ subgroups. Each heat bath updating is supplemented by 4 over-relaxation steps. Details on this methods can be found in [81, 139] and in the standard textbooks, for instance [18].

A2. Temperature scale and string tension

The relation (in QCD/$SU(N)$) between the coupling g and the lattice spacing is in general given by the renormalization group equation,

$$a\frac{dg}{da} = \beta(g), \qquad \text{with } \beta(g) \overset{g\to 0}{=} \beta_0 g^3 + \beta_1 g^5 + \mathcal{O}(g^7) \qquad \text{(A.2)}$$

where $\beta(g)$ denotes the renormalization group β-function. In the limit $g \to 0$ the relation between coupling and lattice spacing a can be calculated perturbatively (see right part of Eq. (A.2)). The first two *universal* coefficient for $SU(3)$ are given by $\beta_0 = 11/(16\pi^2)$ and $\beta_1 = 102/(16\pi^2)^2$ (see for instance [1]). Integrating (A.2) using the low g approximation of $\beta(g)$ leads to

$$a\Lambda_L \equiv R(\beta) \quad = \quad \left(\frac{2N\beta_0}{\beta}\right)^{\frac{-\beta_1}{2\beta_0^2}} \exp\left(-\frac{\beta}{4N\beta_0}\right). \tag{A.3}$$

Note that in this relation $\beta = 6/g^2$ is the lattice coupling in (A.1).

In order to set the scale in lattice calculations one is forced to relate the lattice spacing a to a physical quantity. This can be done in terms of the zero temperature string tension $\sqrt{\sigma}$ that appears in the heavy quark potential. One than uses the renormalization group inspired ansatz [140]

$$\sqrt{\sigma}\, a(\beta) \quad = \quad R(\beta)\left(1 + c_2\hat{a}^2(\beta) + c_4\hat{a}^4(\beta)\right)/c_0, \tag{A.4}$$

where $\hat{a} \equiv R(\beta)/R(\bar{\beta})$. $\bar{\beta}$ is a normalization constant. In [141] this ansatz has been fitted to the string tension data from [86] in the coupling range $\beta \in [4, 5]$ with $\bar{\beta} = 6.0$. We take the values given in Tab. C3 of Ref. [141]: $c_0 = 0.0693(7)$, $c_2 = 0.00392(51)$, $c_4 = 0.0000146(45)$. The temperature scale T/T_c is then fixed through (A.4). For instance, we refer to the temperature given by

$$\frac{\sqrt{\sigma}a(\beta)}{\sqrt{\sigma}a(\beta_c)} \quad = \quad T/T_c, \tag{A.5}$$

where β_c is the critical lattice coupling. β_c is specific to the temporal extent of the lattice, N_τ, and to the parameterization of the continuum action on the lattice. The critical couplings for the lattice gauge action we use are presented in [86].

A3. Tables of simulation parameters and results

We list our results for the Polyakov expectation values from simulations on lattices of size $32^3 \times 4, 8$ and 16. In these tables (see Tabs. A.2,A.3,A.4) we also give the number of independent configurations used in our calculations. The color singlet and octet free energies are calculated by using each tenth of these configurations. In parts of our analyses we also use the high statistics calculations used in the presentations of the color averaged free energies in Ref. [33]. For a corresponding list of results on the Polyakov loop expectation value see Tab. A.1 of Ref. [142]. Our results coincide with the results given in that table.

Tree level improved action								
$N_\tau = 4$			$N_\tau = 8$			$N_\tau = 16$		
β	T/T_c	N_σ	β	T/T_c	N_σ	β	T/T_c	N_σ
3.950	0.792(5)	32,64	4.3212	0.75(1)	32	4.9898	0.90(3)	32
3.974	0.830(5)	32	4.4231	0.86(1)	32	5.2333	1.20(4)	32
4.000	0.874(4)	32,64	4.4472	0.90(1)	32	5.4261	1.50(5)	32
4.020	0.907(3)	32,64	4.4551	0.91(1)	32			
4.040	0.942(3)	32,64	4.4784	0.93(1)	32			
4.050	0.959(1)	32,64	4.4862	0.95(1)	32			
4.060	0.977(1)	32,64	4.4937	0.96(1)	32			
4.070	0.9948(5)	32	4.5592	1.04(1)	32			
4.080	1.0128(5)	32	4.5951	1.10(1)	32			
4.090	1.031(1)	32	4.6290	1.14(2)	32			
4.100	1.049(2)	32	4.6605	1.19(2)	32			
4.127	1.100(3)	32	4.6619	1.20(2)	32			
4.154	1.151(1)	32	4.6874	1.23(1)	32			
4.179	1.200(7)	32	4.7246	1.29(1)	32			
4.200	1.24(1)	32	4.8393	1.49(2)	32			
4.229	1.30(1)	32	4.8661	1.55(2)	32			
4.321	1.50(2)	32	4.8921	1.60(2)	32			
4.343	1.55(2)	32	5.4261	3.00(3)	32			
4.365	1.60(2)	32	6.0434	6.00(3)	32			
4.400	1.68(2)	32	6.3910	9.00(3)	32			
4.600	2.21(5)	32	6.6450	12.0(5)	32			
4.839	3.00(9)	32						

Table A.1: Parameters of the simulations of pure $SU(3)$ gauge theory with tree level improved gauge action. The values for the critical couplings are $\beta_c(N_\tau = 4) = 4.0729(3)$ from [86] and $\beta_c(N_\tau = 8) = 4.5237$, $\beta_c(N_\tau = 16) = 5.0781$. The latter critical couplings follow from Eq. (A.5) with $\beta_c(N_\tau = 4) = 4.0729(3)$.

Tree level improved action, $N_\tau = 4$			
β	measurements	$\lvert\langle \mathrm{Tr}L\rangle\rvert$	
4.080	2220	1.2008566e-01	8.1083231e-04
4.090	1930	1.3414046e-01	6.3148293e-04
4.100	1340	1.4427162e-01	6.6221075e-04
4.127	1730	1.6244043e-01	3.5053976e-04
4.154	1000	1.7582385e-01	2.7351872e-04
4.179	1000	1.8602197e-01	2.3329379e-04
4.200	1176	1.9356189e-01	2.9427799e-04
4.229	1000	2.0279890e-01	2.7679876e-04
4.321	1000	2.2809273e-01	3.0906480e-04
4.343	1000	2.3340925e-01	1.7000425e-04
4.365	1000	2.3869007e-01	1.7026784e-04
4.400	1000	2.4672793e-01	1.3478539e-04
4.600	1000	2.8610242e-01	2.1345168e-04
4.839	1000	3.2553036e-01	1.8535734e-04

Table A.2: The Polyakov loop expectation values from calculations with lattices of size $32^3 \times 4$.

Tree level improved action, $N_\tau = 8$			
β	measurements	$\lvert\langle \mathrm{Tr}L\rangle\rvert$	
4.5592	3881	4.2185466e-02	5.7273022e-04
4.5600	1600	4.2025716e-02	9.1828924e-04
4.5951	1550	4.9586602e-02	5.1584666e-04
4.6290	1358	5.4031650e-02	5.2602321e-04
4.6605	3600	5.8694668e-02	3.0582187e-04
4.6619	1384	5.8744140e-02	3.5625746e-04
4.6874	1200	6.2664022e-02	3.2919255e-04
4.7246	1200	6.6610751e-02	3.1329866e-04
4.8393	4343	7.8954616e-02	2.1751524e-04
4.8661	1200	8.1658141e-02	4.8953539e-04
4.8921	1200	8.4482984e-02	3.4995984e-04
5.4261	4000	1.3747933e-01	1.8004744e-04
6.0434	4502	1.9359154e-01	2.1537250e-04
6.3910	1400	2.2213405e-01	2.8557959e-04
6.6450	1000	2.4220532e-01	3.6100557e-04

Table A.3: The Polyakov loop expectation values from calculations with lattices of size $32^3 \times 8$.

Tree level improved action, $N_\tau = 16$			
β	measurements	$\lvert\langle \mathrm{Tr}L \rangle\rvert$	
5.233300e+00	3350	1.014034e-02	2.574962e-04
5.426100e+00	1692	1.454373e-02	2.373886e-04

Table A.4: The Polyakov loop expectation values from calculations with lattices of size $32^3 \times 16$.

Appendix B

Details on the computations in chapter 1

In this appendix we give notes on the 1-loop perturbative calculations that we referred to in chapter 1. They are organized as follows:

B1. Feynman rules and calculation methods at finite T
B2. The non-static contributions
B3. Diagram calculations of Π_{00}^{ns}
B4. IR and UV properties
B5. Low- and high-T approximation
B6. Fourier transformation to position space

The first part (B1) is aimed to provide an introduction into the calculation techniques of finite temperature Feynman diagrams. It is therefore rather pedagogic. The parts that follow are specific to our calculation and summarize our results.

B.1 Feynman rules and calculation methods at finite T

By involving the auxiliary fields C, $\bar{C}$ (being the ghost fields) and ξ (being the gauge fixing parameter), the gauge action (in static gauge, $\partial_0 A_0 = 0$) can be rewritten with respect to the gauge field boundary conditions as [143]

$$\begin{aligned} S[A_i, A_0, C, \bar{C}] \;=\; & \int dx_0 \int d^3x \Big\{ -\frac{1}{2}\partial_0 A_i^a(x)\partial_0 A_i^a(x) - \frac{1}{2}\partial_i A_0^a(x)\partial_i A_0^a(x) \\ & -\frac{1}{4}F_{ij}^a(x)F_{ij}^a(x) + g f^{abc} A_i^a(x) A_0^b(x)\partial_i A_0^c(x) + g f^{abc} A_0^a(x) A_i^b(x)\partial_0 A_i^c(x) \\ & -\frac{1}{2}g^2 f^{abc} f^{ade} A_i^b(x) A_0^c(x) A_i^d(x) A_0^e(x) - \frac{1}{2\xi}\sum_{i=1}^{3}\left(\partial_i A_i^a(x)\right)^2 \\ & +\mathcal{L}_{GI}(x)\Big\}. \end{aligned} \tag{B.1}$$

where $\mathcal{L}_{GI}(x)$ contains the ghost-field interaction with only static fields. The relations between the static fields (A_i) and the non-static fields (A_0) can be read-off from this

expressions and define the Feynman rules. Here we list our results:

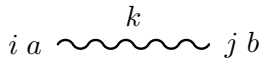

$$= \delta^{ab}\left(\delta_{ij} + \frac{k_i k_j}{k_0^2}\right)\frac{1}{k^2}(1-\delta_{k_0,0}) + \delta^{ab}\frac{1}{\mathbf{k}^2}\left(\delta_{ij} - (1-\xi)\frac{k_i k_j}{\mathbf{k}^2}\right) \tag{B.2}$$

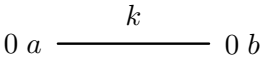

$$= \delta^{ab}\frac{1}{\mathbf{k}^2}\delta_{k_0,0} \tag{B.3}$$

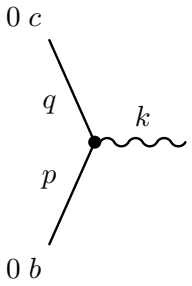

$$= \frac{1}{2}igf^{abc}(p-q)_i \tag{B.4}$$

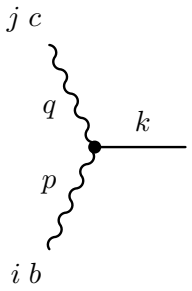

$$= \frac{1}{2}igf^{abc}(p-q)_0\delta_{ij} \tag{B.5}$$

$$= -\frac{1}{2}g^2 f^{abc}f^{ade} \tag{B.6}$$

We note that the non-static modes are not affected by the details of the gauge fixing. More details on this field can be found in [144, 145].

Let us finally give some useful formulas that may help to evaluate Feynman diagrams at finite temperatures. In general, the calculation procedure is the following: In an Euclidean D-dimensional thermal field theory in thermal equilibrium at finite temperature the finite time integration from 0 to $\beta = 1/T$, together with the resulting periodic (anti-periodic) boundary conditions that obey the fields, are often arranged by expanding the fields in

eigenmodes, the so-called *Matsubara frequencies*. This causes that the finite time integration is replaced by a sum over an infinite number of fields which appears in additional to the remaining $(D-1)$-dimensional integrals. In general, the computation of such objects can be performed in *three* steps: In the first step the summation of the frequencies is handled by using the so-called *frequency sum rules*. We only need bosonic rules, *i.e.*

$$T\sum_{n=-\infty}^{+\infty}\frac{1}{\mathbf{p}^2+\omega_n^2} = \frac{1}{|\mathbf{p}|}\Big(1+2n(|\mathbf{p}|)\Big) \tag{B.7}$$

$$T\sum_{n=-\infty}^{+\infty}\frac{1}{[\mathbf{p}^2+\omega_n^2][\mathbf{q}^2+\omega_n^2]} = \frac{1}{2|\mathbf{p}||\mathbf{q}|}\Big[\frac{1+n(|\mathbf{p}|)+n(|\mathbf{q}|)}{|\mathbf{p}|+|\mathbf{q}|}+\frac{n(|\mathbf{q}|)-n(|\mathbf{p}|)}{|\mathbf{p}|-|\mathbf{q}|}\Big]. \tag{B.8}$$

In these relations the four-dimensional momentum (p) is rewritten as $p=(p_0,\mathbf{p})$ where $p_0=\omega_n=2\pi nT$ denotes the Matsubara frequencies. $n(x)$ is the Bose-Einstein distribution function, $n(x)=1/(\exp(-x/T)-1)$. In fact, $n(x)$ represents all the temperature dependence of the finite temperature integrals. In conclusion, there is a temperature dependent part, which is (by construction) convergent in the ultra violet regime and there exists a zero temperature part, which can be divergent in this regime. In general, so, both parts are well separated through (B.7) and (B.8).

This is the initial point for the *second step*: The calculation of the zero temperature part. The zero temperature part, in general divergent, has to be regularized. Regularization means that we separate the divergence from the finite contributions. We make use of the *dimensional regularization*. In this regularization scheme, the dimension of the divergent integral (now $d=3$) gets continuously reduced to an arbitrary dimension, $d=3\to 3-2\epsilon$, in which the integral is supposed to be convergent. In order to ensure a dimension-less (bare) coupling g, it is necessary to introduce a so-called *regularization scale*, ν, on which all dimensions are put, $g\to g\nu^\epsilon$. In principle, the calculation of divergent diagram integrals works, once more, in two steps: In the first step, the divergent integrand is prepared to be of the form that the standard formula of dimensional regularization can be used. This can be achieved by applying to the Feynman parameterization and, if necessary, symmetric integrations. For instance, the *Feynman parameterization formula* is given by

$$\frac{1}{a^\alpha b^\beta}=\frac{\Gamma(\alpha+\beta)}{\Gamma(\alpha)\Gamma(\beta)}\int_0^1 dx\frac{x^{\alpha-1}(1-x)^{\beta-1}}{[b+x(a-b)]^{\alpha+\beta}}. \tag{B.9}$$

One then applies to the *standard formula* in d arbitrary dimensions:

$$\int\frac{d^dp}{(2\pi)^d}\frac{(p^2)^\alpha}{[p^2+R^2]^\beta} = \frac{1}{(4\pi)^{\frac{d}{2}}}\frac{\Gamma(\alpha+\frac{d}{2})\Gamma(\beta-\alpha-\frac{d}{2})}{\gamma(\frac{d}{2})\Gamma(\beta)}[R^2]^{\frac{d}{2}-\beta+\alpha}. \tag{B.10}$$

In order to split-off the divergence from the finite contributions one enlarges the reduced dimension to the initial one, $\epsilon\to 0$. In general, in this limit one results into an expression like $\sim 1/\epsilon+\mathcal{O}(\epsilon)$+finite parts. In this way, the divergence $(\sim 1/\epsilon)$ is well separated from the finite contributions. Useful Laurent expansions for the Γ- and Riemann-Zeta-functions around $\epsilon=0$, which find application in our calculation (see below), are

$$\Gamma(\epsilon) = \frac{1}{\epsilon}-\gamma_E+\mathcal{O}(\epsilon), \tag{B.11}$$

$$\Gamma(\epsilon-1) = -\frac{1}{\epsilon}+\gamma_E-1+\mathcal{O}(\epsilon), \tag{B.12}$$

$$\Gamma(\epsilon+\frac{1}{2}) = \sqrt{\pi}-\sqrt{\pi}(\gamma_E+2\ln 2)\epsilon+\mathcal{O}(\epsilon^2), \tag{B.13}$$

$$\zeta(1+\epsilon) = \frac{1}{\epsilon}+\gamma_E+\mathcal{O}(\epsilon), \tag{B.14}$$

where γ_E denotes the Euler constant, $\gamma_E \simeq 0.577215....$ The separated divergence can be subtracted by *renormalization*. As we use a dimensional regularization, we use in our calculations the $\overline{MS}$-scheme.

The *third step*, unfortunately, is the most expensive part of the calculation of diagrams at finite temperature. It is the calculation of the remaining finite temperature contribution. Indeed we have to work out a d-dimensional finite integral that contains no UV divergences. In general, it is most suitable to introduce spherical coordinates and to apply to numerical integration methods. However, in order to do so, one has to ensure that the integrals behave finite in the low momentum (infra-red) regime. It should be obvious, that the third and second steps can be exchanged.

B2. The non-static contributions

The connected parts of the 2-point Polyakov loop correlation function given in (1.33) define the quark antiquark free energy $\delta F_{q\bar{q}}(r,T)$. We rewrite

$$\begin{aligned}\Pi_{00}(k) &\equiv \tilde{\Pi}_{00}(k)+\Pi_{00}(k\to 0)\\ &= \tilde{\Pi}_{00}(k)+m_D^2,\end{aligned} \tag{B.15}$$

and expand in perturbation theory ($g \ll 1$)

$$\frac{1}{k^2+m_D^2+\tilde{\Pi}_{00}(k)} = \frac{1}{k^2+m_D^2}\left(1+\frac{\Pi_{00}(k)-m_D^2}{k^2+m_D^2}+...\right). \tag{B.16}$$

In general, in a thermal field theory the polarization tensor $\Pi_{00}(k)$ to 1-loop order is given by integrals of the form

$$\Pi_{00}^{1-\text{loop}}(k) \simeq T\sum_{n=0,\pm1,\pm2,...}\int\frac{d^3p}{(2\pi)^3}f(p,k,\omega_n), \tag{B.17}$$

where f represents the contributions of various 1-loop diagrams[1] and $\omega_n = 2\pi nT$ denote the Matsubara frequencies. The contributions with vanishing frequencies, $n=0$, are related to the static contributions while the terms with non-vanishing frequencies $n=\pm1,\pm2,...,\pm\infty$, produce the non-static contributions. As discussed above we are here interested in the *infinite set* of non-static contributions: According to the general decomposition given in (B.17), we refer to the *static polarization tensor*, $\Pi_{00}^{st}(k)$, and to the *non-static polarization tensor*, $\Pi_{00}^{ns}(k)$, via

$$\Pi_{00}(k) = \Pi_{00}^{st}(k)+\Pi_{00}^{ns}(k). \tag{B.18}$$

[1]We will suppress the index '1-loop' from now on as our computations in this chapter are restricted to the 1-loop level.

Due to this separation the free energy consists of a static part, which is known, and of a non-static part, which we aim to work out in the following. In the language of Feynman diagrams, the non-static gauge field polarization tensor to 1-loop order is given by

$\Pi_{00}^{ns}(k)$ = 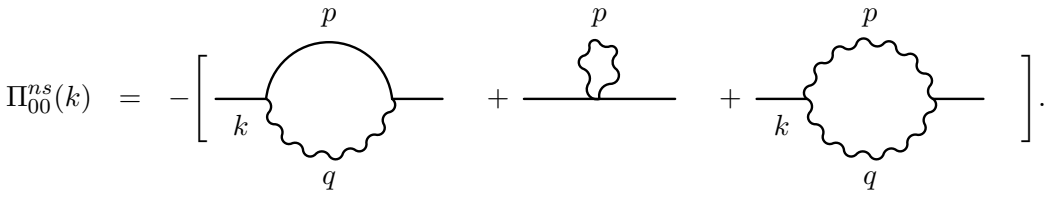

(B.19)

The first diagram in (B.19) vanishes because of energy-momentum conservation as the straight lines denote the non-static fields. The involved δ-functions, which guaranty the conservation laws, lead to a loop integration over zero. Secondly, the 'tadpole' diagram reduces to the well-known formula (see for instance Refs. [11, 12]) $\sum\!\!\!\!\!\!\int_p 1/p^2 = T^2/12$. As a consequence this tadpole diagram does not participate in the dynamics of the field propagation: it is given by $-2N\delta^{ab}g^2T^2/12$. The calculation of the remaining diagram and further details are summarized in B3.

As it is usually the case in a finite temperature field theory, the calculation of $\Pi_{00}^{ns}(k)$ leads to an evaluation of ultraviolet (UV) divergent zero temperature contributions from the vacuum and to UV convergent thermal contributions from the gluonic heat bath. In other words,

$$\Pi_{00}^{ns}(k) = \Pi_{00}^{ns(0)}(k) + \underbrace{\Pi_{00}^{ns(T)}(k) + \Pi_{00}^{ns(T)g}(k)}_{\text{thermal part: } \Pi_{00}^{ns(m)}}, \tag{B.20}$$

where we have split-off from $\Pi_{00}^{ns(m)}$ (matter part) the piece $\Pi_{00}^{(T)g}(k)$ which is specific to our gauge. In conclusion, the contributions from the non-static gauge field sector to the free energy in momentum space result from the quantity

$$\frac{1}{k^2+m_D^2+\tilde{\Pi}_{00}} = \underbrace{\frac{1}{k^2+m_D^2}}_{\text{LO}} + \underbrace{\frac{\Pi_{00}^{st}(k)}{(k^2+m_D^2)^2}}_{\text{static}} + \underbrace{\frac{-m_D^2+\Pi_{00}^{ns(0)}(k)+\Pi_{00}^{ns(T)}(k)+\Pi_{00}^{ns(T)g}(k)}{(k^2+m_D^2)^2}}_{\text{non-static}} + \ldots \tag{B.21}$$

As we are rather interested in the free energy in position space, $\delta F_{q\bar{q}}(r,T)$, than in the free energy in momentum space, the Fourier transformation of (B.21) will lead to the contributions of the non-static fields. According to the decomposition above, we will refer to them as $\delta F_{q\bar{q}}^{ns(0)}$, $\delta F_{q\bar{q}}^{ns(T)}$ and $\delta F_{q\bar{q}}^{ns(T)g}$. The term arising from the Debye mass m_D^2 in the non-static contribution will produce the resummed leading order term. Unfortunately it is not possible to get an analytic expression for $\Pi_{00}^{ns}(k)$ in general. However, this can be achieved in two limits of k: The low temperature approximation with $k \gg p \gg T$ and the high temperature approximation where $k \ll p \ll T$.

In the *low temperature limit* we expect for dimensional reasons

$$\Pi_{00}^{ns}(\mathbf{k} \gg T) \quad = \quad c_0 k^2 + c_1 kT + c_2 T^2, \tag{B.22}$$

with constants c_0, c_1 and c_2. We identify the coefficient proportional to k^2 with contributions from the vacuum which can be taken from [143, 105]:

$$c_0 \quad = \quad -\frac{g^2 N}{16\pi^2}\left(\frac{11}{3}\ln\frac{4\pi\nu^2}{k^2} - \frac{11}{3}\gamma_E + \frac{31}{9}\right). \tag{B.23}$$

The thermal contributions in this approximation lead to

$$c_1 = \frac{1}{4}Ng^2 \quad \text{and} \quad c_2 = -\frac{1}{18}Ng^2. \tag{B.24}$$

In the other limit, the *limit of vanishing* k, one expects to find the Debye mass, *i.e.* $\Pi_{00}^{ns}(\mathbf{k} \ll T) = m_D^2$. In fact we find

$$m_D^2 \equiv \Pi_{00}^{ns}(k=0) = \frac{N_c}{3}g^2T^2. \tag{B.25}$$

Thus our 1-loop computation recovers the well-known gauge independent non-abelian screening mass (see Refs. [57, 24, 60]). We expect, however, that higher order corrections will involve gauge dependent terms.

Our results of the computations presented above are summarized in Fig. B.1 for the case of $SU(3)$. In that figure we show the numerical (full) computation of the matter part of $\Pi_{00}^{ns}(p)$ as a function of the momentum p in units of the temperature T. For the numerical analysis shown in that figure we calculated the matter contributions in steps $p/T = 1$. Fig. B.1 also contains our results from the low (indicated with the dashed line) and the high temperature expansion (see the black line) taken from (B.22) and (B.25). In order to analyze the limits of the validity of the low and high temperature approximation we show $\Pi_{00}^{ns(m)}$ in the range of rather high temperatures, $p/T \lesssim 15$. It can be seen from that figure, that the high temperature approximation of the finite temperature part works indeed quite well at high temperatures. In fact, the high temperature expansion lies on top of the full calculation up to $p/T \lesssim 11$. At larger values, however, the high temperature expansion rapidly deviates from the numerical, exact data. In the low temperature regime the low temperature expansion becomes valid. Indeed, the low temperature expansion works quite well at $p/T \gtrsim 11$. Although we cannot present an analytic expression for the non-static gauge field polarization tensor, it can be quite well described in terms of its low and high T approximations in the whole p/T regime. In fact, we will use the analytic approximations rather than the full expression in the following considerations.

The color averaged quark antiquark free energy $\delta F_{q\bar{q}}(r,T)$ can be written in the 1-loop perturbative approximation as

$$\delta F_{q\bar{q}}(r,T) \quad = \quad \delta F_{q\bar{q}}^{(0)}(r,T) + \delta F^{(1)}(r,T). \tag{B.26}$$

We denote by $\delta F_{q\bar{q}}^{(0)}(r,T)$ the leading order term (see also [57]) and with $\delta F_{q\bar{q}}^{(1)}(r,T)$ the 1-loop ($\mathcal{O}(g^6)$) corrections. Due to the fragmentation of $\Pi_{00}(k)$ in (B.18), the 1-loop

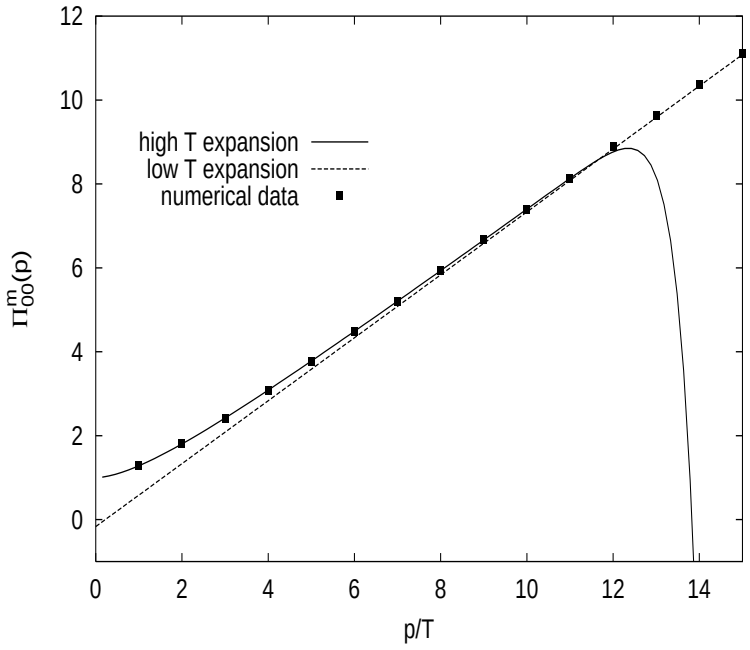

Figure B.1: The matter contribution to the non-static polarization tensor $\Pi_{00}^{ns(m)}$ in the static gauge as a function of the dimension-less momentum p/T. We have chosen the gauge group to be $SU(3)$, $(N = 3)$. The black squares show the numerical computation while the black line denotes the high temperature approximation of $\Pi_{00}^{ns(m)}$ defined in (B.25). The dashed line is the low temperature expansion given in (B.22). In this figure we show the results in terms of Π_{00}/g^2 which allows a study of the polarization tensor independent of the scale in the coupling.

correction term consists of a static (denoted with $\delta F^{st}_{q\bar{q}}(r,T)$) and of a non-static (denoted with $\delta F^{ns}_{q\bar{q}}(r,T)$) part:

$$\delta F^{(1)}_{q\bar{q}}(r,T) \quad = \quad \delta F^{st}_{q\bar{q}}(r,T) + \delta F^{ns}_{q\bar{q}}(r,T). \tag{B.27}$$

It should be obvious that the leading order term does not distinguish between static and non-static contributions. Therefore it is not necessary to indicate explicitly the loop order in the r.h.s. of (B.27). The static contribution $\delta F^{st}_{q\bar{q}}(r,T)$ is well-known [57]. Our results for Eq. (B.26) are shown in Fig. 1.3.

B3. Diagram calculations of Π^{ns}_{00}

We are now prepared to go in detail. We need to calculate:

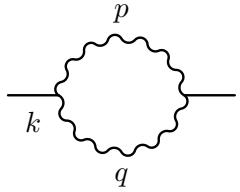

$$= \quad 2N_c g^2 \delta^{ab} T \sum_{n=-\infty}^{+\infty} \int \frac{d^d p}{(2\pi)^d} p_0^2 \tilde{D}_{ij}(p) \tilde{D}_{ij}(q)$$

$$= 2N_c g^2 \delta^{ab}\Big[\frac{3}{2}\frac{T^2}{12} - 2I_1 + I_2 + \frac{1}{2}I_3 + \frac{1}{4}I_4\Big]. \qquad \text{(B.28)}$$

We have indicated (B.2) in this relation as $\delta^{ab}\tilde{D}_{ij}(p)$. The integrals, I_i $(i = 1, ..., 4)$, which appear in (B.28) are defined on

$$I_1 \equiv \sum\!\!\!\!\!\!\int_p \frac{\mathbf{p}^2}{p^2q^2}, \quad I_2 \equiv \sum\!\!\!\!\!\!\int_p \frac{\mathbf{k^2}}{p^2q^2}, \quad I_3 \equiv \sum\!\!\!\!\!\!\int_p \frac{\mathbf{q}^2}{p^2\mathbf{p}^2}, \quad I_4 \equiv \sum\!\!\!\!\!\!\int_p \frac{\mathbf{k}^4}{p^2q^2p_0^2}. \qquad \text{(B.29)}$$

In these notations we have used the short-cut notation $\sum\!\!\!\!\!\!\int = T\sum_{n\neq 0}\int \frac{d^3p}{(2\pi)^3}$. Note that the zero modes ($n = 0$) are missing in this convention. Thus, in order to apply to the frequency sum rules (B.7) and (B.8), we have to add and subtract the zero modes. From power counting of the integrand functions in three dimensions we find that I_1, I_2 and I_3 behave divergent in the ultra violet momentum limit while I_4 is ultra violet convergent. We calculate $I_{1,2,3}$ with the methods introduced above ($P \equiv |\mathbf{p}|/T$):

$$I_1(k) = I_1^{(T=0)}(k) + I_1^{(T)}(k), \text{ with:} \qquad \text{(B.30)}$$

$$\nu^{2\epsilon} I_1^{(T=0)}(k) = \frac{\mathbf{k}^2}{(4\pi)^2}\Big[\frac{1}{12\epsilon} + \frac{1}{12}\ln\frac{4\pi\nu^2}{\mathbf{k}^2} + \frac{2}{3}\gamma_E + \frac{2}{9}\Big] + \mathcal{O}(\epsilon), \qquad \text{(B.31)}$$

$$I_1^{(T)}(k) = \frac{T^2}{(2\pi)^2 K}\int_0^\infty dP P^2 n(P)\Bigg\{\frac{|P+K|^2 - |P-K|^2}{2P^2} + \ln\frac{P+|P+K|}{P+|P-K|} + \ln\frac{P-|P+K|}{P-|P-K|}\Bigg\}, \qquad \text{(B.32)}$$

$$I_2(k) = I_2^{(T=0)}(k) + I_2^{(T)}(k), \text{ with:} \qquad \text{(B.33)}$$

$$\nu^{2\epsilon} I_2^{(T=0)}(k) = \frac{\mathbf{k}^2}{(4\pi)^2}\Big[\frac{1}{\epsilon} + \ln\frac{4\pi\nu^2}{\mathbf{k}^2} + 2 - \gamma_E\Big] + \mathcal{O}(\epsilon), \qquad \text{(B.34)}$$

$$I_2^{(T)}(k) = \frac{KT^2}{(2\pi)^2}\int_0^\infty dP\Bigg\{n(P)\left(\ln\frac{P+|P+K|}{P+|P-K|} + \ln\frac{P-|P+K|}{P-|P-K|}\right) - \frac{1}{P}\ln\frac{|P+K|}{|P-K|}\Bigg\}, \qquad \text{(B.35)}$$

$$\nu^{2\epsilon} I_3(k) = \frac{\mathbf{k}^2}{(4\pi)^2}\Big[\frac{2}{\epsilon} + 2\ln\frac{4\pi\nu^2}{\mathbf{k}^2} + 2\ln\frac{\mathbf{k}^2}{(2\pi T)^2} + 2\gamma_E + 4 - \ln 4\Big] + \mathcal{O}(\epsilon) \qquad \text{(B.36)}$$

Let us give some notes: Firstly, the finite temperature integrals $I_1^{(T)}$ and $I_2^{(T)}$ are infra-red (IR) finite which allows us to handle them with standard numerical methods. Secondly, a straight forward separation of the temperature and the zero temperature contributions in (B.30) and (B.33) is obvious, however, the separation in (B.36) is rather problematic. Fortunately, a separation of the thermal contributions from the vacuum contributions can be done as the vacuum part is well-known (see f.i. [105, 143]).

We now compute I_4. In order to perform the frequency summations it is convenient to rewrite I_4 for in terms of $I_4 \equiv I_{4a} - I_{4b} - I_{4c}$, with

$$I_{4a} \equiv \sum\!\!\!\!\!\!\int_p \frac{\mathbf{k}^4}{\mathbf{p}^2\mathbf{q}^2p_0^2}, \quad I_{4b} \equiv \sum\!\!\!\!\!\!\int_p \frac{\mathbf{k}^4}{\mathbf{p}^2\mathbf{q}^2q^2}, \quad I_{4c} \equiv \sum\!\!\!\!\!\!\int_p \frac{\mathbf{k}^4}{\mathbf{p}^2p^2q^2}.$$

By performing the frequency sums in I_{4a}, I_{4b} and I_{4c} and integrating out the angular dependence we obtain:

$$I_{4a} = \frac{K^3T^2}{12(2\pi)^2}\int_0^\infty dP\frac{1}{P}\ln\frac{|P+K|}{|P-K|} = \frac{k^3}{96}, \tag{B.37}$$

$$I_{4b} = \frac{K^3T^2}{(2\pi)^2}\int_0^\infty dP\left(\frac{1+2n(P)}{2P^2}-\frac{T}{P^3}\right)\ln\frac{|P+K|}{|P-K|}, \tag{B.38}$$

$$\begin{aligned} I_{4c} &= \frac{K^3T^2}{(2\pi)^2}\int_0^\infty dP\Bigg[\frac{1}{2P^2}\ln\frac{P+|P+K|}{P+|P-K|}-\frac{1}{P^3}\ln\frac{|P+K|}{|P-K|} \\ &\quad +\frac{n(P)}{P^2}\Big(\ln\frac{P+|P+K|}{P+|P-K|}+\ln\frac{P-|P+K|}{P-|P-K|}+\ln\frac{|P-K|}{|P+K|}\Big)\Bigg]. \end{aligned} \tag{B.39}$$

We identify I_{4a} being the term which is specific to our gauge; we have extracted this term in (B.20). While I_4 does not produce ultra violet divergences, we note here however, that I_4 contains non-trivial vacuum contributions.

B4. IR and UV properties

One may check the ν-scale independence of the zero temperature parts. We find

$$\Big(\Pi_{00}^{ns}\Big)_{\nu-\mathrm{dep}} = \frac{11}{3}Ng^2k^2\delta^{ab}\ln\nu^2 \tag{B.40}$$

This factor, $\frac{11N}{3}$, appears indeed in the perturbative β-function for $N_f=0$.

We check the convergence in the infra-red limit $p\to 0$. We give a detailed proof of the convergence of $I_4^{(T)}$. Infra-red behaviour, this means $P\ll K\ll T$, $|P-K|=K-P$, of I_{4a}:

$$\begin{aligned} I_{4a} &= \frac{1}{(2\pi T)^2K}\frac{1}{12}\int_0^\infty dP\frac{1}{P}\ln\frac{P+K}{K-P} \\ &= \frac{1}{(2\pi T)^2K}\frac{1}{12}\int_0^\infty dP\frac{1}{P}\Big\{2\frac{P}{K}+\frac{2}{3}\Big(\frac{P}{K}\Big)^3+...\Big\} \\ &= \frac{1}{(2\pi T)^2K}\frac{1}{12}\int_0^\infty dP\Big\{\frac{P}{K}+\mathcal{O}(P^2)\Big\}. \end{aligned} \tag{B.41}$$

I_{4a} is infra-red convergent.

Now: I_{4b} is convergent in the infra-red limit:

$$\begin{aligned} I_{4b} &= \frac{1}{(2\pi)^2K}\int_0^\infty dP\Big(\frac{1+2n(P)}{2P^2}-\frac{1}{P^3}\Big)\ln\frac{|P+K|}{|P-K|} \\ &= \frac{1}{(2\pi)^2K}\int_0^\infty dP\Big(\frac{1}{2P^2}+\frac{n(P)}{P^2}-\frac{1}{P^3}\Big)\Big(2P+...\Big). \end{aligned} \tag{B.42}$$

In the last expression we have only expand the logarithm. By expanding $n(P)$ we are led to only convergent contributions:

$$I_{4b} = \frac{1}{(2\pi)^2 K}\int_0^\infty dP\Big(\frac{1}{6}+\mathcal{O}(P)\Big) \tag{B.43}$$

We finally show that $I_{4c} \equiv A+B+C-D$ is itself convergent in the infra-red limit with:

$$A := \frac{1}{(2\pi)^2 K}\int_0^\infty dP \frac{1}{2P^2}\ln\frac{P+|P+K|}{P+|P-K|} \tag{B.44}$$

$$B := \frac{1}{(2\pi)^2 K}\int_0^\infty dP \frac{n(P)}{2P^2}\Big(\ln\frac{P+|P+K|}{P+|P-K|}+\ln\frac{P-|P+K|}{P-|P-K|}\Big) \tag{B.45}$$

$$C := \frac{1}{(2\pi)^2 K}\int_0^\infty dP \frac{n(P)}{2P^2}\Big(2\ln\frac{|P-K|}{|P+K|}+\ln\frac{P+|P+K|}{P+|P-K|}+\ln\frac{P-|P+K|}{P-|P-K|}\Big) \tag{B.46}$$

$$D := \frac{1}{(2\pi)^2 K}\int_0^\infty dP \frac{1}{P^3}\ln\frac{|P+K|}{|P-K|}. \tag{B.47}$$

We proof: C is alone infra-red convergent and $A+B-D$ is infra-red convergent. In order to do so, we expand C in the limit $P/K \ll 1$. This leads to

$$\begin{aligned} C &= \frac{1}{(2\pi)^2 K}\int_0^\infty dP \frac{n(P)}{2P^2}\Big\{2\Big[-\frac{P}{K}-\frac{2}{3}\Big(\frac{P}{K}\Big)^3+...\Big]+4\frac{P}{K}+\frac{16}{3}\Big(\frac{P}{K}\Big)^3+...\Big\} \\ &= \frac{1}{(2\pi)^2 K}\int_0^\infty dP \frac{n(P)}{2P^2}\Big\{4\Big(\frac{P}{K}\Big)^3+...\Big\}. \end{aligned} \tag{B.48}$$

Now we only need to expand $n(P)$ in this regime to get the convergent expression

$$C = \frac{1}{(2\pi)^2 K}\int_0^\infty dP\Big[\frac{2}{K^3}+\mathcal{O}(P)\Big]. \tag{B.49}$$

Finally we show: $A+B-D$ is convergent for $P\to 0$:

$$A+B-D = \frac{1}{(2\pi)^2 K}\int_0^\infty dP\Big\{\frac{1}{PK}-\frac{2}{P^2K}+2\frac{n(P)}{KP}+\mathcal{O}(P^0)\Big\} \tag{B.50}$$

By expanding the Bose Einstein distribution the divergent parts cancel out:

$$A+B-D = \frac{1}{(2\pi)^2 K}\int_0^\infty dP\ \mathcal{O}(P^0). \tag{B.51}$$

B5. Low- and high-T approximation

In the low temperature approximation of the finite temperature integrals we make use of some integrals that are calculated in [146].
In the high temperature limit we find ($k \ll p \ll T$), $\tilde{\Pi}^m_{00} = \Pi^m_{00}/g^2$:

$$\begin{aligned}\tilde{\Pi}^m_{00}(k \ll p \ll T) &= 1 + 0.01192947179834837\, k^2 + 0.015625\, k^3 \\ &\quad -0.00044347934570314947\, k^4 + 6.470230045218389\, 10^{-7}\, k^6 \\ &\quad -2.1929620925010094\, 10^{-9}\, k^8 + 9.453105666167652\, 10^{-12}\, k^{10} \\ &\quad -4.541986644640096\, 10^{-14}\, k^{12} + 2.3191838919038833\, 10^{-16}\, k^{14} \\ &\quad -1.231059165419055\, 10^{-18}\, k^{16} + 6.7129162217446455\, 10^{-21}\, k^{18} \\ &\quad -3.7335965865922323\, 10^{-23}\, k^{20} + 2.1082165069000592\, 10^{-25}\, k^{22} \\ &\quad -1.2047473535474273\, 10^{-27}\, k^{24} + 6.951585898777381\, 10^{-30}\, k^{26} \\ &\quad -4.043428554828764\, 10^{-32}\, k^{28} + 3.2370809486341554\, 10^{-35}\, k^{30} \\ &\quad -2.767372364279353\, 10^{-36}\, k^{32} \\ &\quad +0.06965831375410722\, k^2 \ln(39.47841760435743/k^2) \end{aligned} \tag{B.52}$$

This parameterization is shown in Fig. B.1.

B6. Fourier transformation to position space

At HTL-like re-summed 1-loop level we identify in accordance with (B.16)

$$\beta\delta F^{ns}_{q\bar{q}}(r,T) = -g^4\beta^2 \frac{2(N^2-1)}{8N^2}\left(\frac{e^{-m_D r}}{4\pi r}\right)\int \frac{d^3k}{(2\pi)^3}\left(\Pi^{ns}_{00}(k) - m_D^2\right)\frac{e^{i\mathbf{kr}}}{(k^2+m_D^2)^2}, \tag{B.53}$$

where we have included the Fourier transformation to position space. Because of the segmentation of $\Pi^{ns}_{00}(k)$ defined in (B.20) we have:

$$\begin{aligned}\beta\delta F^{ns}_{q\bar{q}}(r,T) &= \beta\delta F^{ns(0)}_{q\bar{q}}(r,T) + \beta\delta F^{ns(T)}_{q\bar{q}}(r,T) + \beta\delta F^{ns(T)g}_{q\bar{q}}(r,T) \\ &\quad + g^4\beta^2 \frac{2(N^2-1)}{8N^2}\left(\frac{e^{-m_D r}}{4\pi r}\right)\underbrace{\int \frac{d^3k}{(2\pi)^3}\frac{m_D^2}{(k^2+m_D^2)^2}e^{i\mathbf{kr}}}_{=\frac{m_D}{8\pi}e^{-m_D r}}, \end{aligned} \tag{B.54}$$

where the integral in the under-bracket follows from the residual calculi. We first concentrate on the 1-loop vacuum corrections defined on

$$\beta\delta F^{ns(0)}_{q\bar{q}}(r,T) \equiv -g^4\beta^2 \frac{2(N^2-1)}{8N^2}\left(\frac{e^{-m_D r}}{4\pi r}\right)\int \frac{d^3k}{(2\pi)^3}\,\Pi^{ns(0)}_{00}(k)\frac{e^{i\mathbf{kr}}}{(k^2+m_D^2)^2}, \tag{B.55}$$

where we take $\Pi^{ns(0)}_{00}(k)$ from [103]. By inserting the scale $\bar{\nu}^2 \equiv 4\pi e^{-\gamma_E}\nu^2$, with ν defined in the $\overline{MS}$ scheme, we rewrite $\Pi^{ns(0)}_{00}(k)$ in the form

$$\Pi^{ns(0)}_{00}(k) = -\frac{g^2 N\mathbf{k}^2}{(4\pi)^2}\Big(\frac{11}{3}\ln\bar{\nu}r^2 + \frac{31}{9} + \frac{11}{3}\ln\frac{1}{\mathbf{k}^2r^2}\Big). \tag{B.56}$$

After some basic steps we are led to:

$$\beta\delta F_{q\bar{q}}^{ns(0)}(r,T) = g^6\beta^2\frac{N^2-1}{64N\pi^2}\left(\frac{e^{-m_D r}}{4\pi r}\right)\left[\frac{11}{3}\underbrace{\int\frac{d^3k}{(2\pi)^3}\frac{e^{i\mathbf{kr}}}{(k^2+m_D^2)^2}k^2\ln\frac{1}{k^2r^2}}_{\equiv J_0(r,T)}\right.$$
$$\left.+\left(\frac{11}{3}\ln\bar{\nu}^2r^2+\frac{31}{9}\right)\left(\int\frac{d^3k}{(2\pi)^3}\frac{e^{i\mathbf{kr}}}{k^2+m_D^2}-\int\frac{d^3k}{(2\pi)^3}\frac{m_D^2e^{i\mathbf{kr}}}{(k^2+m_D^2)^2}\right)\right], \quad \text{(B.57)}$$

where $J_0(r,T)$ defined in (B.57) can be reduced to

$$J_0(r,T) \;=\; \frac{1}{2\pi^2 r}\int_0^\infty d\tilde{p}\frac{\tilde{p}^3\ln\frac{1}{\tilde{p}^2(rT)^2}}{(\tilde{p}^2+\tilde{m}_D^2)^2}\sin(\tilde{p}rT) \quad \text{(B.58)}$$

with $\tilde{m}_D \equiv m_D/T$. We calculate this integral with numerical methods.
The 1-loop contributions specific to our gauge is given by

$$\beta\delta F_{q\bar{q}}^{ns(T)g}(r,T) \equiv -g^4\beta^2\frac{2N^2-1}{8N^2}\left(\frac{e^{-m_D r}}{4\pi r}\right)\int\frac{d^3k}{(2\pi)^3}\Pi_{00}^{(T)g}(k)\frac{e^{i\mathbf{kr}}}{(k^2+m_D^2)^2}, \quad \text{(B.59)}$$

with

$$\Pi_{00}^{(T)g} \;=\; -\frac{Ng^2}{2}I_{4a} \;=\; -\frac{Ng^2}{2}\frac{k^3}{96}. \quad \text{(B.60)}$$

In order to perform the Fourier transformation we re-organize

$$\frac{1}{(k^2+m_D^2)^2} \;=\; \frac{1}{k^4}+\left(\frac{1}{(k^2+m_D^2)^2}-\frac{1}{k^4}\right) \quad \text{(B.61)}$$

as the first term cancels the k^3 in (B.60). We then arrive at:

$$\beta\delta F_{q\bar{q}}^{ns(T)g}(r,T) \;=\; g^6\beta^3\frac{N^2-1}{768N}\left(\frac{e^{-m_D r}}{4\pi r}\right)^2 J_g(r,T)$$
$$+g^6\beta^3\frac{N^2-1}{96N}e^{-m_D r}\left(\frac{1}{4\pi r}\right)^3. \quad \text{(B.62)}$$

(The factor $(N^2-1)/(768N)$ results from $N/96\times 2(N^2-1)/(8N^2)\times 1/4$, where the first term is from (B.60), the second term is from (B.53) and the last factor results from angular integration and some re-organizations.) $J_g(r,T)$ appearing in (B.62) originates from the second term in (B.61) and can be written as

$$J_g(r,T) = e^{m_D r}\frac{2}{\pi}\int_0^\infty d\tilde{p}\left(\frac{\tilde{p}^4}{(\tilde{p}^2+\tilde{m}_D^2)^2}-1\right)\sin(\tilde{p}rT) \quad \text{(B.63)}$$

where we refer to the notations as clarified above. We have solved this integral by applying numerical methods - and even the remaining thermal contribution $\delta F^{ns(T)}$ defined on

$$\beta\delta F_{q\bar{q}}^{ns(T)}(r,T) \equiv -g^4\beta^2\frac{2N^2-1}{8N^2}\left(\frac{e^{-m_D r}}{4\pi r}\right)\int\frac{d^3k}{(2\pi)^3}\Pi_{00}^{ns(T)}(k)\frac{e^{i\mathbf{kr}}}{(k^2+m_D^2)^2} \quad \text{(B.64)}$$

has to be computed with numerical methods since $\Pi_{00}^{ns(T)}(k)$ is non-analytic in our presentation.

Bibliography

[1] T. Muta. Foundations of Quantum Chromodynamics, An Introduction to Perturbative Methods in Gauge Theories, World Scientific (1987).

[2] G. t'Hooft. unpublished (1972).

[3] H. D. Politzer, "Reliable perturbative results for strong interactions?", *Phys. Rev. Lett.* **30** (1973) 1346.

[4] D. J. Gross and F. Wilczek, "Ultraviolet behavior of non-abelian gauge theories", *Phys. Rev. Lett.* **30** (1973) 1343.

[5] J. C. Collins and M. J. Perry, "Superdense matter: Neutrons or asymptotically free quarks?", *Phys. Rev. Lett.* **34** (1975) 1353.

[6] U. W. Heinz, "The little bang: Searching for quark-gluon matter in relativistic heavy-ion collisions", *Nucl. Phys.* **A685** (2001) 414, `hep-ph/0009170`.

[7] H. Satz, "Limits of confinement: The first 15 years of ultra- relativistic heavy ion studies", *Nucl. Phys.* **A715** (2003) 3, `hep-ph/0209181`.

[8] R. D. Pisarski, "Theory at quark matter '02", *Nucl. Phys.* **A715** (2003) 412, `nucl-th/0212015`.

[9] L. D. McLerran and B. Svetitsky, "Quark liberation at high temperature: A monte carlo study of su(2) gauge theory", *Phys. Rev.* **D24** (1981) 450.

[10] L. D. McLerran and B. Svetitsky, "A monte carlo study of su(2) yang-mills theory at finite temperature", *Phys. Lett.* **B98** (1981) 195.

[11] M. LeBellac. Thermal field theory, Cambridge University Press (1996).

[12] J. I. Kapusta. Finite-temperature field theory, Cambridge University Press (1988).

[13] E. Braaten and R. D. Pisarski, "Soft amplitudes in hot gauge theories: A general analysis", *Nucl. Phys.* **B337** (1990) 569.

[14] F. Karsch, A. Patkos, and P. Petreczky, "Screened perturbation theory", *Phys. Lett.* **B401** (1997) 69, `hep-ph/9702376`.

[15] A. D. Linde, "Infrared problem in thermodynamics of the yang-mills gas", *Phys. Lett.* **B96** (1980) 289.

[16] D. J. Gross, R. D. Pisarski, and L. G. Yaffe, "Qcd and instantons at finite temperature", *Rev. Mod. Phys.* **53** (1981) 43.

[17] J.-P. Blaizot and E. Iancu, "The quark-gluon plasma: Collective dynamics and hard thermal loops", *Phys. Rept.* **359** (2002) 355, `hep-ph/0101103`.

[18] I. Montvay and G. Munster. Quantum Fields on a Lattice, Cambridge Monographs on Mathematical Physics (1997).

[19] F. Karsch and E. Laermann, "Thermodynamics and in-medium hadron properties from lattice qcd", `hep-lat/0305025`.

[20] F. Karsch (ed.) and H. Satz (ed.). Statistical QCD, Symposium on Statistical QCD, Bielefeld, Germany, 26-30 Aug. 2001.

[21] K. G. Wilson, "Confinement of quarks", *Phys. Rev.* **D10** (1974) 2445.

[22] R. D. Pisarski, "Notes on the deconfining phase transition", `hep-ph/0203271`.

[23] O. Philipsen, "Non-perturbative formulation of the static color octet potential", *Phys. Lett.* **B535** (2002) 138, `hep-lat/0203018`.

[24] S. Nadkarni, "Nonabelian debye screening. 2. the singlet potential", *Phys. Rev.* **D34** (1986) 3904.

[25] R. D. Pisarski, "Quark-gluon plasma as a condensate of su(3) wilson lines", *Phys. Rev.* **D62** (2000) 111501, `hep-ph/0006205`.

[26] A. Dumitru and R. D. Pisarski, "Two-point functions for su(3) polyakov loops near t(c)", *Phys. Rev.* **D66** (2002) 096003, `hep-ph/0204223`.

[27] P. N. Meisinger, T. R. Miller, and M. C. Ogilvie, "Phenomenological equations of state for the quark-gluon plasma", *Phys. Rev.* **D65** (2002) 034009, `hep-ph/0108009`.

[28] P. N. Meisinger, T. R. Miller, and M. C. Ogilvie, "Theory and phenomenology of the polyakov loop in qcd thermodynamics", `hep-lat/0309097`.

[29] S. Digal, P. Petreczky, and H. Satz, "Quarkonium feed-down and sequential suppression", *Phys. Rev.* **D64** (2001) 094015, `hep-ph/0106017`.

[30] S. Digal, P. Petreczky, and H. Satz, "Sequential quarkonium suppression", `hep-ph/0110406`.

[31] T. Matsui and H. Satz, "J / psi suppression by quark - gluon plasma formation", *Phys. Lett.* **B178** (1986) 416.

[32] F. Karsch and H. Satz, "The spectral analysis of strongly interacting matter", *Z. Phys.* **C51** (1991) 209.

[33] O. Kaczmarek, F. Karsch, E. Laermann, and M. Lutgemeier, "Heavy quark potentials in quenched qcd at high temperature", *Phys. Rev.* **D62** (2000) 034021, `hep-lat/9908010`.

[34] I. T. Drummond and R. R. Horgan, "Lattice string breaking and heavy meson decays", *Phys. Lett.* **B447** (1999) 298, `hep-lat/9811016`.

[35] A. Duncan, E. Eichten, and H. Thacker, "String breaking in four dimensional lattice qcd", *Phys. Rev.* **D63** (2001) 111501, `hep-lat/0011076`.

[36] C. DeTar, O. Kaczmarek, F. Karsch, and E. Laermann, "String breaking in lattice quantum chromodynamics", *Phys. Rev.* **D59** (1999) 031501, `hep-lat/9808028`.

[37] D. Antonov, L. Del Debbio, and A. Di Giacomo, "A model for string-breaking in qcd", *JHEP* **08** (2003) 011, `hep-lat/0302015`.

[38] J. F. Arvis, "The exact q anti-q potential in nambu string theory", *Phys. Lett.* **B127** (1983) 106.

[39] Y. Nambu, "Qcd and the string model", *Phys. Lett.* **B80** (1979) 372.

[40] M. Luscher, K. Symanzik, and P. Weisz, "Anomalies of the free loop wave equation in the wkb approximation", *Nucl. Phys.* **B173** (1980) 365.

[41] M. Luscher, "Symmetry breaking aspects of the roughening transition in gauge theories", *Nucl. Phys.* **B180** (1981) 317.

[42] C. J. Morningstar, K. J. Juge, and J. Kuti, "Where is the string limit in qcd?", *Nucl. Phys. Proc. Suppl.* **73** (1999) 590, `hep-lat/9809098`.

[43] A. M. Polyakov, "Gauge fields as rings of glue", *Nucl. Phys.* **B164** (1980) 171.

[44] A. M. Polyakov, "Quantum geometry of bosonic strings", *Phys. Lett.* **B103** (1981) 207.

[45] P. de Forcrand, G. Schierholz, H. Schneider, and M. Teper, "The string and its tension in su(3) lattice gauge theory: Towards definitive results", *Phys. Lett.* **B160** (1985) 137.

[46] R. D. Pisarski and O. Alvarez, "Strings at finite temperature and deconfinement", *Phys. Rev.* **D26** (1982) 3735.

[47] J. D. Stack and M. Stone, "Elementary derivation of the universal attractive coulomb term in the interquark potential", *Phys. Lett.* **B100** (1981) 476.

[48] A. Ukawa, "Qcd phase transitions at finite temperatures", *Nucl. Phys. Proc. Suppl.* **17** (1990) 118.

[49] M. Gao, "Heavy quark potential at finite temperature from a string picture", *Phys. Rev.* **D40** (1989) 2708.

[50] S. W. Otto and J. D. Stack, "The su(3) heavy quark potential with high statistics", *Phys. Rev. Lett.* **52** (1984) 2328.

[51] G. S. Bali, "Qcd forces and heavy quark bound states", *Phys. Rept.* **343** (2001) 1, `hep-ph/0001312`.

[52] G. Munster, "High temperature expansions for the free energy of vortices, respectively the string tension in lattice gauge theories", *Nucl. Phys.* **B180** (1981) 23.

[53] G. S. Bali, C. Schlichter, and K. Schilling, "Probing the qcd vacuum with static sources in maximal abelian projection", *Prog. Theor. Phys. Suppl.* **131** (1998) 645, `hep-lat/9802005`.

[54] M. Luscher and P. Weisz, "Quark confinement and the bosonic string", *JHEP* **07** (2002) 049, `hep-lat/0207003`.

[55] S. Necco and R. Sommer, "The n(f) = 0 heavy quark potential from short to intermediate distances", *Nucl. Phys.* **B622** (2002) 328, `hep-lat/0108008`.

[56] J. Engels and V. K. Mitrjushkin, "Mass gap and finite size effects in finite temperature su(2) lattice gauge theory", *Phys. Lett.* **B282** (1992) 415.

[57] S. Nadkarni, "Nonabelian debye screening. 1. the color averaged potential", *Phys. Rev.* **D33** (1986) 3738.

[58] L. S. Brown and W. I. Weisberger, "Remarks on the static potential in quantum chromodynamics", *Phys. Rev.* **D20** (1979) 3239.

[59] C. Gale and J. Kapusta, "Modification of debye screening in gluon plasma", *Phys. Lett.* **B198** (1987) 89.

[60] A. K. Rebhan, "Nonabelian debye screening in one loop resummed perturbation theory", *Nucl. Phys.* **B430** (1994) 319, `hep-ph/9408262`.

[61] E. Braaten and A. Nieto, "Next-to-leading order debye mass for the quark - gluon plasma", *Phys. Rev. Lett.* **73** (1994) 2402, `hep-ph/9408273`.

[62] P. Arnold and L. G. Yaffe, "The nonabelian debye screening length beyond leading order", *Phys. Rev.* **D52** (1995) 7208, `hep-ph/9508280`.

[63] T. A. DeGrand and C. E. DeTar, "Static screening lengths in the gluon plasma", *Phys. Rev.* **D34** (1986) 2469.

[64] K. Kanaya and H. Satz, "Correlation and screening in finite temperature su(2) gauge theory", *Phys. Rev.* **D34** (1986) 3193.

[65] J. Engels, J. Fingberg, K. Redlich, H. Satz, and M. Weber, "The onset of deconfinement in su(2) lattice gauge theory", *Z. Phys.* **C42** (1989) 341.

[66] U. M. Heller, F. Karsch, and J. Rank, "Gluon propagator at high temperature: Screening, improvement and nonzero momenta", *Phys. Rev.* **D57** (1998) 1438, `hep-lat/9710033`.

[67] N. Attig, F. Karsch, B. Petersson, H. Satz, and M. Wolff, "Polyakov loop correlations in landau gauge and the heavy quark potential", *Phys. Lett.* **B209** (1988) 65.

[68] P. Lacock and T. Reisz, "Dimensional reduction of qcd and screening masses in the quark - gluon plasma", *Nucl. Phys. Proc. Suppl.* **30** (1993) 307.

[69] S. Digal, S. Fortunato, and P. Petreczky, "Heavy quark free energies and screening in su(2) gauge theory", *Phys. Rev.* **D68** (2003) 034008, `hep-lat/0304017`.

[70] J. Engels, F. Karsch, and H. Satz, "A finite size analysis of the heavy quark potential in a deconfining medium", *Nucl. Phys.* **B315** (1989) 419.

[71] E. Manousakis and J. Polonyi, "Nonperturbative length scale in high temperature qcd", *Phys. Rev. Lett.* **58** (1987) 847.

[72] C. DeTar and J. B. Kogut, "Measuring the hadronic spectrum of the quark plasma", *Phys. Rev.* **D36** (1987) 2828.

[73] F. Zantow, O. Kaczmarek, F. Karsch, and P. Petreczky, "Short distance physics with heavy quark potentials", *Nucl. Phys. Proc. Suppl.* **106** (2002) 519, `hep-lat/0110103`.

[74] P. Petreczky *et al.*, "Lattice calculation of medium effects at short and long distances", *Nucl. Phys.* **A698** (2002) 400, `hep-lat/0103034`.

[75] K. Holland and U.-J. Wiese, "The center symmetry and its spontaneous breakdown at high temperatures", `hep-ph/0011193`.

[76] G. 't Hooft, "On the phase transition towards permanent quark confinement", *Nucl. Phys.* **B138** (1978) 1.

[77] A. M. Polyakov, "Thermal properties of gauge fields and quark liberation", *Phys. Lett.* **B72** (1978) 477.

[78] V. A. Belavin, V. G. Bornyakov, and V. K. Mitrjushkin, "On the gauge dependence of the singlet and adjoint potentials", `hep-lat/0310033`.

[79] P. Weisz, "Continuum limit improved lattice action for pure yang-mills theory. 1", *Nucl. Phys.* **B212** (1983) 1.

[80] P. Weisz and R. Wohlert, "Continuum limit improved lattice action for pure yang-mills theory. 2", *Nucl. Phys.* **B236** (1984) 397. Erratum ibid. **B247** (1984) 544.

[81] K. Symanzik, "Continuum limit and improved action in lattice theories. 1. principles and phi**4 theory", *Nucl. Phys.* **B226** (1983) 187.

[82] F. Zantow, O. Kaczmarek, F. Karsch, and P. Petreczky, "A new order parameter with renormalized polyakov loops", `hep-lat/0110106`.

[83] O. Kaczmarek, F. Karsch, P. Petreczky, and F. Zantow. Static quark-antiquark free energy and the running coupling at finite temperature, (in preparation).

[84] I. Wetzorke. Lattice QCD Calculations of Hadron Spectra and Spectral Functions in the Vacuum and in a Thermal Heath Bath, PhD thesis, Bielefeld, Germany (2001).

[85] O. Kaczmarek. The heavy quark mass limit of QCD at non-zero baryon number density, PhD thesis, Bielefeld, Germany (2000).

[86] B. Beinlich, F. Karsch, and A. Peikert, "Su(3) latent heat and surface tension from tree level and tadpole improved actions", *Phys. Lett.* **B390** (1997) 268, `hep-lat/9608141`.

[87] G. S. Bali and K. Schilling, "Running coupling and the lambda parameter from su(3) lattice simulations", *Phys. Rev.* **D47** (1993) 661, `hep-lat/9208028`.

[88] S. Datta and S. Gupta, "Does the qcd plasma contain propagating gluons?", *Phys. Rev.* **D67** (2003) 054503, `hep-lat/0208001`.

[89] A. Nakamura, I. Pushkina, T. Saito, and S. Sakai, "Screening of hot gluon", *Phys. Lett.* **B549** (2002) 133, `hep-lat/0208075`.

[90] E. V. Shuryak and I. Zahed, "Rethinking the properties of the quark gluon plasma at t approx. t(c)", `hep-ph/0307267`.

[91] V. S. Dotsenko and S. N. Vergeles, "Renormalizability of phase factors in the nonabelian gauge theory", *Nucl. Phys.* **B169** (1980) 527.

[92] O. Kaczmarek, F. Karsch, P. Petreczky, and F. Zantow, "Heavy quark anti-quark free energy and the renormalized polyakov loop", *Phys. Lett.* **B543** (2002) 41, `hep-lat/0207002`.

[93] F. Zantow, "On the renormalization of the polyakov loop", `hep-lat/0301014`.

[94] S. Pokorski. Gauge Field Theories, Cambridge Monographs on Mathematical Physics, Cambridge University Press (2000).

[95] N. N. Bogoliubov and D. V. Shirkov. Introduction to the theory of quantized fields Interscience, New York (1959).

[96] E. Gava and R. Jengo, "Perturbative evaluation of the thermal wilson loop", *Phys. Lett.* **B105** (1981) 285.

[97] I. Y. Arefeva, "Quantum contour field equations", *Phys. Lett.* **B93** (1980) 347.

[98] J.-L. Gervais and A. Neveu, "The slope of the leading regge trajectory in quantum chromodynamics", *Nucl. Phys.* **B163** (1980) 189.

[99] C. P. Korthals Altes, "Constrained effective potential in hot qcd", *Nucl. Phys.* **B420** (1994) 637, `hep-th/9310195`.

[100] P. de Forcrand and L. von Smekal, "'t hooft loops, electric flux sectors and confinement in su(2) yang-mills theory", *Phys. Rev.* **D66** (2002) 011504, `hep-lat/0107018`.

[101] A. Dumitru, Y. Hatta, J. Lenaghan, K. Orginos, and R. D. Pisarski, "Deconfining phase transition as a matrix model of renormalized polyakov loops", `hep-th/0311223`.

[102] U. M. Heller and F. Karsch, "One loop perturbative calculation of wilson loops on finite lattices", *Nucl. Phys.* **B251** (1985) 254.

[103] G. Curci, G. Paffuti, and R. Tripiccione, "Perturbative background to monte carlo calculations in lattice gauge theories", *Nucl. Phys.* **B240** (1984) 91.

[104] G. S. Bali, K. Schilling, and A. Wachter, "Complete o(v**2) corrections to the static interquark potential from su(3) gauge theory", *Phys. Rev.* **D56** (1997) 2566, `hep-lat/9703019`.

[105] W. Fischler, "Quark - anti-quark potential in qcd", *Nucl. Phys.* **B129** (1977) 157.

[106] M. Peter, "The static quark-antiquark potential in qcd to three loops", *Phys. Rev. Lett.* **78** (1997) 602, `hep-ph/9610209`.

[107] S. Necco and R. Sommer, "Testing perturbation theory on the n(f) = 0 static quark potential", *Phys. Lett.* **B523** (2001) 135, `hep-ph/0109093`.

[108] S. Kratochvila and P. de Forcrand, "Qcd at zero baryon density", `hep-lat/0309146`.

[109] D. E. Miller, "Entropy for su(3)c quark states", `hep-ph/0306302`.

[110] R. Sommer, "A new way to set the energy scale in lattice gauge theories and its applications to the static force and alpha-s in su(2) yang-mills theory", *Nucl. Phys.* **B411** (1994) 839, `hep-lat/9310022`.

[111] F. Zantow, O. Kaczmarek, F. Karsch, and P. Petreczky, "Renormalized quark anti-quark free energy", `hep-lat/0301015`.

[112] K. Hubner. Freie Energien schwerer Quarks in reiner Eichtheorie, Diploma thesis, Bielefeld, Germany (2003).

[113] O. Vogt. Diploma thesis in preparation, Bielefeld, Germany.

[114] K. G. Wilson, "Nonlagrangian models of current algebra", *Phys. Rev.* **179** (1969) 1499.

[115] W. Zimmermann. Local Operator Products and Renormalization in Quantum Field Theory, in Lectures on Elementary Particles and Quantum Filed Theory (Brandeis Summer Institute) (1970).

[116] G. P. Lepage and P. B. Mackenzie, "On the viability of lattice perturbation theory", *Phys. Rev.* **D48** (1993) 2250, `hep-lat/9209022`.

[117] F. Karsch, E. Laermann, and A. Peikert, "Quark mass and flavor dependence of the qcd phase transition", *Nucl. Phys.* **B605** (2001) 579, `hep-lat/0012023`.

[118] S. Fortunato. Private communication (2003).

[119] O. Kaczmarek, S. Ejiri, F. Karsch, E. Laermann, and F. Zantow, "Heavy quark free energies and the renormalized polyakov loop in full qcd", `hep-lat/0312015`.

[120] O. Kaczmarek. Private communication (2003).

[121] J. E. Kiskis and P. Vranas, "Adjoint wilson line in su(2) lattice gauge theory", *Phys. Rev.* **D49** (1994) 528, `hep-lat/9307012`.

[122] P. Bacilieri *et al.*, "On the order of the deconfining phase transition in pure gauge qcd", *Phys. Rev. Lett.* **61** (1988) 1545.

[123] F. R. Brown, N. H. Christ, Y. F. Deng, M. S. Gao, and T. J. Woch, "Nature of the deconfining phase transition in su(3) lattice gauge theory", *Phys. Rev. Lett.* **61** (1988) 2058.

[124] M. Wingate and S. Ohta, "Deconfinement transition and string tensions in su(4) yang- mills theory", *Phys. Rev.* **D63** (2001) 094502, `hep-lat/0006016`.

[125] E. Braaten, "Thermodynamics of hot qcd", *Nucl. Phys.* **A702** (2002) 13–24.

[126] F. Karsch, M. T. Mehr, and H. Satz, "Color screening and deconfinement for bound states of heavy quarks", *Z. Phys.* **C37** (1988) 617.

[127] G. Boyd *et al.*, "Thermodynamics of su(3) lattice gauge theory", *Nucl. Phys.* **B469** (1996) 419, `hep-lat/9602007`.

[128] O. Kaczmarek, F. Karsch, P. Petreczky, and F. Zantow, "Heavy quark free energies, potentials and the renormalized polyakov loop", `hep-lat/0309121`.

[129] E. Seiler, "Upper bound on the color confining potential", *Phys. Rev.* **D18** (1978) 482.

[130] O. Alvarez, "The static potential in string models", *Phys. Rev.* **D24** (1981) 440.

[131] H. v. Beijeren and I. Nolden, "The roughening transition",. in Structure and Dynamics of Surfaces II, Topics in Current Physics, Vol. 43 (1987), Springer, Berlin.

[132] C. Itzykson, M. E. Peskin, and J. B. Zuber, "Roughening of wilson's surface", *Phys. Lett.* **B95** (1980) 259.

[133] M. Luscher, G. Munster, and P. Weisz, "How thick are chromoelectric flux tubes?", *Nucl. Phys.* **B180** (1981) 1.

[134] A. Hasenfratz, E. Hasenfratz, and P. Hasenfratz, "Generalized roughening transition and its effect on the string tension", *Nucl. Phys.* **B180** (1981) 353.

[135] W. Buchmuller and S. H. H. Tye, "Quarkonia and quantum chromodynamics", *Phys. Rev.* **D24** (1981) 132.

[136] S. Digal, O. Kaczmarek, F. Karsch, H. Satz, P. Petreczky, and F. Zantow. in progress.

[137] K. Fabricius and O. Haan, "Heat bath method for the twisted eguchi-kawai model", *Phys. Lett.* **B143** (1984) 459.

[138] A. D. Kennedy and B. J. Pendleton, "Improved heat bath method for monte carlo calculations in lattice gauge theories", *Phys. Lett.* **B156** (1985) 393.

[139] K. Symanzik, "Continuum limit and improved action in lattice theories. 2. o(n) nonlinear sigma model in perturbation theory", *Nucl. Phys.* **B226** (1983) 205.

[140] C. R. Allton, "Lattice monte carlo data versus perturbation theory", *Nucl. Phys. Proc. Suppl.* **53** (1997) 867, `hep-lat/9610014`.

[141] A. Peikert. QCD thermodynamics with $2 + 1$ quark flavours in lattice simulations, PhD thesis, Bielefeld, Germany (2000).

[142] O. Kaczmarek. Korrelationsfunctionen und Potentiale mit verbesserten Wirkungen, Diploma thesis, Bielefeld, Germany (1997).

[143] G. Curci and P. Menotti, "Temporal gauges and periodic boundary conditions", *Z. Phys.* **C21** (1984) 281.

[144] S. Nadkarni, "Dimensional reduction in hot qcd", *Phys. Rev.* **D27** (1983) 917.

[145] B. Petersson and T. Reisz, "Polyakov loop correlations at finite temperature", *Nucl. Phys.* **B353** (1991) 757.

[146] P. Arnold and C.-X. Zhai, "The three loop free energy for pure gauge qcd", *Phys. Rev.* **D50** (1994) 7603, `hep-ph/9408276`.